Aus der

Radiologischen Universitätsklinik Tübingen

Nuklearmedizin und Klinische Molekulare Bildgebung

Enhanced imaging in oncology: novel clinical applications of new-generation PET/CT Scanners with a long axial field-of-view

Inaugural-Dissertation
zur Erlangung des Doktorgrades
der Medizin

der Medizinischen Fakultät
der Eberhard Karls Universität
zu Tübingen

vorgelegt von

Calderón Ochoa, Eduardo Enrique

2026

Dekanin: Professorin Dr. S. Y. Brucker

1. Berichterstatter: Professor Dr. C. la Fougère
2. Berichterstatter: Professor Dr. J. Leibold

Tag der Disputation: 26.06.2026

Table of Contents

List of Abbreviations

Abbreviation	Definition
ACT	Activity Concentrations
aFOV	Axial field of view
ANOVA	Analysis of Variance
Bq	Becquerel
cm	Centimetre
CoV	Coefficient of Variation
cps	Counts per second
CT	Computed Tomography
Cu	Copper
CUP	Cancer of Uknown Primary
DOTA	Tetraxetan
EANM	European Association of Nuclear Medicine
EFOMP	European Federation of Organisations for Medical Physics
EMA	European Medicines Agency
ENETS	European Neuroendocrine Tumor Society
ESMO	European Society of Medical Oncology
eV	electron Volt
F	Fluorine
FDA	Food and Drug Administration
FDG	Fluorodeoxyglucose
G	Grade
Ga	Gallium
Ge	Germanium
GEP	Gastroenteropancreatic
GLUT	Glucose transporter
Gy	Gray
h	hour
H&E	Hematoxylin and Eosin
HER2	Human Epidermal Growth Factor Receptor 2
HS	High Sensitivity
ICRP	International Commission on Radiological Protection
In	Indium
ITB	Interdisciplinary Tumorboard
kg	Kilogram
L	Liter
LAFOV	Long axial field of view
LOR	Line of response
Lu	Lutetium

mg	milligram
min	minute
MIP	Maximum Intensity Projection
mm	millimetre
MRI	Magnetic Resonance Imaging
MTV	Metabolic or Molecular Tumor Volume
NEC	Neuroendocrine Carcinoma
NEMA	National Electrical Manufacturers Association
NEN	Neuroendocrine Neoplasia
NET	Neuroendocrine Tumor
NOC	[1-Nal3]-octreotide
OP-OSEM	Ordinary-Poisson Ordered-Subsets Expectation-Maximization
OS	Overall Survival
p.i.	Post-injection
p53	Tumor suppressor protein p53
PET	Positron Emission Tomography
PRRT	Peptide Receptor Radionuclide Therapy
PSF	Point-Spread-Function
PSMA	Prostate Specific Membrane Antigen
RB	Retinoblastoma Tumor Suppressor Gene
RLT	Radioligand Therapy
RS	Radiosensitizing
SAFOV	Short axial field of view
SD	Standard Deviation
SE	Standard Error
Si	Silicium
SIRT	Selective Internal Radiation Therapy
SNR	Signal-to-noise ratio
SSA	Somatostatin Analogue
SSTR	Somatostatin Receptor
SUV	Standardized Uptake Value
Sv	Sievert
TATE	[Tyr3]-octreotate
TBR	Tumor-to-Background Ratio
TLR	Tumor-to-Liver Ratio
TOC	[Tyr3]-octreotide
TOF	Time-of-Flight
UHS	Ultra-high sensitivity
VOI	Volume of Interest
Y	Yttrium
Zr	Zirconium
β	beta

1. Introduction

1.1 Positron emission tomography imaging

Positron emission tomography (PET) is a nuclear medicine imaging technique that visualizes and quantifies the in vivo distribution of specific radiolabeled molecules. Like other nuclear medicine methods, it employs the tracer principle, using very small amounts of a radiolabeled substance to study physiological or biochemical processes without significantly disturbing them. Specifically for PET imaging, a biologically active molecule (e.g., a glucose analogue, a receptor ligand, or an amino acid) is labeled with a positron-emitting radionuclide and administered in tracer quantities following the same transport, binding, and metabolic pathways as the unlabeled compound.

Following intravenous injection of radiotracers that undergo beta-plus decay (β^+), the radionuclides emit a positron that travels a short distance before annihilating with an electron. This annihilation produces two 511 keV photons emitted almost back-to-back at 180 degrees, which are detected in time coincidence by a ring of detectors. Each coincident detection defines a so-called line of response (LOR), i.e., the straight line connecting the two detectors that registered the photons and along which the annihilation event must have occurred. By reconstructing a large number of coincident events, PET generates three-dimensional images of tracer distribution(Gambhir 2002, Basu, Kwee et al. 2011). Since its development in 1975 by Michael E. Phelps and colleagues(Phelps, Hoffman et al. 1975), PET technology has advanced significantly, contributing to its widespread adoption in medical practice and playing a key role in contemporary oncological imaging and patient care management.

1.2 Semi-Quantification of PET radiotracers

An important hallmark of PET imaging, compared with other nuclear medicine imaging techniques, is the possibility to quantify tracer distribution, which is

particularly important for monitoring the course of pathological processes in vivo. Semi-quantitative analysis in PET imaging is performed using the standardized uptake value (SUV). SUV is defined as the tissue activity concentration at a specific time point, normalized to the injected activity of a radiotracer and the patient's body weight, yielding a dimensionless number that enables comparison of radiotracer uptake between tumor lesions and across different time points(Weber 2005).

For this assessment, specialized software is used to generate three-dimensional volumes of interest (VOIs) in areas of suspected pathology and/or reference organs. Thereby, a tumor lesion’s volume is delineated by including all voxels above a fixed uptake threshold, usually expressed as a percentage of the lesion’s maximum voxel value (e.g., 50% of SUVmax). This approach is simple, fast, and reproducible, making it widely used to quantify three SUV metrics: SUVmax (the highest voxel value within the VOI), SUVmean (average activity in the measured volume), and SUVpeak (the activity measured in a one-cubic-centimeter VOI centered on the area with the highest uptake). Furthermore, SUV-based tumor segmentations enable estimation of a patient’s total tumor burden, thereby generating image biomarkers for prognostic assessment, as in patients with lymphoma (Boellaard, Buvat et al. 2024).

Although SUV measurements are common in oncologic PET applications, SUV values can be affected by several factors, including scanner sensitivity and PET data reconstruction settings. For example, because SUVmax is measured in a single voxel, it is highly susceptible to bias from statistical noise in PET image data(Lodge, Chaudhry et al. 2012), which hampers reliable quantification between examinations at different time points and may lead to incorrect clinical interpretations. Because of this characteristic, scanners with high-count sensitivity, and therefore improved count statistics, will provide more accurate measurements of SUVmax.

On the other hand, SUVmean is much less susceptible to noise because it reflects the average activity across a specific population of voxels. Nonetheless, it can be more user-dependent, as it depends on proper VOI delineation that covers the exact tumor area to be assessed(Lucignani 2009).
In the case of SUVpeak, quantification of small lesions may be affected because it reflects the local average around the voxel with the highest uptake(Adams, Turkington et al. 2010). For these reasons, depending on the clinical scenario and PET/CT scanner in question, some SUV metrics may be preferred for clinical use over others.

1.3 Conventional PET/CT imaging with short axial field of view (SAFOV) scanners

Conventional PET/CT systems have a short axial field of view (SAFOV) of typically 16-30 cm(Surti, Pantel et al. 2020). As a result, whole-body scans are performed in multiple step-and-shoot bed positions with partial overlap or by continuous motion of the scanner bed, typically covering from the skull base to the mid-thigh, or extended from the vertex to the toes if clinically needed. The PET/CT exam duration varies depending on the scanner and radiotracer used, typically around 20-45 minutes. Additionally, a low-dose CT is performed for attenuation correction, with an optional contrast-enhanced diagnostic CT scan. These lengthy examination times, along with preparation and uptake periods, typically require a patient to stay about 2-3 hours at a PET/CT center for each exam. This can add to the burden on often severely ill cancer patients, frequently necessitating additional measures such as more pain medication and suitable waiting areas to manage the logistics of this complex procedure. Furthermore, due to the limited axial coverage, dynamic studies that require image acquisition at the beginning of tracer administration are usually restricted to a single bed position or body area.

Since approximately 85 to 90% of the body lies outside the axial FOV (aFOV), these scanners provide volume sensitivities in the range of 6-20 kcps/MBq(Rausch, Mannheim et al. 2022). Consequently, obtaining diagnostic PET images requires high radiotracer activity. For standard adult patients, [^{18}F]FDG protocols administer ~3–5 MBq/kg (typically 200–370 MBq) with a scan time of 2–4 minutes per bed position(Boellaard, Delgado-Bolton et al. 2015). Using the ICRP effective dose coefficient for [^{18}F]FDG (~0.019 mSv/MBq), this corresponds to an effective dose from the PET examination alone of about 7 mSv for a 70 kg adult(Mattsson, Johansson et al. 2015). Depending on the chosen CT protocol, a single PET/CT examination can result in up to 39 mSv of whole-body radiation exposure(Guttikonda, Herts et al. 2014), with the CT scan contributing most of the radiation.

From the PET standpoint, many of these factors and constraints stem from the limited count sensitivity of these SAFOV PET systems, which can be mitigated to some extent by extending the scanner's axial coverage(Vandenberghe, Moskal et al. 2020). This drove the development of long axial field of view (LAFOV) PET/CT systems, which have an aFOV of 70 cm or longer (Schmidt, Mannheim et al. 2023), leading to notable improvements in sensitivity and timing resolution, thereby potentially enabling whole-body dynamic studies, low-dose imaging, multi-tracer examinations, and many other novel applications(Dimitrakopoulou-Strauss, Pan et al. 2023).

1.4 LAFOV PET/CT systems and the Biograph Vision Quadra

Of the commercially available LAFOV PET/CT systems, the Biograph Vision Quadra (Siemens Healthineers, Knoxville, TN, USA) offers an aFOV of 106 cm. According to phantom evaluations performed in accordance with the NEMA NU 2-2018 standard, this scanner provides volume sensitivities of 83.4 kcps/MBq and 176 kcps/MBq for its available sensitivity modes—the high sensitivity mode and the ultra-high sensitivity mode, respectively(Prenosil, Sari et al. 2022). This leads to a considerable increase in count sensitivity, up to 10-fold compared to

its SAFOV predecessor, the Biograph Vision 600, in UHS mode(Prenosil, Hentschel et al. 2022).

A head-to-head comparative study in 44 patients using different radiotracers ([^{18}F]FDG, [^{18}F]PSMA-1007, and [^{68}GA]DOTA-TOC) compared SAFOV PET (16.06 minutes scan time) with LAFOV PET scans with a duration of 0.5, 1.0, 2.0, 6.0, and 10.0 minutes. In this study, 2-minute LAFOV PET images showed comparable signal-to-noise ratios (SNR) and image quality to SAFOV PET datasets, indicating that clinically diagnostic images are achievable with extremely short scan times or, analogously, with a significantly reduced applied tracer dose(Alberts, Hunermund et al. 2021). Clinically, these capabilities have the potential to unlock several exciting PET applications, such as low-dose and ultra-late PET examinations, as well as ultra-fast PET examinations(van Sluis, Borra et al. 2022). Nonetheless, the framework for many of these PET applications remains to be developed and established, marking an exciting era for clinical PET research.

1.5 Hybrid imaging in clinical oncology

The additional molecular information provided by PET imaging has led to the development of systems that integrate PET with morphological modalities such as CT and MRI, resulting in combined PET/CT and PET/MRI scanners. These hybrid systems have become standard in clinical practice, and their use and applications are collectively referred to as hybrid imaging. Across a broad range of oncological diseases, the diagnostic advantages of this approach over conventional imaging alone have established hybrid imaging with various radiotracers as an essential tool in modern oncology.

1.5.1 [^{18}F]FDG PET

Among the available radiotracers for PET imaging, 2-deoxy-2-[^{18}F]fluoroglucose ([^{18}F]FDG) is by far the most commonly used tracer for various clinical scenarios.

After intravenous injection, [^{18}F]FDG distributes throughout the bloodstream and is taken up into cells via glucose transporters (primarily GLUT1 and GLUT3 in tumor cells), competing directly with unlabeled glucose (Mochizuki, Tsukamoto et al. 2001). Once inside the cell, [^{18}F]FDG is phosphorylated by hexokinase to [^{18}F]FDG-6-phosphate, analogous to the first step of glycolysis. However, unlike glucose-6-phosphate, [^{18}F]FDG-6-phosphate is not a substrate for further metabolism. Dephosphorylation by glucose-6-phosphatase is slow and considered irrelevant for clinical imaging, so [^{18}F]FDG-6-phosphate is effectively trapped intracellularly (Pauwels, Ribeiro et al. 1998). This results in radiotracer accumulation in areas of increased glucose metabolism, such as many malignant tumors, inflammatory tissue, and certain organs with physiologically increased glucose consumption (e.g., the brain or myocardium). The resulting “hot spots” can be analyzed visually and semi-quantitatively, enabling the detection and localization of viable tumors in oncological patients.

Through the well-known increased glucose consumption observed in several tumor entities, first described by Warburg et al. and correspondingly referred to as the Warburg Effect(Warburg, Wind et al. 1927), [^{18}F]FDG PET in combination with cross-sectional imaging such as CT or MRI, has become essential for staging, treatment response assessment, and surveillance across a wide range of malignancies, including various lymphomas, lung cancer, melanoma, and colorectal tumors(Petersen, Hess et al. 2014, Forschner, Olthof et al. 2017, Ayati, Sadeghi et al. 2021, Lewis and Trotman 2023, Sathekge, Maes et al. 2025).

In lymphoma, [^{18}F]FDG PET is the standard for initial staging and therapy monitoring in both Hodgkin lymphoma and non-Hodgkin lymphoma (Barrington and Kluge 2017). When combined with conventional imaging such as CT, it improves the detection of nodal and extranodal disease compared with PET or CT alone(Fueger, Yeom et al. 2009). Furthermore, interim and end-of-treatment [^{18}F]FDG PET scans, evaluated using the Deauville 5-point scale, are crucial for assessing response. The Deauville 5-point scale is a visual scoring system used to interpret [^{18}F]FDG PET uptake in lymphoma lesions by comparing lesion

uptake with that of reference tissues, such as the mediastinal blood pool and liver. In the current protocol, scores 1–3 are considered a complete metabolic response, whereas scores 4–5 indicate residual active disease, triggering treatment escalation(Cheson, Fisher et al. 2014, Yoo 2022). For melanoma, [^{18}F]FDG PET is recommended in the European Society of Medical Oncology (ESMO) guidelines for patients with an initial tumor stage of IIB or higher, as well as for therapy response assessment(Amaral, Ottaviano et al. 2025). Compared with CT alone, [^{18}F]FDG PET/CT improves detection of in-transit disease, nodal involvement, and distant metastases, often altering management(Forschner, Olthof et al. 2017). Given these diagnostic benefits across several tumor entities, [^{18}F]FDG has become the most widely used radiotracer in oncology PET imaging.

1.5.2 PSMA-targeted PET in prostate cancer

In addition to [^{18}F]FDG imaging, PET has become a key tool for several other tumor entities by targeting cell membrane proteins that are highly expressed in specific tumor types. In prostate cancer, PET imaging is performed by targeting the prostate-specific membrane antigen(Hofman, Lawrentschuk et al. 2020), a transmembrane protein that is overexpressed in prostate cancer metastases and primary tumors compared to benign tissues(Queisser, Hagedorn et al. 2015).

These ligands are mainly labelled with gallium-68 or fluorine-18, such as [^{68}Ga]Ga-PSMA-11 and [^{18}F]PSMA-1007, and replaced previous tracers used in prostate cancer staging, such as [^{18}F]Fluoroethylcholine, due to improved image quality and diagnostic performance(Afshar-Oromieh, Avtzi et al. 2015, Giesel, Hadaschik et al. 2017). Since its introduction in the first half of the last decade, an increasing body of evidence has shown that PSMA-PET provides improved diagnostic performance compared with conventional imaging techniques such as CT and bone scans, particularly in clinical scenarios such as primary staging in high-risk patients and the evaluation of biochemical recurrence(Hofman, Lawrentschuk et al. 2020, Pozdnyakov, Kulanthaivelu et al. 2023).

1.5.3 Somatostatin-receptor PET in NEN

NENs are a heterogeneous group of tumors that can be subdivided based on cell morphology and proliferation index, that is, into well-differentiated NET and poorly differentiated NEC(Rindi, Mete et al. 2022). Well-differentiated NETs typically exhibit increased somatostatin receptor (SSTR) expression, notably higher expression of the SSTR-2 receptor subtype(Geijer and Breimer 2013, Pavel, Oberg et al. 2020, Leupe, Ahenkorah et al. 2023), making them a suitable target for molecular imaging. Until the mid-2010s, the most widely used molecular imaging technique exploiting the increased SSTR expression in NET was somatostatin receptor scintigraphy, or octreotide scan, using mainly ^{111}In-labelled somatostatin analogues (SSAs)(Squires, Volkan Adsay et al. 2015). Of note, the non-labelled or “cold” variant of SSAs are an essential part of the therapeutic regime for well-differentiated NETs.

Afterward, with the introduction of ^{68}Ga-labelled SSAs suitable for PET imaging, such as [^{68}Ga]DOTA-TATE or [^{68}Ga]DOTA-TOC, the octreotide scan was replaced because of the notably improved diagnostic performance. In a study comparing [^{68}Ga]DOTA-TATE PET/CT, multiphasic CT scans, and the octreotide scan in GEP-NET and CUP-NET, lesion detection rates of 95.1%, 45.3%, and 30.9%, respectively, were reported(Sadowski, Neychev et al. 2016). These significant improvements led to FDA approval in June 2016 for the localization of SSTR-positive NETs in adult and pediatric patients. In Europe, [^{68}Ga]DOTA-TOC received EMA market approval in December 2016 for SSTR-PET imaging in patients with confirmed or suspected well-differentiated GEP-NET to localize primary tumors and metastases. Since then, SSAs labelled with fluorine-18 and copper-64, such as [^{18F}]SiTATE and [^{64}Cu]DOTA-TATE, have also become viable tracer alternatives for PET imaging in well-differentiated, SSTR-positive NET patients(Delpassand, Ranganathan et al. 2020, Beyer, Gosewisch et al. 2021).

1.6 Theranostic approaches

Theranostics is a two-step approach that integrates diagnostic imaging with targeted therapies. A ligand specific to a tumor-associated target, e.g., a membrane protein, is first labeled with an imaging radionuclide (such as fluorine-18) to confirm target expression and tumor burden. The same ligand is then labeled with a therapeutic radionuclide, usually one with β^- decay (typically lutetium-177), to deliver radiation doses capable of producing a therapeutic effect. Subsequent scans are used to assess response.

For prostate cancer, PSMA-PET is used to assess sufficient target expression to consider treatment with ^{177}Lu-labelled PSMA ligands (e.g., [^{177}Lu]Lu-PSMA-617), known as radioligand therapy (RLT) (Olivier, Powell et al. 2023). In NEN, SSTR-PET helps select candidates for peptide receptor radionuclide therapy (PRRT), which is commonly performed with [^{177}Lu]Lu-DOTA-TATE(Strosberg, Caplin et al. 2021). In both settings, variations in tracer uptake across lesions have prognostic relevance and may indicate when alternative systemic or locoregional strategies should be preferred if target expression is insufficient for effective radioligand delivery. As of today, these therapeutic approaches have become a staple in nuclear medicine and have significantly contributed to the specialty's growth by substantially expanding its therapeutic repertoire.

Nonetheless, it is often debated whether these targeted imaging approaches provide sufficient information for selecting patients before radionuclide therapy, with some authors recommending multi-parametric imaging using other radiotracers that are not routinely used for prostate cancer or NEN, such as [^{18}F]FDG(Alevroudis, Spei et al. 2021, Hofman, Emmett et al. 2024). However, a second PET examination typically requires an additional patient visit to a PET center, which, for many logistical reasons, has hampered the clinical implementation of such approaches. However, this problem can be potentially solved by the capabilities of LAFOV PET/CT scanners.

1.7 Promising novel oncology applications with LAFOV PET/CT scanners: low-dose imaging

Some studies have systemically examined clinically feasible low-dose PET protocols, mainly using [^{18}F]FDG, thereby evaluating optimal scan time, lesion detectability, and image quality on LAFOV PET/CT systems. In the case of the Biograph Vision Quadra, a study evaluating 45 melanoma patients showed that a dose reduction to 2.0 MBq/kg with a scan time of 5 minutes provides diagnostic quality comparable to standard acquisition times(Sachpekidis, Pan et al. 2023). Investigations on the uEXPLORER, another commercially available LAFOV PET/CT scanner with an aFOV of 194 cm(Spencer, Berg et al. 2021), have shown that injected activities can be reduced to 1.85 MBq/kg or even below 1.0 MBq/kg if acquisition times of 10–15 min are used, while maintaining adequate lesion detectability(Tan, Sui et al. 2021, He, Gu et al. 2022). In these studies, image evaluation typically combines subjective visual assessment using point scales for overall image quality, objective noise evaluations assessing SNRs, and lesion detectability. To evaluate the influence of reduced activity doses in semi-quantification, the SUVmean, SUVpeak, and SUVmax of tumor lesions and of reference organs were assessed.

Nevertheless, several questions remain insufficiently answered from the perspective of routine oncologic imaging. Many published low-dose studies have focused on specific tumor entities or used extended acquisition times, thereby losing one of the main benefits of LAFOV PET/CT scanners: shorter scan times. Furthermore, studies evaluating the Biograph Vision Quadra have not systematically examined the advantages of recently introduced advanced sensitivity settings (e.g., HS vs UHS) in achieving significant reductions in activity, nor the extent to which the increased sensitivity of LAFOV scanners can compensate for low-count conditions. From a practical viewpoint, there is a need to define realistic working ranges for injected [^{18}F]FDG activity and acquisition times that preserve diagnostic confidence and quantitative reliability while offering a meaningful reduction in radiation dose and shorter examination times.

Answering these questions requires carefully designed studies in clinical cohorts that reflect everyday oncologic practice, with stepwise reductions in activity, consistent reconstruction settings, and standardized evaluation of both subjective and objective metrics. Such work will form the basis for developing practical, implementable low-dose protocols compatible with existing guidelines and adoptable across different centers.

1.8 Proposed one-day dual-tracer PET examinations

A potential benefit of low-dose PET examinations is not only reduced radiation exposure but also the possibility of performing one-day PET examinations in cohorts that may benefit from dual-tracer PET assessments, such as patients with prostate cancer and NEN. The rationale for combining standard receptor-targeted PET imaging with PSMA- or SSTR-targeting tracers and [^{18}F]FDG PET is to integrate information on differentiation status and glycolytic activity, both of which are related to tumor aggressiveness(Alevroudis, Spei et al. 2021, Hofman, Emmett et al. 2024).

As previously described, well-differentiated NETs typically overexpress SSTRs, which provides the biological basis for theranostic approaches. International guidelines from ESMO and the European Neuroendocrine Tumor Society (ENETS) recommend SSTR-PET/CT for primary staging, candidate selection for PRRT, and response assessment in well-differentiated NENs(Sundin, Arnold et al. 2017, Pavel, Oberg et al. 2020). Most clinical experience is available for ^{68}Ga-labeled SSAs, DOTA-peptides such as [^{68}Ga]Ga-DOTA-TATE, [^{68}Ga]Ga-DOTA-TOC, and [^{68}Ga]Ga-DOTA-NOC(Geijer and Breimer 2013). Furthermore, while the recently introduced ^{18}F-labeled SSAs, including [^{18}F]SiTATE, offer higher production yields, a longer half-life, and favorable imaging characteristics, they require further clinical evaluation (Lindner, Wangler et al. 2020, Beyer, Gosewisch et al. 2021).

On the other hand, poorly differentiated NECs and many grade 3 NETs often exhibit more aggressive behavior and lower or heterogeneous SSTR expression. In these entities, [^{18}F]FDG PET/CT has emerged as a significant prognostic tool, correlating increased glucose metabolism with shorter progression-free and overall survival(Binderup, Knigge et al. 2010, Chan, Bernard et al. 2020), and can reveal lesions by displaying mismatched [^{18}F]FDG-positive, SSTR-negative lesions, with significant implications for SSTR-targeted therapies.

As a consequence, combined imaging with SSTR-PET and [^{18}F]FDG PET has been advocated, particularly for high-grade or clinically aggressive NEN(Ambrosini, Caplin et al. 2024). Dual-tracer approaches are considered to provide more refined characterization of intra-patient tumor heterogeneity, help identify discordant lesions, and improve risk stratification beyond what either modality alone can achieve. Furthermore, combined evaluation with SSTR-PET and [^{18}F]FDG PET has been shown to influence therapy stratification for PRRT, systemic chemotherapy, and loco-regional interventions(Chan, Pavlakis et al. 2017). In routine practice, dual-tracer PET/CT is usually performed as two separate examinations on different days. This separation prevents tracer overlap and maintains accurate semi-quantification. However, it increases logistical challenges for both patients and imaging centers, lengthens the diagnostic work-up, and can delay treatment for rapidly progressing diseases. For these reasons, implementing dual-tracer PET exams in clinical practice has been challenging.

Few groups have already explored dual-tracer PET protocols within a single imaging session. In these protocols, imaging of each tracer is performed sequentially with no meaningful time gap between scans. For example, a study by Alberts et al. evaluated the feasibility of a single-session dual-tracer PET in an LAFOV PET/CT scanner using [^{68}Ga]Ga-PSMA-11 and [^{18}F]FDG in prostate cancer patients being considered for radioligand therapy(Alberts, Schepers et al. 2023). In this study, PSMA-PET was performed with a standard tracer activity of 150 MBq of [^{68}Ga]Ga-PSMA-11 after a 1-hour uptake time. After completion of the first scan, a fixed 40 MBq dose of [^{18}F]FDG was administered, and PET

acquisition was performed 1 hour p.i. (scan time 15 minutes). Of the 14 examined patients, one patient showed lesions with low or missing PSMA expression but increased [^{18}F]FDG avidity. However, due to the short intervals between tracer injections and PET acquisition, the independent semi-quantification of each tracer was not feasible, including SUV-based evaluation of the entire [^{18}F]FDG-avid tumor burden. Thus, existing single-session dual-tracer protocols mainly serve to identify discordant lesions rather than to provide two independent, quantitatively robust PET datasets.

LAFOV PET/CT scanners could provide a practical and elegant solution to this problem. The key concept is to exploit the increased sensitivity of these scanners to reduce the injected activity of the first applied radiotracer, thereby preserving diagnostic performance. After an appropriate waiting period, the first tracer has decayed to a small fraction of its initial activity, so that a second tracer administered at standard activity can be imaged with minimal to no interference from residual activity of the first tracer. For dual-tracer protocols involving two ^{18}F-labeled tracers, such as [^{18}F]FDG and an [^{18}F]SiTATE, this approach is desirable. From a technical perspective, two key conditions must be met for a one-day dual-tracer protocol to be viable. First, the low-activity [^{18}F]FDG scan must provide sufficient image quality and quantitative reliability for clinical interpretation. This requirement depends on the LAFOV PET system's sensitivity, acquisition duration, and reconstruction settings. Second, residual [^{18}F]FDG activity at the time of the SSTR-PET scan must not distort lesion classification or SUV-based semi-quantitative parameters.

Clinically, a one-day low-dose [^{18}F]FDG plus standard-dose SSTR-PET protocol on an LAFOV PET/CT scanner could reduce patient visits and compress the diagnostic work-up, which is relevant for patients with aggressive NEN who often face complex treatment decisions. At the same time, such a protocol aligns with the broader trend toward multiparametric imaging, in which different radiotracers are combined to provide a more comprehensive description of tumor biology within a single clinical workflow. Despite these potential advantages, the concept

still requires systematic evaluation. Open questions include determining the optimal reduction in injected activities, acquisition times, and injection intervals; assessing the effects of residual tracer activity; and evaluating the extent to which dual-tracer information obtained in a one-day LAFOV protocol alters treatment decisions in NEN patients.

1.9 Hypotheses

Existing dual-tracer PET studies have primarily been performed on SAFOV PET/CT systems and have usually employed standard activities for both tracers with examinations on separate days. Data on one-day dual-tracer protocols with ^{18}F-labelled radiotracers on LAFOV PET/CT remain limited, and their technical feasibility and clinical utility need further exploration.

Therefore, this cumulative dissertation aimed to explore how the increased sensitivity of LAFOV PET/CT could be used to develop practical low-dose [^{18}F]FDG PET protocols and to translate these protocols into feasible one-day dual-tracer PET examinations. The work aimed to define the qualitative and quantitative boundaries of low-dose [^{18}F]FDG PET/CT by evaluating image quality, lesion detectability, and the influence on semi-quantitative parameters under different simulated reduced-activity levels across both sensitivity modes of the Biograph Vision Quadra. After the selection of an optimal low-dose [^{18}F]FDG PET protocol, the feasibility of a one-day dual-tracer examination in patients with NEN using an [^{18}F]FDG and [^{18}F]SiTATE was explored, thereby evaluating [^{18}F]FDG activity by assessing organs with physiologically increased glucose consumption and [^{18}F] FDG-avid tumor lesions as well as the clinical impact of this approach in patient management.

2. Results and Discussion

2.1 Research Article: "Image Quality and Quantitative PET Parameters of Low-Dose [^{18}F]FDG PET in a Long Axial Field-of-View PET/CT Scanner"

Authors: Eduardo Calderón, Fabian P. Schmidt, Wenhong Lan, Salvador Castaneda-Vega, Andreas S. Brendlin, Nils F. Trautwein, Helmut Dittmann, Christian la Fougère, Lena S. Kiefer.

Published in: Diagnostics (Basel), **Volume:** 13**, Article Number:** 20**, Year:** 2023

diagnostics

MDPI

Article

Image Quality and Quantitative PET Parameters of Low-Dose [^{18}F]FDG PET in a Long Axial Field-of-View PET/CT Scanner

Eduardo Calderón [1], Fabian P. Schmidt [1,2], Wenhong Lan [1], Salvador Castaneda-Vega [1,2], Andreas S. Brendlin [3], Nils F. Trautwein [1], Helmut Dittmann [1], Christian la Fougère [1,4,5] and Lena Sophie Kiefer [1,*]

1 Department of Nuclear Medicine and Clinical Molecular Imaging, University Hospital Tuebingen, 72076 Tuebingen, Germany; eduardo.calderon-ochoa@med.uni-tuebingen.de (E.C.); f.schmidt@med.uni-tuebingen.de (F.P.S.); wenhong.lan@med.uni-tuebingen.de (W.L.); salvador.castaneda@med.uni-tuebingen.de (S.C.-V.); nils.trautwein@med.uni-tuebingen.de (N.F.T.); helmut.dittmann@med.uni-tuebingen.de (H.D.); christian.lafougere@med.uni-tuebingen.de (C.l.F.)
2 Werner Siemens Imaging Center, Department of Preclinical Imaging and Radiopharmacy, Eberhard-Karls University Tuebingen, 72076 Tuebingen, Germany
3 Department of Diagnostic and Interventional Radiology, University Hospital Tuebingen, 72076 Tuebingen, Germany; andreas.brendlin@med.uni-tuebingen.de
4 Cluster of Excellence iFIT (EXC 2180) "Image Guided and Functionally Instructed Tumor Therapies", University of Tuebingen, 72074 Tuebingen, Germany
5 German Cancer Consortium (DKTK), Partner Site Tuebingen, 72074 Tuebingen, Germany
* Correspondence: lena.kiefer@med.uni-tuebingen.de

Abstract: PET/CT scanners with a long axial field-of-view (LAFOV) provide increased sensitivity, enabling the adjustment of imaging parameters by reducing the injected activity or shortening the acquisition time. This study aimed to evaluate the limitations of reduced [^{18}F]FDG activity doses on image quality, lesion detectability, and the quantification of lesion uptake in the Biograph Vision Quadra, as well as to assess the benefits of the recently introduced ultra-high sensitivity mode in a clinical setting. A number of 26 patients who underwent [^{18}F]FDG-PET/CT (3.0 MBq/kg, 5 min scan time) were included in this analysis. The PET raw data was rebinned for shorter frame durations to simulate 5 min scans with lower activities in the high sensitivity (HS) and ultra-high sensitivity (UHS) modes. Image quality, noise, and lesion detectability (n = 82) were assessed using a 5-point Likert scale. The coefficient of variation (CoV), signal-to-noise ratio (SNR), tumor-to-background ratio (TBR), and standardized uptake values (SUV) including SUV_{mean}, SUV_{max}, and SUV_{peak} were evaluated. Subjective image ratings were generally superior in UHS compared to the HS mode. At 0.5 MBq/kg, lesion detectability decreased to 95% (HS) and to 98% (UHS). SNR was comparable at 1.0 MBq/kg in HS (5.7 $\pm$ 0.6) and 0.5 MBq/kg in UHS (5.5 $\pm$ 0.5). With lower doses, there were negligible reductions in SUV_{mean} and SUV_{peak}, whereas SUV_{max} increased steadily. Reducing the [^{18}F]FDG activity to 1.0 MBq/kg (HS/UHS) in a LAFOV PET/CT provides diagnostic image quality without statistically significant changes in the uptake parameters. The UHS mode improves image quality, noise, and lesion detectability compared to the HS mode.

Keywords: total-body PET/CT scanner; LAFOV PET/CT; low-dose [^{18}F]FDG PET; [^{18}F]FDG

Citation: Calderón, E.; Schmidt, F.P.; Lan, W.; Castaneda-Vega, S.; Brendlin, A.S.; Trautwein, N.F.; Dittmann, H.; la Fougère, C.; Kiefer, L.S. Image Quality and Quantitative PET Parameters of Low-Dose [^{18}F]FDG PET in a Long Axial Field-of-View PET/CT Scanner. *Diagnostics* **2023**, *13*, 3240. https://doi.org/10.3390/diagnostics13203240

Academic Editors: Andor W.J.M. Glaudemans, Riemer H.J.A. Slart and Joyce van Sluis

Received: 29 September 2023
Revised: 15 October 2023
Accepted: 15 October 2023
Published: 18 October 2023

1. Introduction

Positron emission tomography and computed tomography (PET/CT) hybrid imaging plays a fundamental role in current medical practice. Thereby, [^{18}F]fluoro-deoxy-glucose (FDG) PET/CT has become an essential pillar in the diagnosis and follow-up of various oncological diseases, such as lymphoma, melanoma, and lung cancer [1–3]. Recent advances in the field of PET/CT technology have led to the introduction of PET/CT scanners with a long axial field-of-view (LAFOV), enabling the improvement of existing clinical

applications and the establishment of new ones [4,5]. The extended axial field-of-view (aFOV) of these scanners, ranging between 64 to 200 cm, increases solid angle coverage for the detection of coincident events, providing a higher sensitivity and relevant improvements in the signal-to-noise ratio (SNR) compared to conventional PET scanners with a short axial field-of-view (SAFOV) [6,7]. Notably, the improved sensitivity is advantageous for examinations with low event statistics, such as PET imaging with radioisotopes that have low branching ratios such as Y-90 [8,9], allowing for post-therapeutic PET scans after trans-arterial radioembolization with Y-90 microspheres; immuno-PET imaging with long half-life radioisotopes such as Zr-89 [10,11], which allows the improved in vivo characterization of various tumors such as HER2-positive breast cancer [12]; and examinations with reduced doses of injected activity, contributing to a reduction in radiation exposure [13,14].

Conventional PET/CT scanners with a SAFOV of approximately 20 to 25 cm typically have a sensitivity in the range of 6 to 20 cps/kBq [15]. In these scanners, roughly 85 to 90% of the body is located outside the aFOV, and only around 3 to 5% of the available signal within the FOV can be used [16]. In contrast, the Biograph Vision Quadra PET/CT scanner (Siemens Healthineers, Knoxville, TN, USA) provides an aFOV of 106 cm and a sensitivity of 83 cps/kBq using its standard high-sensitivity (HS) mode with an acceptance angle of 18°. Compared to its predecessor model with a SAFOV (Biograph Vision 600), the Biograph Vision Quadra features an approximately fivefold sensitivity increase [17].

The ultra-high sensitivity (UHS) mode, representing the latest sensitivity mode for the Biograph Vision Quadra, allows for the unlimited acceptance angle of 52°, further improving the sensitivity to 176 cps/kBq [18]. This improvement translates into an approximately two-fold increase in sensitivity compared to the standard HS mode [19]. This enables a further reduction in acquisition time while maintaining the noise performance and might also provide advantages for the low-dose examination protocols while maintaining diagnostic reliability. Despite these encouraging results, the standardization of short acquisition time and low-dose protocols in clinical routine remains to be achieved. Specifically, to the best of our knowledge, no studies have yet been published systematically evaluating the limits of the reduction in injected activity regarding the qualitative and quantitative image parameters in the [^{18}F]FDG PET/CT of oncological patients on the Biograph Vision Quadra system. Therefore, this study aimed to assess the impact of reduced [^{18}F]FDG activity doses on image quality and noise, lesion detectability, and uptake quantification while comparing the HS and UHS modes in the Siemens Biograph Vision Quadra LAFOV PET/CT scanner.

2. Materials and Methods

2.1. Study Design and Patient Population

Twenty-six patients who underwent a whole-body [^{18}F]FDG PET/CT on a Biograph Vision Quadra PET/CT scanner were included in this retrospective analysis. PET/CT examinations were clinically indicated for oncological purposes. Different tumor entities were included in this analysis (e.g., melanoma, lymphoma, lung cancer, esophageal cancer, colon cancer, rectal and anal cancer, and a cancer of unknown primary). Detailed patient characteristics are provided in Supplementary Table S1.

2.2. Imaging Protocol

Patients were required to fast for at least 10 h prior to the examination. A venous blood glucose measurement was conducted to confirm the blood glucose levels <130 mg/dL. A clinical standard dose of 3.0 MBq/kg [^{18}F]FDG was injected intravenously, and PET/CT image acquisition was started at 60 min. p.i.. Whole-body scans were acquired in a supine position covering an area from the head to the mid-thighs. Technical details of the CT image acquisition and protocol are provided in Supplementary Table S2. The PET emission data with a routine acquisition time of 5 min were acquired directly after the CT scan.

2.3. Image Reconstruction

PET image reconstruction was performed using the proprietary e7 tools software (Version VR20, Siemens Healthineers, Knoxville, TN, USA). According to our standard clinical reconstruction protocol, an Ordinary-Poisson Ordered-Subsets Expectation-Maximization algorithm with four iterations and five subsets (OP-OSEM 4i5s) was applied, using point-spread-function (PSF) modeling and time-of-flight (TOF) information. The PET images were reconstructed with a matrix of 440 × 440 × 645 with a 1.65 × 1.65 × 1.65 mm^3 isotropic voxel size, and no image filter was applied. Attenuation correction was performed based on the diagnostic CT scan acquired before the emission measurements. All reconstructions were performed for both the HS and the UHS modes. The PET raw data (5 min scan, 3.0 MBq/kg) was consecutively rebinned for shorter frame durations to simulate lower activities of injected [^{18}F]FDG as follows: 1.0 MBq/kg, 0.5 MBq/kg, 0.25 MBq/kg, and 0.125 MBq/kg. An example of a data set reconstructed with the different simulated doses and both sensitivity modes is shown in Figure 1.

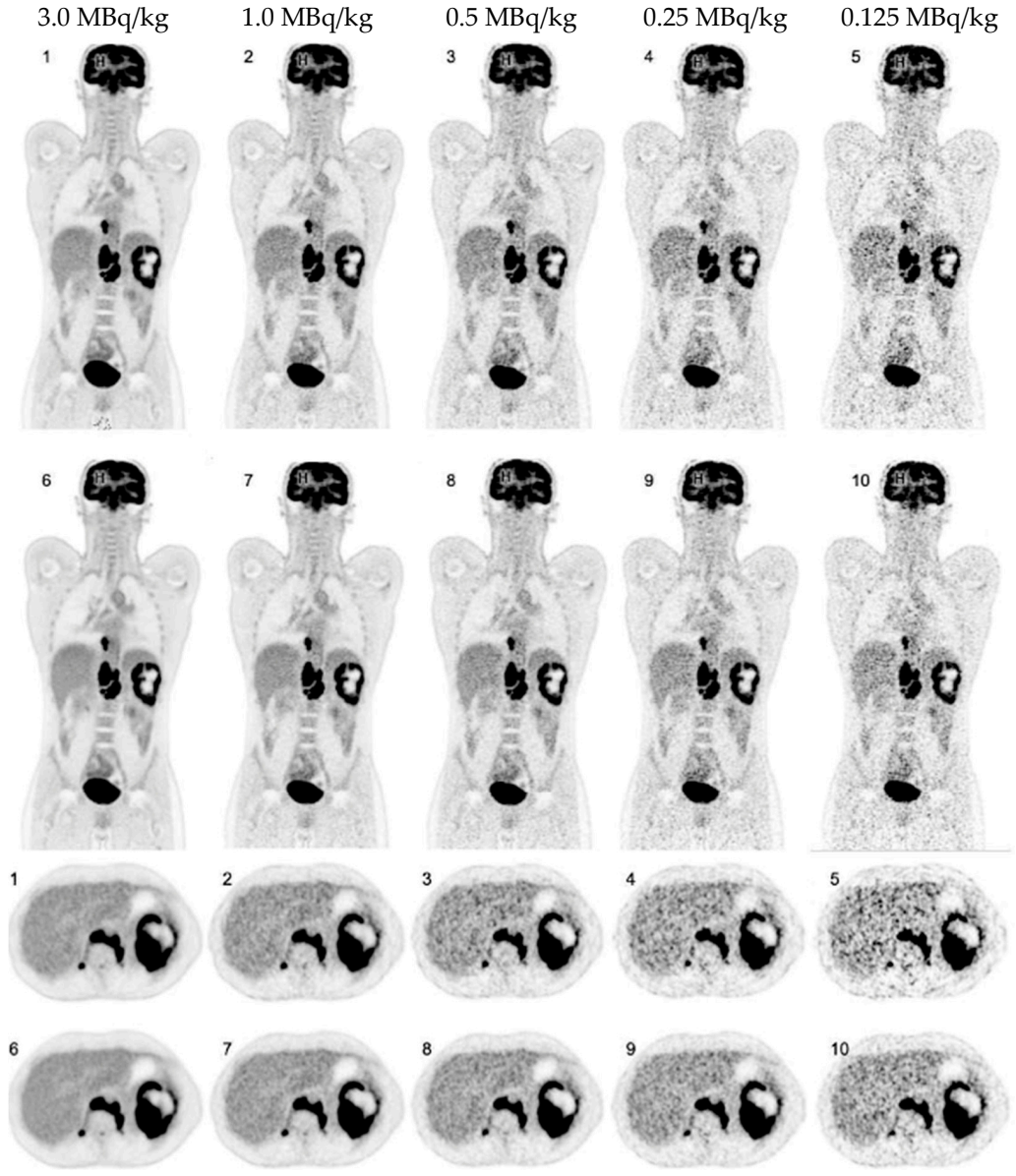

Figure 1. Coronal and axial [^{18}F]FDG PET images of a 37-year-old patient with Hodgkin lymphoma reconstructed in high-sensitivity (1–5) and ultra-high sensitivity (6–10) mode.

2.4. Image Analysis and Evaluation

Image analysis and evaluation were performed on a dedicated workstation using the SyngoVia® software (Version 2.3.1, Siemens Healthineers; Knoxville, TN, USA) by two experienced resident nuclear medicine physicians (one being a board-certified radiology physician, both with multi-year experience in the reading of oncological PET/CT scans) in consensus. Both readers were blinded to the patient demographics and clinical information. Scans were read in multiple sessions in a randomized order. Afterward, all reconstructions per patient were re-read simultaneously to analyze the lesion uptake. In patients with a multifocal disease, a maximum of five lesions per patient were analyzed to reduce over-representation.

2.5. Subjective PET Image Quality

Subjective overall impression of image quality, subjective image noise, and conspicuity of suspected pathological lesions were assessed using a 5-point Likert scale. The criteria for the Likert scoring system are provided in Table 1.

Table 1. 5-Point Likert scoring system for subjective PET image rating.

Score	Image Quality	Lesion Conspicuity	Image Noise
5	state-of-the-art quality	well-defined	near-imperceptible noise
4	superior to the average	fairly defined	lower than regular image of daily practice
3	regular quality of daily practice	hazy, recognizable	similar to regular image of daily practice
2	barely diagnostic	ill-defined, impairing diagnostic confidence	increased noise, slightly worse than regular image of daily practice
1	non-diagnostic	un-recognizable	excessive noise

2.6. Quantitative PET Analyses

Target lesion uptake was determined by placing a 40% isocontour volume of interest (VOI) around the lesion. Thereby, the mean, peak, and maximum standardized uptake values (SUV_{mean}, SUV_{peak}, and SUV_{max}) were evaluated. As previously described, the liver was chosen to measure the background activity [20]. Background uptake was determined using a 14 cm^3 VOI in the healthy tissue of the right liver lobe. Target lesions were manually segmented in the standard scan (3.0 MBq/kg, 5 min., HS mode). Afterwards, corresponding VOIs were automatically overlayed onto the simulated scans, ensuring that the placement of the respective VOIs was identical in all data sets.

The tumor-to-background ratio (TBR) was calculated as an estimate for the objective lesion contrast and lesion visibility as previously described [6], utilizing Equation (1):

$$\mathrm{TBR} = \frac{\mathrm{SUVpeakLesion}}{\mathrm{SUVmeanBackground}} \quad (1)$$

Furthermore, to quantitatively assess image noise, the coefficient of variation (CoV) was calculated using Equation (2) as previously published [21]:

$$\mathrm{CoV} = \frac{\mathrm{SUVSD}}{\mathrm{SUVmean}} \quad (2)$$

A CoV of <15% (as a recommended threshold by the EFOMP and EANM [22]) was considered for interpretation. According to [19], the SNR was defined as the reciprocal variable of (CoV) for the liver background. To account for physiological uptake differences between patients, the measured SUV from the different simulations was normalized to the

corresponding SUV derived from the standard scan (3.0 MBq/kg, 5 min., HS mode). Subsequently, the normalized mean SUV values and standard deviations (SD) were determined.

2.7. Radiation Exposure

The effective radiation dose of the simulated examinations was calculated using the conversion factor of 0.019 mSv/MBq, as proposed by the International Commission on Radiological Protection publication 106 [23].

2.8. Statistical Analysis

Two-way ANOVA was performed to analyze the effect of the simulated reduced dose and sensitivity modes on the uptake values and SNR. Bonferroni's multiple comparison tests were used to point out specific statistical significances following two-way ANOVA. The results of the two-way ANOVA are shown with *p*-values. An alpha level of 0.05 and a confidence interval of 95% were used for analysis. Corresponding degrees of freedom (df), F-values (F), and the results of multiple comparison tests are provided in Supplementary Tables S3 and S4. p values < 0.05 were considered statistically significant. Statistical analysis was performed using GraphPad Prism (Version 9.4.1, GraphPad Software, San Diego, CA, USA).

3. Results

3.1. Overall PET Image Quality

The standard clinical scans with a dose of 3.0 MBq/kg in the HS mode were subjectively rated with a mean Likert score of 4.0 ± 0.4 (superior to the average quality). The reconstructed images with a dose reduction to 1.0, 0.5, 0.25, and 0.125 MBq/kg in the HS mode were subsequently rated with mean Likert scores of 3.1 ± 0.3, 2.0 ± 0.3, 1.0 ± 0.2, and 1.0 ± 0.0, respectively.

As shown in Figure 2A, the subjective image quality of image reconstructions in the UHS mode was generally rated superior compared to the images in HS mode. At full doses of 3.0 MBq/kg in the UHS mode, image quality was rated best, corresponding to "state-of-the-art quality" (Likert score 5.0 ± 0.0). The reconstructed images with the UHS mode received a Likert score of 4.1 ± 0.3 and 2.9 ± 0.3 for 1.0 and 0.5 MBq/kg, respectively, as well as 1.9 ± 0.3 and 1.1 ± 0.3 for 0.25 and 0.125 MBq/kg, respectively. However, the images at very low doses of 0.125 MBq/kg were not better rated as the images in the HS mode.

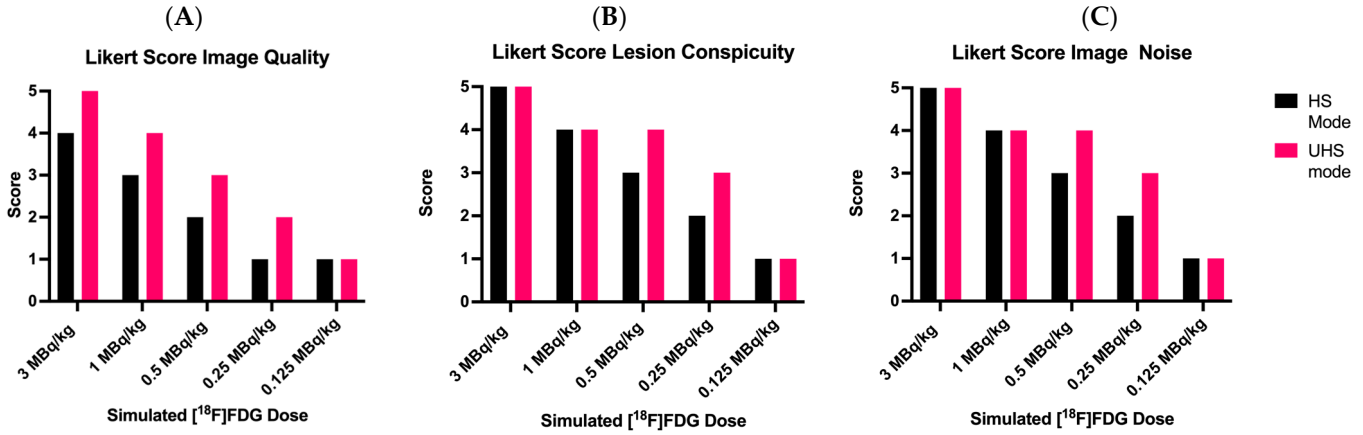

Figure 2. Results of subjective PET image quality ratings. (**A**): Overall Image Quality; (**B**): Lesion Conspicuity; and (**C**): Image Noise. UHS: ultra-high sensitivity; HS: high sensitivity.

3.2. Detectability and Conspicuity of Suspected Pathological Lesions

In total, 82 lesions were selected in the standard reference scan with 3.0 MBq/kg in the HS mode and were considered for further analysis. Lesion detectability was not affected

by the sensitivity modes in dose reductions down to 1.0 MBq/kg. The lesion detection rate decreased to 95%, 71%, and 49% (HS) and 98%, 83%, and 60% (UHS) for 0.5 MBq/kg, 0.25 MBq/kg, and 0.125 MBq/kg, respectively. The results of lesion detection rates for each simulated dose and sensitivity mode with the number of detected lesions are shown in Table 2.

Table 2. Lesion detection rate according to simulated dose and sensitivity mode.

[^{18}F]FDG MBq/kg	Sensitivity Mode	Number of Lesions Detected	Lesion Detection Rate in %
3.0	UHS	82	100%
3.0	HS	82	100%
1.0	UHS	82	100%
1.0	HS	82	100%
0.5	UHS	80	98%
0.5	HS	78	95%
0.25	UHS	68	83%
0.25	HS	58	71%
0.125	UHS	49	60%
0.125	HS	40	49%

UHS: ultra-high sensitivity; HS: high sensitivity.

Concerning subjective lesion conspicuity, all lesions were rated as "well-defined" at 1.0 MBq/kg with no notable different scoring between the HS and UHS mode (Likert score HS 3.8 ± 0.4 and UHS 4.1 ± 0.3), as shown in Figure 2B. At 0.5 MBq/kg in the HS mode, the lesions were "hazy but recognizable" (Likert score 3.0 ± 0.2). For 0.25 MBq/Kg in the HS mode, the lesions were considered "ill-defined, significantly impairing diagnostic confidence" (Likert score 2.0 ± 0.5). PET image reconstructions in the UHS mode at 0.5 MBq/Kg (Likert score 3.9 ± 0.3) and 0.25 MBq/kg (Likert score HS 3.2 ± 0.4) improved the lesion conspicuity. However, at the lowest simulated dose of 0.125 MBq/kg, the lesions were rated as mostly "unrecognizable" (Likert score HS 1.0 ± 0.0 and UHS 1.1 ± 0.3), independent of the sensitivity mode.

Regarding lesion morphology in the CT scan, the mean size of every undetected lesion was 1.5 ± 0.57 cm and comprised almost exclusively of small lymph nodes with a low to moderate [^{18}F]FDG uptake (SUV_{mean} 4.7 ± 2.8). An example of a lesion being undetected in reconstructions with lower doses is provided in Figure 3.

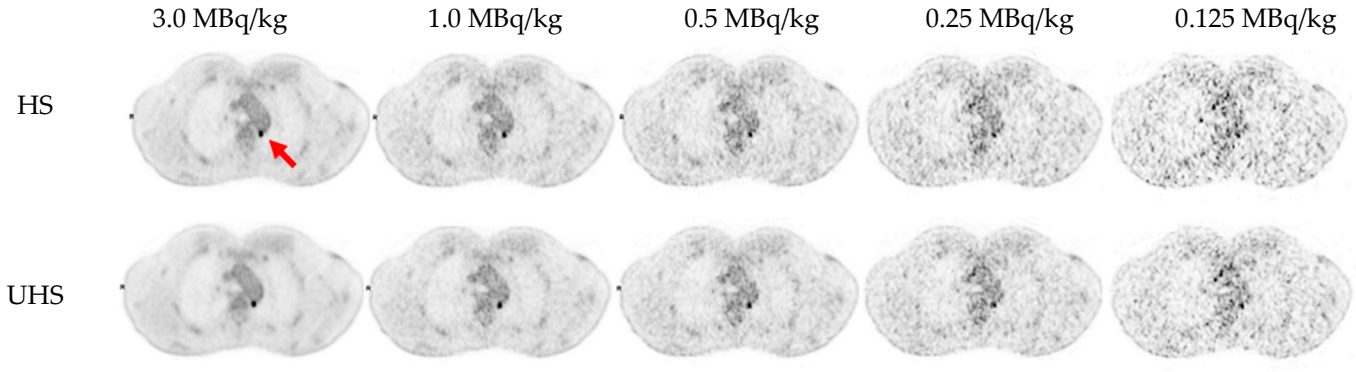

Figure 3. Example of a small retro-aortic lymph node (red arrow, 7 × 6 mm^2) undetected in reconstructions with lower doses (0.25 MBq/kg in HS mode and 0.125 MBq/kg in both HS and UHS mode). UHS: ultra-high sensitivity; HS: high sensitivity.

3.3. Image Noise

Regarding subjective image noise ratings according to the Likert score (Figure 2C), the standard clinical images (3.0 MBq/kg, both in the HS and UHS mode) were considered

to show a "near imperceptible noise", corresponding to a Likert score of 5. Subjective image noise Likert scores of 4.8 ± 0.4, 4.0 ± 0.3, 3.0 ± 0.3, 2.1 ± 0.3, and 1.0 ± 0.2 (HS) and 5.0 ± 0.0, 4.3 ± 0.5, 4.0 ± 0.2, 3.2 ± 0.4, and 1.2 ± 0.4 (UHS) corresponded to 3.0, 1.0, 0.5, 0.25, and 0.125 MBq/kg, respectively.

At 1.0 MBq/kg in the HS mode, a mean CoV of 17.9 ± 2.0% was recorded, slightly surpassing the recommended CoV < 15.0% threshold. The mean CoV in the HS mode for 0.5 MBq/kg, 0.25 MBq/kg, and 0.125 MBq/Kg were 25.3 ± 2.6%, 35.5 ± 4.0%, and 49.0 ± 6.3%, respectively. For the UHS mode, the CoV was always lower; therefore, the same image noise could be obtained for UHS as for HS for lower doses, e.g., a CoV of 18.3% ± 1.8% (0.5 MBq/kg, UHS), which is comparable to 17.9 ± 2.0% with 1.0 MBq/kg in the HS mode. All mean values and standard deviations (SD) of the CoV and SNR measurements are provided in Table 3.

Table 3. Coefficient of Variation and signal-to-noise ratio mean values according to simulated dose and sensitivity mode.

[^{18}F]FDG MBq/kg	Sensitivity Mode	Mean CoV and STD in %	Mean SNR and STD
3.0	UHS	7.9 ± 1.0	12.8 ± 1.6
3.0	HS	10.4 ± 1.2	9.7 ± 1.1
1.0	UHS	13.0 ± 1.3	7.8 ± 0.8
1.0	HS	17.9 ± 2.0	5.7 ± 0.6
0.5	UHS	18.3 ± 1.8	5.5 ± 0.5
0.5	HS	25.3 ± 2.6	4.0 ± 0.4
0.25	UHS	26.0 ± 3.3	3.9 ± 0.5
0.25	HS	35.5 ± 4.0	2.9 ± 0.3
0.125	UHS	35.7 ± 4.5	2.9 ± 0.4
0.125	HS	49.0 ± 6.3	2.1 ± 0.3

UHS: ultra-high sensitivity; HS: high sensitivity; CoV: coefficient of variation; STD: standard deviation; SNR: signal-to-noise ratio.

Two-way ANOVA on the SNR values revealed a statistically significant interaction between the effects of the sensitivity mode and simulated dose reduction ($p < 0.0001$). Furthermore, the results of the main effects showed that, in general, the sensitivity mode and simulated dose reduction independently have a statistically significant effect on the SNR values ($p < 0.0001$ for each main effect).

The Post-hoc multiple comparison test revealed that the mean values of SNR were significantly different between almost every simulated dose and sensitivity mode. This was, however, not the case between the reconstructions in the HS mode and the reconstructions in the UHS mode with half the simulated dose (e.g., 1.0 MBq/kg HS mode vs. 0.5 MBq/kg UHS mode, $p > 0.99$), as shown in Figure 4. Furthermore, a mean SNR UHS/HS ratio of all reconstructed images of 1.36 ± 0.02 was reported.

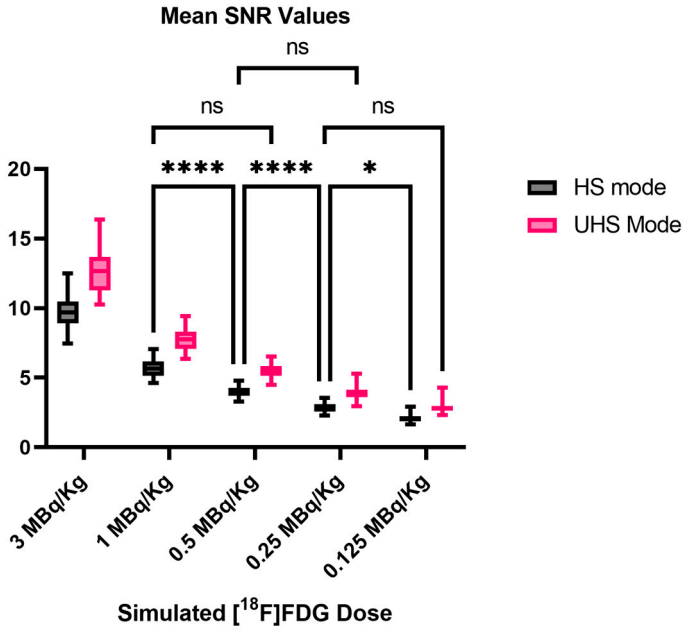

Figure 4. Mean SNR values of liver background according to simulated dose and sensitivity mode. SNR values were statistically significantly different between almost all reconstructed images. Dose reduction and sensitivity mode had relevant effects on SNR values. However, in UHS images, SNR was not statistically significantly different to values in HS images but with twice the dose (e.g., 0.5 MBq/kg UHS vs. 1.0 MBq/kg HS). Each boxplot shows the median value (central line) and the 25–75th percentiles. Whiskers represent the minimum and maximum values. Two-way ANOVA was performed for statistical analysis followed by Bonferroni's multiple comparison test. Not every comparison between every simulated dose and sensitivity mode is displayed to avoid an overcrowded graph. * Refers to $p < 0.05$ and **** refers to $p < 0.0001$. HS: high sensitivity; UHS: ultra-high sensitivity; SNR: signal-to-noise ratio; ns: non-significant.

3.4. Quantitative PET Parameters

SUV_{mean} and SUV_{peak} only showed minimal decreases in the simulated low-dose reconstructions. Regarding the lowest dose of 0.125 MBq/kg, SUV_{mean} decreased by only 8%, whereas SUV_{peak} decreased by only 3%**.** The impact of the sensitivity mode on the SUV_{mean} and SUV_{peak} values was negligible. Two-way ANOVA revealed no statistically significant interaction between the effects of the sensitivity mode and the reduced doses, neither for SUV_{mean} nor SUV_{peak} ($p > 0.99$). The main effects analysis showed that neither sensitivity mode nor simulated dose reduction alone had a statistically significant effect on the SUV_{mean} or SUV_{peak} values ($p = 0.76$, $p = 0.76$, $p = 0.93$, and $p = 0.81$, respectively).

SUV_{max} increased steadily for lower doses. However, the increase was less prominent for UHS in comparison to the HS mode, e.g., we reported an increase of 16% (HS) and 6% (UHS) at 0.5 MBq/kg and 27% (HS) and 13% (UHS) at 0.25 MBq/kg.

Two-way ANOVA showed no statistically significant interaction between the effects of the sensitivity mode and the simulated dose reduction ($p = 0.92$) on SUV_{max}. The main effects analysis shows that both the simulated dose reduction and the sensitivity mode had a statistically significant effect on the SUV_{max} values ($p = 0.003$, $p = 0.04$). Consistently, as shown in Figure 5C, post-hoc multiple comparison tests revealed that the significant difference in SUV_{max} values was present only when comparing the values between the standard scan (3.0 MBq/kg, HS mode) with 0.125 MBq/kg in the HS mode ($p = 0.0135$), where a mean increase of 41% was recorded. This was, however, not the case when comparing the standard scan SUV_{max} values (3.0 MBq/kg, HS mode) with values at 0.125 MBq/kg in the UHS mode ($p > 0.99$).

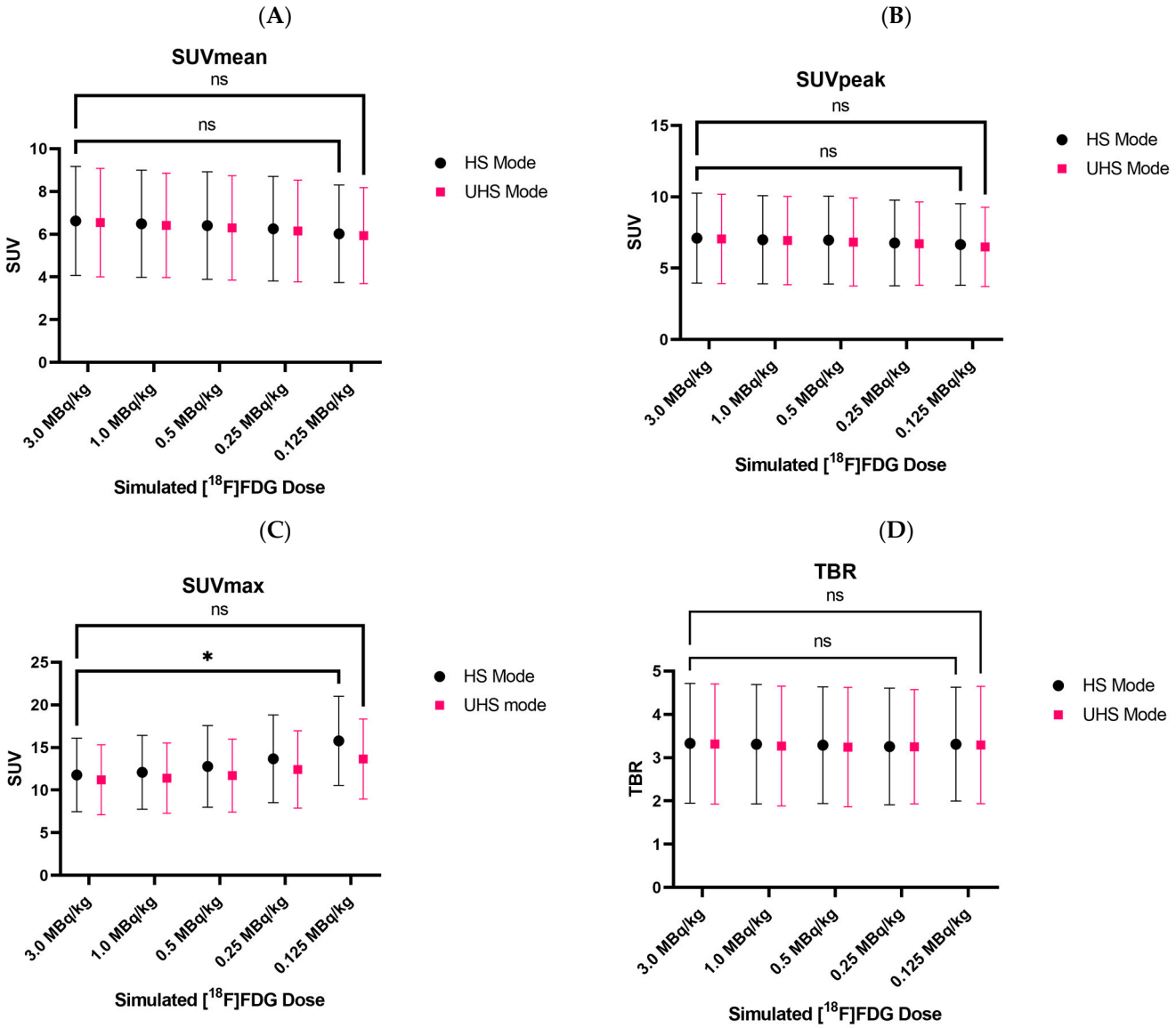

Figure 5. Average standard uptake values of all lesions for SUV_{mean} (**A**), SUV_{peak} (**B**), SUV_{max} (**C**), and TBR (**D**) for all simulated doses in both sensitivity modes. No statistically significant differences in SUV_{mean}, SUV_{peak}, and TBR values were reported between the standard scan (3 MBq/kg, HS mode) and all simulated doses, regardless of sensitivity mode and even at the lowest dose. SUV_{max} values were, however, statistically significantly different between the standard scan and simulated dose of 0.125 Mbq/kg in HS mode (**C**). Each dot represents the mean value and error bars represent the standard deviations. Two-way ANOVA was performed for statistical analysis, followed by Bonferroni's multiple comparison test. Not every comparison between every simulated dose and sensitivity mode is displayed to avoid an overcrowded graph. * Refers to $p < 0.05$. UHS: ultra-high sensitivity: HS, high sensitivity; STD: standard deviation; AU: arbitrary unit; ns: non-significant.

Regarding TBR (as a function of SUV_{peak}), two-way ANOVA revealed no statistically significant interaction between the effects of the simulated dose reduction and the sensitivity mode ($p > 0.99$, $p = 0.88$). Moreover, the main effects analysis showed that neither the simulated dose reduction nor the sensitivity mode had a statistically significant effect on the TBR values.

4. Discussion

Recent studies have demonstrated the improved performance characteristics of LAFOV PET/CT scanners. For example, studies evaluating the uEXPLORER, another commercially available LAFOV PET/CT scanner with an aFOV of approximately 2 m, showed that low- (1.85 MBq/kg) or ultra-low-dose (0.37 MBq/kg) imaging protocols [24,25] may be clinically feasible, usually requiring longer scan times (>5 min.).

For the Biograph Vision Quadra, a study in melanoma patients showed that a dose reduction down to 2.0 MBq/Kg with a 5 min scan was not associated with a worsening clinical performance [14]. Such protocols may profit from the recently introduced UHS mode, which has the potential to further lower the applicated activity and/or the acquisition time by fully exploiting the largely increased sensitivity of this LAFOV PET/CT scanner. However, before the low-dose protocols involving the latest sensitivity mode can be implemented into routine clinical practice, evaluating their limitations and diagnostical reliability is necessary. Therefore, we assessed the influence of reduced [^{18}F]FDG activity doses for both the HS and UHS modes on the qualitative and quantitative PET parameters in the Biograph Vision Quadra.

Regarding subjective image rating, we determined that the images at 0.5 MBq/kg (1/6th of the standard clinical dose) with a 5 min acquisition in the HS mode were "barely diagnostic". In this regard, simulations with very low doses in the HS mode (0.25 MBq/kg and 0.125 MBq/kg) were rated as biased via the poor image quality and affected diagnostic reliability. However, using the same protocols in the UHS mode, improved diagnostic image quality was consistently achieved, e.g., the images at 0.25 MBq/kg in the UHS mode were then also rated as "barely diagnostic". Nonetheless, we would still recommend that these very low doses should not be considered for clinical application unless compensated by a scan time considerably longer than 5 min. In general, the enhanced SNR in the UHS mode led to an overall improvement in the subjectively evaluated image characteristics, except for 0.125 MBq/kg, where no tangible improvements were noted.

Lesion detectability decreased at the dose of 0.5 MBq/kg to a detection rate of 95% in the HS mode and could be partly recovered to 98% in the UHS mode. Lesion morphology and tracer uptake evidently influenced lesion detection. The mean size of undetected lesions was 1.5 $\pm$ 0.57 cm with a SUV_{mean} of 4.7 $\pm$ 2.8, mainly indicating an increased risk of smaller and low to moderate metabolic active lesions remaining undetected.

A dose of 1.0 MBq/kg combined with the HS mode resulted in a CoV of 17.9% $\pm$ 2.0, exceeding the threshold of 15.0% recommended by EFOMP and EANM [22]. The UHS mode could meet this criterion with a CoV of 13.0 $\pm$ 1.3%. To further reduce the dose and maintain an acceptable image noise, filtering of the images can be performed. In this regard, Rausch et al. [26] showed that for the Biograph Vision Quadra, using a 6 mm Gaussian filter instead of a 2 mm filter helped to increase the useful aFOV (CoV < 15%) from 83 cm to 103 cm. Subjective image noise ratings considered noise as excessive and impairing the diagnostic quality starting at 0.25 MBq/Kg while having acceptable image noise levels even at 0.5 MBq/kg, implying that higher noise values may still be acceptable in clinical settings.

Furthermore, two-way ANOVA showed that the SNR values of the images reconstructed in the UHS mode have comparable SNRs to the images reconstructed in the HS mode but with twice the simulated activity, e.g., 0.5 MBq/kg (UHS) vs. 1.0 MBq/kg (HS), which is another way of interpreting the similar results previously published, where 30 s/60 s acquisitions in UHS showed comparable SNRs to 60 s/120 s acquisitions in the HS mode [19]. Furthermore, a mean SNR UHS to the HS ratio of 1.36 $\pm$ 0.02 was reported, which also aligns with the previously published values. The UHS mode is, thus, useful for acquiring clinically diagnostic images with lower activity protocols.

Of note, image noise is not uniformly improved across the FOV. Schmidt et al. [27] reported that for the Biograph Vision Quadra, the improvement in CoV in the center FOV can be as high as a factor of 1.49, comparing the UHS and HS mode. However, no improvement was observed with the UHS mode beyond the central 80 cm of the aFOV.

Concerning the quantitative PET parameters, SUV_{mean}, SUV_{peak}, and TBR showed only minimal decreases of <10% and two-way ANOVA revealed no statistically significant differences, including at the lowest simulated dose. $SUV_{max,}$ however, was steadily considerably higher in the HS mode compared to the values in the UHS mode and increased towards lower doses, which is comparable to the previously published results, where 600 s acquisitions had statistically significant differences in the SUV_{max} values of evaluated lesions compared to 120 s and 60 s acquisitions [28], whereas SUV_{mean} and SUV_{peak} remained relative stable. This is expected to be caused by the influence of noise on SUV_{max} [29,30]. In our study, two-way ANOVA and multiple comparisons revealed only statistically significant differences while comparing the SUV_{max} values of the standard 3.0 MBq/kg scan (HS) with values at 0.125 MBq/kg (HS), whereas when comparing to SUV_{max} values at 0.125 MBq/kg in UHS mode two-way ANOVA showed no statistically significantly differences. SUV_{max} is known to be overestimated due to the PSF reconstruction [31,32] and prone to noise distortion as it is based on the value of only a single voxel. Therefore, using SUV_{peak} or SUV_{mean} for quantification instead of SUV_{max} seems reasonable, especially in scenarios with low event statistics. The fact that the uptake values remained relatively constant at lower doses down to 0.125 MBq/kg (=1/24th of the standard applied dose, UHS mode) indicates that the fundamental limitations regarding dose reduction were based on insufficient diagnostic image quality.

Considering the results of this study, the Biograph Vision Quadra and LAFOV PET/CT scanners, in general, provide an emerging flexibility in the adjustment of applied activities and scan times. Of note, instead of altering the dose, a change in scan duration can also have a comparable impact. As such, considering the short half-life of F-18 of 109.8 min, a 5 min scan with 1.0 MBq/kg would yield approximately the same count statistics as a 10 min scan with 0.5 MBq/kg. As with 1.0 MBq/kg, no degradations were reported in our work compared to the full 3.0 MBq/kg with a 5 min scan. This implies the same is true for 0.5 MBq/kg with a 10 min scan time. This would allow high image quality, quantification accuracy, and diagnostic reliability with an effective dose of less than 1 mSv (for a 70 kg patient).

Utilizing this protocol with 0.5 MBq/kg and a 10 min scan would also allow feasible dual-tracer same-day protocols; for example, by performing an [^{18}F]FDG PET early in the day. Approximately three half-lives later, one could perform a second PET scan with a different radiotracer and standard activity doses (2.0–3.0 MBq/kg) of, e.g., [^{18}F]PSMA-1007 or [^{18}F]SiFAlin-TATE, since no relevant activity of [^{18}F]FDG remains at the time point of the second scan. Such protocols would come into question where the [^{18}F]FDG PET supports clinical decision-making; for example, for patient selection or therapy control in patients with prostate cancer or neuroendocrine tumors that may receive or are receiving radioligand therapy. This type of examination aims to find radiotracer mismatches (FDG-positive and PSMA/SSR negative), which may indicate more aggressive tumor types that may warrant more aggressive therapy regimens instead of radioligand therapy [33]. The benefit of this protocols compared to previously published ones, e.g., first completion of [^{68}Ga]Ga-PSMA-11 PET scan followed immediately by a standard 40 MBq injection of [^{18}F]FDG [34], is that the semi-quantitative assessment of both FDG and PSMA would be less problematic at the cost of longer patient waiting times. Nonetheless, both protocols would be able to assess radiotracer mismatches.

Considering the reduced radiation exposure, pediatric patients could also benefit, and hybrid imaging could become more feasible in this patient population. The flexibility of LAFOV PET/CT scanners comes to note in pediatric patients since, depending on the clinical setting, one would be able to apply a standard activity dose and perform a fast scan while avoiding the use of anesthesia, as Reichkendler M et al. showed [35], or reduce applied activity in children that do not require sedation. Our results might be transferable for hybrid imaging studies in the pediatric population, but this requires further evaluation.

One limitation of this study is that only a relatively small sample size of 26 patients with a total of 82 pathological target lesions was included for analysis. Only two patients

included were obese with a BMI > 35 kg/m^2. Previous studies reported that a dose reduction was feasible only in non-obese patients with a BMI < 30 kg/m^2, thus limiting the generalizability of our results to the obese patient population [36]. Furthermore, different FDG-avid tumor entities were included in this study, while other entities were not represented in our clinical cohort. We recognize that this might limit the generalizability of our results. Further studies including low-metabolic tumors are needed to further evaluate the performance of low-dose [^{18}F]FDG PET in these entities. However, we believe that our study provides a satisfactory foundation for possible future evaluations in this regard. Another limitation is that only [^{18}F]FDG in oncological patients was considered in this study, and no non-oncological indications for PET/CT (e.g., search for florid inflammation or fever of unknown origin) were analyzed. Moreover, the transferability to tracers based on isotopes different than F-18, which have a larger positron range (such as Ga-68) or typically require lower activities (such as Zr-89), need to be elaborated as these factors impact the quantification accuracy and noise performance [37]. Further studies are warranted to assess the feasibility of low-dose PET examinations in these scenarios.

5. Conclusions

Due to their high sensitivity, LAFOV PET/CT scanners allow for a considerable reduction in the applied activity of radiotracers. In this study, we showed that reducing the injected [^{18}F]-FDG activity to 1.0 MBq/kg in a LAFOV PET/CT still offered clinically diagnostic image quality without relevant changes in the uptake parameters. Further reductions appear feasible by prolonging the scan times (e.g., 10 min) and by using the UHS mode. Fundamental limitations of further dose reduction were based on insufficient diagnostic image quality, the diminishing performance, and did not involve any possible alterations in the quantitative uptake parameters. These novel insights may further expand the implementation in clinical routine, possibly allowing for e.g., same-day multi-tracer protocols and applications in pediatric patient populations.

Supplementary Materials: The following supporting information can be downloaded at: https://www.mdpi.com/article/10.3390/diagnostics13203240/s1. Table S1: Patient and dose characteristics and clinical information; Table S2: Details of the CT imaging protocol; Table S3: Results of two-way ANOVA between simulated dose reduction and sensitivity modes for uptake parameters and SNR values; Table S4: Multiple comparisons test for SUVmax and SNR.

Author Contributions: Conceptualization, E.C., F.P.S., C.l.F. and L.S.K.; Data curation, E.C., F.P.S., W.L. and S.C.-V.; Formal analysis, E.C., F.P.S., S.C.-V., N.F.T. and L.S.K.; Funding acquisition, C.l.F. and L.S.K.; Investigation, E.C., F.P.S. and L.S.K.; Methodology, E.C., F.P.S., W.L. and L.S.K.; Project administration, E.C., F.P.S., H.D. and C.l.F.; Resources, F.P.S., A.S.B. and C.l.F.; Software, E.C., F.P.S., W.L. and S.C.-V.; Supervision, F.P.S., H.D., C.l.F. and L.S.K.; Validation, E.C., F.P.S., H.D. and L.S.K.; Visualization, E.C. and L.S.K.; Writing—original draft, E.C. and L.S.K.; Writing—review and editing, E.C., F.P.S., W.L., S.C.-V., N.F.T., H.D., C.l.F. and L.S.K. All authors have read and agreed to the published version of the manuscript.

Funding: The LAFOV PET/CT scanner was funded by the Deutsche Forschungsgemeinschaft (DFG, German Research Foundation)—INST 37/1145-1 FUGG, and the Deutsche Forschungsgemeinschaft (DFG, German Research Foundation) under Germany's Excellence Strategy—EXC 2180—390900677. Lena Sophie Kiefer received a grant from the Faculty of Medicine, Tuebingen, Germany (TÜFF, No. 2727-0-0).

Institutional Review Board Statement: The study was conducted according to the guidelines of the Declaration of Helsinki and approved by the Institutional Review Board of the University Hospital of Tuebingen (#167/2020BO2).

Informed Consent Statement: Patient consent was waived due to retrospective data acquisition.

Data Availability Statement: The data presented in this study are available on request from the corresponding author. The data are not publicly available due to privacy and ethical reasons.

Conflicts of Interest: Schmidt F. and la Fougère C. received a research grant from Siemens Healthineers. No other potential conflict of interest relevant to this article exist. The funders had no role in the design of the study; in the collection, analyses, or interpretation of the data; in the writing of the manuscript; or in the decision to publish the results.

References

1. Farsad, M. FDG PET/CT in the Staging of Lung Cancer. *Curr. Radiopharm.* **2020**, *13*, 195–203. [CrossRef] [PubMed]
2. Ayati, N.; Sadeghi, R.; Kiamanesh, Z.; Lee, S.T.; Zakavi, S.R.; Scott, A.M. The Value of 18F-FDG PET/CT for Predicting or Mon-itoring Immunotherapy Response in Patients with Metastatic Melanoma: A Systematic Review and Meta-Analysis. *Eur. J. Nucl. Med. Mol. Imaging* **2021**, *48*, 428–448. [CrossRef] [PubMed]
3. Zanoni, L.; Bezzi, D.; Nanni, C.; Paccagnella, A.; Farina, A.; Broccoli, A.; Casadei, B.; Zinzani, P.L.; Fanti, S. PET/CT in Non-Hodgkin Lymphoma: An Update. *Semin. Nucl. Med.* **2023**, *53*, 320–351. [CrossRef]
4. Nadig, V.; Herrmann, K.; Mottaghy, F.M.; Schulz, V. Hybrid Total-Body Pet Scanners—Current Status and Future Perspectives. *Eur. J. Nucl. Med. Mol. Imaging* **2022**, *49*, 445–459. [CrossRef] [PubMed]
5. Alavi, A.; Saboury, B.; Nardo, L.; Zhang, V.; Wang, M.; Li, H.; Raynor, W.Y.; Werner, T.J.; Høilund-Carlsen, P.F.; Revheim, M.-E. Potential and Most Relevant Applications of Total Body PET/CT Imaging. *Clin. Nucl. Med.* **2022**, *47*, 43–55. [CrossRef]
6. Alberts, I.; Hünermund, J.-N.; Prenosil, G.; Mingels, C.; Bohn, K.P.; Viscione, M.; Sari, H.; Vollnberg, B.; Shi, K.; Afshar-Oromieh, A.; et al. Clinical Performance of Long Axial Field of View PET/CT: A Head-to-Head Intra-Individual Comparison of the Bi-ograph Vision Quadra with the Biograph Vision PET/CT. *Eur. J. Nucl. Med. Mol. Imaging* **2021**, *48*, 2395–2404. [CrossRef]
7. Dimitrakopoulou-Strauss, A.; Pan, L.; Sachpekidis, C. Long Axial Field of View (LAFOV) PET-CT: Implementation in Static and Dynamic Oncological Studies. *Eur. J. Nucl. Med. Mol. Imaging* **2023**, *50*, 3354–3362. [CrossRef]
8. Attarwala, A.A.; Molina-Duran, F.; Büsing, K.-A.; Schönberg, S.O.; Bailey, D.L.; Willowson, K.; Glatting, G. Quantitative and Qualitative Assessment of Yttrium-90 PET/CT Imaging. *PLoS ONE* **2014**, *9*, e110401. [CrossRef]
9. Dryák, P.; Šolc, J. Measurement of the Branching Ratio Related to the Internal Pair Production of Y-90. *Appl. Radiat. Isot.* **2020**, *156*, 108942. [CrossRef]
10. van Sluis, J.; Borra, R.; Tsoumpas, C.; van Snick, J.H.; Roya, M.; Ten Hove, D.; Brouwers, A.H.; Lammertsma, A.A.; Noordzij, W.; Dierckx, R.A.J.O.; et al. Extending the Clinical Capabilities of Short- and Long-Lived Positron-Emitting Radionuclides through High Sensitivity PET/CT. *Cancer Imaging* **2022**, *22*, 69. [CrossRef]
11. Mohr, P.; van Sluis, J.; Providência, L.; van Snick, J.H.; Hooge, M.N.L.; Willemsen, A.T.; Glaudemans, A.W.J.M.; Boellaard, R.; Lammertsma, A.A.; Brouwers, A.H.; et al. Long Versus Short Axial Field of View Immuno-PET/CT: Semiquantitative Evalu-ation for 89Zr-Trastuzumab. *J. Nucl. Med.* **2023**. [CrossRef]
12. Lugat, A.; Bailly, C.; Chérel, M.; Rousseau, C.; Kraeber-Bodéré, F.; Bodet-Milin, C.; Bourgeois, M. Immuno-PET: Design Options and Clinical Proof-of-Concept. *Front. Med.* **2022**, *9*, 1026083. [CrossRef] [PubMed]
13. Tan, H.; Sui, X.; Yin, H.; Yu, H.; Gu, Y.; Chen, S.; Hu, P.; Mao, W.; Shi, H. Total-Body PET/CT Using Half-Dose FDG and Compared with Conventional PET/CT Using Full-Dose FDG in Lung Cancer. *Eur. J. Nucl. Med. Mol. Imaging* **2021**, *48*, 1966–1975. [CrossRef] [PubMed]
14. Sachpekidis, C.; Pan, L.; Kopp-Schneider, A.; Weru, V.; Hassel, J.C.; Dimitrakopoulou-Strauss, A. Application of the Long Axial Field-of-View PET/CT with Low-Dose [18F]FDG in Melanoma. *Eur. J. Nucl. Med. Mol. Imaging* **2023**, *50*, 1158–1167. [CrossRef] [PubMed]
15. Surti, S.; Pantel, A.R.; Karp, J.S. Total Body PET: Why, How, What For? *IEEE Trans. Radiat. Plasma Med. Sci.* **2020**, *4*, 283–292. [CrossRef]
16. Cherry, S.R.; Jones, T.; Karp, J.S.; Qi, J.; Moses, W.W.; Badawi, R.D. Total-Body PET: Maximizing Sensitivity to Create New Opportunities for Clinical Research and Patient Care. *J. Nucl. Med.* **2018**, *59*, 3–12. [CrossRef]
17. Prenosil, G.A.; Hentschel, M.; Weitzel, T.; Sari, H.; Shi, K.; Afshar-Oromieh, A.; Rominger, A. EARL Compliance Measure-ments on the Biograph Vision Quadra PET/CT System with a Long Axial Field of View. *EJNMMI Phys.* **2022**, *9*, 26. [CrossRef]
18. Prenosil, G.A.; Sari, H.; Fürstner, M.; Afshar-Oromieh, A.; Shi, K.; Rominger, A.; Hentschel, M. Performance Characteristics of the Biograph Vision Quadra PET/CT System with a Long Axial Field of View Using the NEMA NU 2-2018 Standard. *J. Nucl. Med.* **2022**, *63*, 476–484. [CrossRef]
19. Mingels, C.; Weidner, S.; Sari, H.; Buesser, D.; Zeimpekis, K.; Shi, K.; Alberts, I.; Rominger, A. Impact of the New Ultra-High Sensitivity Mode in a Long Axial Field-of-View PET/CT. *Ann. Nucl. Med.* **2023**, *37*, 310–315. [CrossRef]
20. Boellaard, R.; Delgado-Bolton, R.; Oyen, W.J.G.; Giammarile, F.; Tatsch, K.; Eschner, W.; Verzijlbergen, F.J.; Barrington, S.F.; Pike, L.C.; Weber, W.A.; et al. FDG PET/CT: EANM Procedure Guidelines for Tumour Imaging: Version 2.0. *Eur. J. Nucl. Med. Mol. Imaging* **2015**, *42*, 328–354. [CrossRef]
21. De Luca, G.M.R.; Habraken, J.B.A. Method to Determine the Statistical Technical Variability of SUV Metrics. *EJNMMI Phys.* **2022**, *9*, 40. [CrossRef] [PubMed]
22. EFOMP Protocol for Quality Control in PET/CT and PET/MRI. Available online: https://www.efomp.org/index.php?r=news/view&id=277 (accessed on 22 May 2023).

23. Mattsson, S.; Johansson, L.; Leide Svegborn, S.; Liniecki, J.; Noßke, D.; Riklund, K.Å.; Stabin, M.; Taylor, D.; Bolch, W.; Carlsson, S.; et al. Radiation Dose to Patients from Radiopharmaceuticals: A Compendium of Current Information Related to Frequently Used Substances. *Ann. ICRP* **2015**, *44*, 7–321. [CrossRef] [PubMed]
24. He, Y.; Gu, Y.; Yu, H.; Wu, B.; Wang, S.; Tan, H.; Cao, Y.; Chen, S.; Sui, X.; Zhang, Y.; et al. Optimizing Acquisition Times for Total-Body Positron Emission Tomography/Computed Tomography with Half-Dose 18F-Fluorodeoxyglucose in Oncology Patients. *EJNMMI Phys.* **2022**, *9*, 45. [CrossRef] [PubMed]
25. Tan, H.; Cai, D.; Sui, X.; Qi, C.; Mao, W.; Zhang, Y.; Liu, G.; Yu, H.; Chen, S.; Hu, P.; et al. Investigating Ultra-Low-Dose To-tal-Body [18F]-FDG PET/CT in Colorectal Cancer: Initial Experience. *Eur. J. Nucl. Med. Mol. Imaging* **2022**, *49*, 1002–1011. [CrossRef] [PubMed]
26. Rausch, I.; Mannheim, J.G.; Kupferschläger, J.; la Fougère, C.; Schmidt, F.P. Image Quality Assessment along the One Metre Axial Field-of-View of the Total-Body Biograph Vision Quadra PET/CT System for 18F-FDG. *EJNMMI Phys.* **2022**, *9*, 87. [CrossRef] [PubMed]
27. Schmidt, F.P.; Mannheim, J.G.; Linder, P.; Will, P.; Kiefer, L.S.; Conti, M.; la Fougère, C.; Rausch, I. Impact of the maximum ring difference on image quality and noise characteristics of a total-body PET/CT scanner. *Z. Med. Phys.* 2023, *in press*. [CrossRef]
28. van Sluis, J.; van Snick, J.H.; Brouwers, A.H.; Noordzij, W.; Dierckx, R.A.J.O.; Borra, R.J.H.; Slart, R.H.J.A.; Lammertsma, A.A.; Glaudemans, A.W.J.M.; Boellaard, R.; et al. EARL Compliance and Imaging Optimisation on the Biograph Vision Quadra PET/CT Using Phantom and Clinical Data. *Eur. J. Nucl. Med. Mol. Imaging* **2022**, *49*, 4652–4660. [CrossRef]
29. Koopman, D.; van Osch, J.A.C.; Jager, P.L.; Tenbergen, C.J.A.; Knollema, S.; Slump, C.H.; van Dalen, J.A. Technical Note: How to Determine the FDG Activity for Tumour PET Imaging That Satisfies European Guidelines. *EJNMMI Phys.* **2016**, *3*, 22. [CrossRef]
30. Lodge, M.A.; Chaudhry, M.A.; Wahl, R.L. Noise Considerations for PET Quantification Using Maximum and Peak Standard-ized Uptake Value. *J. Nucl. Med.* **2012**, *53*, 1041–1047. [CrossRef]
31. Tsai, Y.-J.; Liu, C. Pitfalls on PET/CT Due to Artifacts and Instrumentation. *Semin. Nucl. Med.* **2021**, *51*, 646–656. [CrossRef]
32. Alessio, A.M.; Stearns, C.W.; Tong, S.; Ross, S.G.; Kohlmyer, S.; Ganin, A.; Kinahan, P.E. Application and Evaluation of a Measured Spatially Variant System Model for PET Image Reconstruction. *IEEE Trans. Med. Imaging* **2010**, *29*, 938–949. [CrossRef]
33. Buteau, J.P.; Martin, A.J.; Emmett, L.; Iravani, A.; Sandhu, S.; Joshua, A.M.; Francis, R.J.; Zhang, A.Y.; Scott, A.M.; Lee, S.-T.; et al. PSMA and FDG-PET as Predictive and Prognostic Biomarkers in Patients given [177Lu]Lu-PSMA-617 versus Cabazitaxel for Metastatic Castration-Resistant Prostate Cancer (TheraP): A Biomarker Analysis from a Randomised, Open-Label, Phase 2 Trial. *Lancet Oncol.* **2022**, *23*, 1389–1397. [CrossRef] [PubMed]
34. Alberts, I.; Schepers, R.; Zeimpekis, K.; Sari, H.; Rominger, A.; Afshar-Oromieh, A. Combined [68 Ga]Ga-PSMA-11 and Low-Dose 2-[18F]FDG PET/CT Using a Long-Axial Field of View Scanner for Patients Referred for [177Lu]-PSMA-Radioligand Therapy. *Eur. J. Nucl. Med. Mol. Imaging* **2023**, *50*, 951–956. [CrossRef] [PubMed]
35. Reichkendler, M.; Andersen, F.L.; Borgwardt, L.; Nygaard, U.; Albrecht-Beste, E.; Andersen, K.F.; Ljunggren, A.; Abraham-sen, N.; Loft, A.; Højgaard, L.; et al. A Long Axial Field of View Enables PET/CT in Toddler Without Sedation. *J. Nucl. Med.* **2022**, *63*, 1962. [CrossRef] [PubMed]
36. Sekine, T.; Delso, G.; Zeimpekis, K.G.; de Galiza Barbosa, F.; Ter Voert, E.E.G.W.; Huellner, M.; Veit-Haibach, P. Reduction of 18F-FDG Dose in Clinical PET/MR Imaging by Using Silicon Photomultiplier Detectors. *Radiology* **2018**, *286*, 249–259. [CrossRef]
37. Mannheim, J.G.; Rausch, I.; Conti, M.; la Fougère, C.; Schmidt, F.P. Characterization of the Partial Volume Effect along the Axial Field-of-View of the Biograph Vision Quadra Total-Body PET/CT System for Multiple Isotopes. *EJNMMI Phys.* **2023**, *10*, 33. [CrossRef]

2.2 **Research article**: “One-day dual-tracer examination in neuroendocrine neoplasms: a real advantage of low activity LAFOV PET imaging”

Authors: Eduardo Calderón, Lena S. Kiefer, Fabian P. Schmidt, Wenhong Lan, Andreas S. Brendlin, Christian P. Reinert, Stephan Singer, Gerald Reischl, Martina Hinterleitner, Helmut Dittmann, Christian la Fougère, Nils F. Trautwein. **Published in:** European Journal of Nuclear Medicine and Molecular Imaging, **Volume:** 52**, Issue:** 7**, Pages:** 2463-2476**, Year:** 2025

European Journal of Nuclear Medicine and Molecular Imaging (2025) 52:2463–2476
https://doi.org/10.1007/s00259-025-07073-w

ORIGINAL ARTICLE

One-day dual-tracer examination in neuroendocrine neoplasms: a real advantage of low activity LAFOV PET imaging

Eduardo Calderón[1] · Lena S. Kiefer[1] · Fabian P. Schmidt[1,2] · Wenhong Lan[1] · Andreas S. Brendlin[3] · Christian P. Reinert[3] · Stephan Singer[4] · Gerald Reischl[2,7] · Martina Hinterleitner[5,6,7] · Helmut Dittmann[1,6] · Christian la Fougère[1,6,7,8] · Nils F. Trautwein[1,6]

Received: 13 September 2024 / Accepted: 30 December 2024 / Published online: 30 January 2025

Abstract

Purpose Somatostatin receptor (SSTR)-PET is crucial for effective treatment stratification of neuroendocrine neoplasms (NENs). In highly proliferating or poorly differentiated NENs, dual-tracer approaches using additional [^{18}F]FDG PET can effectively identify SSTR-negative disease, usually requiring separate imaging sessions. We evaluated the feasibility of a one-day dual-tracer imaging protocol with a low activity [^{18}F]FDG PET followed by an SSTR-PET using the recently introduced [^{18}F]SiFA*lin*-TATE tracer in a long axial field-of-view (LAFOV) PET/CT scanner and its implications in patient management.

Methods Twenty NEN patients were included in this study. Initially, a low activity [^{18}F]FDG PET was performed (0.5 ± 0.01 MBq/kg; PET scan 60 min p.i.). After 4.2 ± 0.09 h after completion of the [^{18}F]FDG PET, a standard activity of [^{18}F]SiFA*lin*-TATE was administered (3.0 MBq/kg; PET scan 90 min p.i.). To ensure the quantification accuracy of the second scan, we evaluated the potential impact of residual [^{18}F]FDG activity by segmenting organs with minimal physiological SSTR-tracer uptake, such as the brain and myocardium, and assessing the activity concentrations (ACTs) of tumor lesions. Residual tumor lesion ACTs of [^{18}F]FDG were calculated by factoring fluorine-18 decay, identifying a maximum residual ACT of 15% (R15%). To account for increased [^{18}F]FDG trapping over time, higher residual ACTs of 20% (R20%) were considered. These simulated [^{18}F]FDG ACTs were compared with those measured in the second PET scan with [^{18}F]SiFA*lin*-TATE. The influence of the dual-tracer PET/CT results on therapeutic strategies was evaluated.

Results [^{18}F]FDG cerebral uptake significantly decreased in the subsequent SSTR-PET (mean uptake [^{18}F]FDG: SUV_{mean} 6.0 ± 0.4; mean uptake in [^{18}F]SiFA*lin*-TATE PET: SUV_{mean} 0.2 ± 0.01; $p < 0.0001$); with similar results recorded for the myocardium. Simulated residual [^{18}F]FDG ACTs represented only a minimal percentage of ACTs measured in the tumor lesions from the second PET scan (R15%: mean 5.2 ± 0.9% and R20%: mean 6.8 ± 1.2%), indicating only minimal residual activity of [^{18}F]FDG that might interfere with the second PET scan using [^{18}F]SiFA*lin*-TATE and preserved semi-quantification of the latter. Dual-tracer PET/CT findings directly influenced changes in therapy plans in eleven (55%) of the examined patients.

Conclusion LAFOV PET scanners enable a one-day dual-tracer protocol, providing diagnostic image quality while preserving the semi-quantification of two ^{18}F-labeled radiotracers, potentially simplifying the assessment of tumor biology and improving the clinical patient management while reducing logistical challenges. Additionally, low-activity PET imaging facilitates one-day dual-tracer PET examinations.

Keywords Dual-tracer PET · LAFOV PET/CT · Low activity [^{18}F]FDG PET · Neuroendocrine neoplasms

Extended author information available on the last page of the article

Introduction

Neuroendocrine neoplasms (NENs) comprise a group of heterogeneous tumors originating from various anatomical sites, which are subcategorized into well-differentiated neuroendocrine tumors (NETs) and poorly differentiated neuroendocrine carcinomas (NECs) [1, 2]. Moreover, NETs are subdivided according to their proliferation index in G1 (Ki67 < 3%), G2 (Ki67 3–20%), and G3 (Ki67 > 20%). Well-differentiated NETs are usually characterized by the overexpression of somatostatin receptors (SSTRs) [3], providing a viable target structure for theranostic approaches [4]. In this context, PET imaging is performed through a non-invasive assessment of SSTR expression using radiolabeled somatostatin analogues (SSAs) [5], where [^{68}Ga]Ga-DOTA-SSAs are the current gold standard. New ^{18}F-labeled radiotracers, such as [^{18}F]SiFA*lin*-TATE, have recently been established in clinical practice [6] and might facilitate access to SSTR-PET imaging due to the longer half-life of fluorine-18 and the associated higher production scalability.

Regarding clinical management of patients with NENs, SSTR-PET imaging is crucial for the assessment of disease extent and prognosis, and specifically for adequate patient selection for peptide receptor radionuclide therapy (PRRT) with [^{177}Lu]Lu-DOTA-TATE, which has proven to be an essential therapy option especially considered for G1/G2 gastroenteropancreatic NETs [7–9]. Besides this patient group, the NETTER2 trial recently revealed promising results for [^{177}Lu]Lu-DOTA-TATE PRRT as a first-line therapy in high-proliferating G2 (≥ 10%) and even G3 (< 55%) tumors [10]. However, NENs with a Ki67 greater than 10% or poor differentiation may exhibit tumor biology changes, leading to increased glucose metabolism and decreased SSTR expression [11]. In these patients, the entire disease burden would be potentially underrepresented in the SSTR-PET, thus leading to inappropriate therapy stratification and worsened outcomes, e.g., for SSTR-targeted therapies.

To address this problem and assist the clinical management of patients with high-grade NENs, dual-tracer PET approaches combining [^{18}F]FDG and radiolabeled SSAs have been proposed [12–14]. However, conventional PET/CT scanners with a short axial field-of-view (SAFOV) necessitate two separate imaging sessions on different days to prevent "spill-over" between the applied radiotracers.

New-generation PET/CT scanners with a long axial field-of-view (LAFOV) offer technical advantages compared to SAFOV PET/CT scanners due to their significantly higher sensitivity up to a factor of 10 [15, 16], leading to many new possibilities in hybrid imaging, including the activity reduction of radiotracers. Thereby, activity reductions down to 2.0 MBq/kg of [^{18}F]FDG have been proposed and introduced in our standard clinical practice [17]. Furthermore, a previous study showed that further activity reductions down to 0.5 MBq/kg [^{18}F]FDG with a 10 min PET acquisition time offers reliable diagnostic performance with preserved lesion detection rate and accurate quantification compared to standard activity (3.0 MBq/kg) PET images [18]. This relevant activity reduction can shorten the required interval between two separate PET scans, making quantifiable dual-tracer PET examinations feasible in one day.

Therefore, we decided to explore the feasibility of a one-day dual-tracer PET imaging protocol for patients with NENs (Ki67 ≥ 10%), combining a low activity [^{18}F]FDG PET with 0.5 MBq/kg followed by a standard activity [^{18}F]SiFA*lin*-TATE PET with 3.0 MBq/kg and to evaluate its impact in the clinical management of NEN patients.

Materials and methods

Study cohort

This study was based on a prospective PET/CT registry, including 20 patients with histologically confirmed G2 (≥ 10%) and G3 (> 20%) NEN. The [^{18}F]FDG PET and SSTR-PET with [^{18}F]SiFAlin-TATE were performed on a LAFOV PET/CT scanner (Siemens Biograph Vision Quadra, Siemens Healthineers, Knoxville, TN, USA). Written informed consent was obtained from all patients prior to the PET/CT examination. The study was approved by the Institutional Review Board of the University Hospital of Tuebingen (#082/2024BO2).

Dual-Tracer PET protocol and PET image reconstruction

Detailed information on applied activity and elapsed time between PET scans are provided in Supplementary Table 1. Patients first received a low activity [^{18}F]FDG PET after an intravenous (i.v.) injection of 0.5 ± 0.01 MBq/kg. A 10 min PET image acquisition was started at 60 min post-injection (p.i.). Whole-body scans were acquired in supine position and a single bed position (106 cm) covering an area from the skull apex to the mid-thighs. Patients were required to fast for at least 10 h prior to the examination. A venous blood glucose measurement was conducted to confirm blood glucose levels ≤ 200 mg/dl, as described by the European Association of Nuclear Medicine (EANM) procedures guidelines [19]. A low-dose CT scan for attenuation correction was performed before PET acquisition.

A minimum of three and a half hours (mean 4.2 ± 0.09 h) after completing the [^{18}F]FDG PET was kept until i.v. injection of 3.0 MBq/kg [^{18}F]SiFA*lin*-TATE. Afterward, a 5 min PET image acquisition was started at 90 min p.i., as

previously described [20]. [^{18}F]SiFA*lin*-TATE was synthesized following a modified procedure of Lindner et al. [21]. A full diagnostic contrast-enhanced dual-energy CT scan in arterial and portal venous phase was acquired and used for attenuation correction. Technical specificities of CT scan protocols are provided in Supplementary Table 2. The average time span until completion of both PET/CT examinations was 6.7 ± 0.09 h. Patients were allowed to leave our center after completion of the first scan and return later for the second PET examination.

PET reconstruction was performed according to the standard clinical reconstruction protocol, with an Ordinary-Poisson Ordered-Subsets Expectation-Maximization algorithm with four iterations and five subsets (OP-OSEM 4i5s), using point-spread-function (PSF) modeling, time-of-flight (TOF) information. For low activity [^{18}F]FDG scans, images were reconstructed in both the high-sensitivity mode (HS) and ultra-high sensitivity (UHS) mode with an acceptance angle of 18° and 52°, respectively. For two patients, reconstructions in UHS mode were not available. Images were reconstructed with a 440 × 440 × 645 matrix and a 1.65 × 1.65 × 1.65 mm^3 isotropic voxel size. No image filter was applied.

PET image and residual [^{18}F]FDG activity analysis

Two experienced nuclear medicine physicians with at least three years of experience in hybrid imaging performed image analysis in consensus reading, analyzing both PET scans simultaneously, thereby reflecting the procedure in clinical practice. Affinity Hybrid Viewer software (Version 3.0.5, Hermes Medical Solution, Sweden) was used for image analysis. For blood pool measurements, the SUV_{mean} of a 3 cm^3 cylindrical VOI placed in the thoracic descending aorta was recorded in both PET images. Furthermore, a 14 m^3 VOI was used to measure background uptake in the healthy tissue of the liver lobe.

To evaluate the residual [^{18}F]FDG activity in the subsequent [^{18}F]SiFA*lin*-TATE PET scan, the brain parenchyma and the myocardium, which are known to have physiological high glucose metabolism but no physiological SSTR tracer uptake, were segmented and assessed. Thereby, a whole-brain threshold-based automatic segmentation was performed, choosing a threshold of 2 x SUV_{mean} of the blood pool volume of interest (VOI). In the case of the myocardium, a 1 cm^3 cylindrical VOI was placed in the posterior myocardial wall of the left ventricle. Segmented VOIs were consecutively co-registered to the corresponding [^{18}F]SiFA*lin*-TATE PET/CT examination, and the magnitude of SUV_{mean} was assessed for residual [^{18}F]FDG activity.

Furthermore, to assess the potential impact of residual [^{18}F]FDG activity on [^{18}F]SiFA*lin*-TATE semi-quantification, we first determined the activity concentrations (ACTs) of all segmented tumor lesions from the [^{18}F]FDG PET scan. Secondly, we calculated the residual [^{18}F]FDG ACTs present when performing the second PET scan considering the decay of fluorine-18 (half-life 109.8 min). The estimated mean residual ACTs were 12% of the initially measured ACTs in the [^{18}F]FDG PET, considering the mean elapsed half-lives of 3.1 ± 0.05 between examinations. In this study, the shortest time interval between the scans was 298 min (approx. 5 h), corresponding to a maximum residual ACT of 15% (R15%).

To account for this worst-case scenario, we used the estimated R15% ACTs for each tumor lesion and determined the percentual proportion in relation to tumor lesion ACTs obtained from the [^{18}F]SiFA*lin*-TATE PET scan. However, it is recognized that in certain malignancies, the uptake of [^{18}F]FDG can further increase over time. This phenomenon remains to be studied for NENs. However, to address this issue and to simulate an increase in [^{18}F]FDG uptake over time, we incorporated a higher estimated residual [^{18}F]FDG activity of 20% (R20%) in our analysis.

The coefficient of variation (CoV) was calculated to assess objective image noise on [^{18}F]FDG images, as previously described [22]. The recommended CoV of < 15% by the EANM and the European Federation of Organisations for Medical Physics (EFOMP) was considered for interpretation of adequate noise performance [23].

Tumor lesion segmentation, semi-quantification, and assessment of metabolic tumor volume

A maximum of five representative lesions (lesion volume ≥ 0.5 mL) per organ for each patient were segmented. Tumor lesion uptake was quantified by measuring the SUV_{mean}, SUV_{peak}, and SUV_{SD} in a VOI using a 41% threshold. VOIs were manually segmented where pathological uptake suspicious for malignancy was recorded. The tumor-to-liver ratio (TLR) was calculated as previously described [21]. Lesions with a TLR equal to or below 1.0 were then categorized as FDG or SSTR negative. Considering the dual-tracer uptake, lesions were classified as follows: FDG+/SSTR-, FDG+/SSTR+, and FDG-/SSTR+. The metabolic tumor volume of [^{18}F]FDG (FDG-MTV) images was segmented using a threshold of SUV 4, as described previously [24]. For the SSTR-PET, the molecular tumor volumes (SSTR-MTV) were assessed using a threshold of 1.5 times the SUV_{mean} plus 2 times the standard deviation (SD) of the liver VOI [25].

$$SSTR-MTV = SUV_{tumor} > 1.5 \times SUVmean_{liver} + 2 \times SD_{liver}$$

Impact on clinical management

To assess the impact of dual-tracer PET on the clinical management of patients, information on the current stage of disease and treatment prior to dual-tracer PET was collected. In addition, we examined the decision-making of the interdisciplinary tumor board (ITB) involving dual-tracer PET findings. In particular, PET parameters that significantly influenced these decisions, i.e., FDG-MTV and SSTR-MTV and individual dual-tracer uptake of tumor lesions, were analyzed. Subsequent treatment changes were documented. The mentioned radiosensitizing (RS) regimen denotes a chemotherapy protocol previously outlined with capecitabine and temozolomide [26], designed to complement and improve the effectiveness of PRRT in high proliferating NENs.

Statistical analysis

Statistical analysis and figures were performed using GraphPad Prism (Version 9.4.1, GraphPad Software, San Diego, CA, USA) and an open-source software (SankeyMATIC®). D'Agostino & Pearson test was performed to test for normality distribution. Continuous variables were compared with the non-parametric Wilcoxon matched-pairs signed rank test and the Kruskal-Wallis test when comparing more than two groups, followed by Dunn´s multiple comparisons. p values <0.05 were considered statistically significant. Summary statistics are presented as mean and standard error (SE).

Table 1 Patient characteristics of the study cohort

Patient characteristics	
Age (y)	67.2 ± 9.3
Sex– n (%)	
Male	12 (60%)
Female	8 (40%)
Primary tumor site– n (%)	
Midgut	4 (20%)
Pancreas	5 (25%)
CUP	7 (35%)
Lung	4 (20%)
Grading– n (%)	
G2 (Ki67: 10–20%)	5 (25%)
G3 (Ki67: >20%)	15 (75%)
Previous therapy– n (%)	
Surgery	11 (55%)
SSA	5 (25%)
Chemotherapy	13 (65%)
PRRT	2 (10%)
SIRT	3 (15%)
Everolimus	1 (5%)

CUP = cancer of unknown primary, G = grading, SSA = somatostatin analogue, PRRT = peptide receptor radionuclide therapy, SIRT = selective internal radiation therapy

Results

Patient characteristics

Table 1 summarizes the clinical characteristics of the study population. Imaging procedures and time intervals are presented in Supplementary Table 1. Twenty patients were scanned according to our protocol: 12 (60%) males and 8 (40%) females. All patients had a histologically confirmed diagnosis of an NEN with a Ki67 index ≥ 10%.

Low activity [^{18}F]FDG PET and residual [^{18}F]FDG activity

Semi-quantitative evaluation of brain and myocardial tracer uptake and activity concentrations of segmented tumor lesions, as well as the estimated residual [^{18}F]FDG activity concentrations (R15% and R20%), are displayed in Fig. 1. The mean elapsed half-lives of fluorine-18 between both PET data acquisitions were 3.1 ± 0.05. Cerebral [^{18}F]FDG uptake was assessed in the first PET images (mean [^{18}F]FDG uptake: SUV_{mean} 6.0 ± 0.4) and showed a statistically significant decrease in the corresponding subsequent PET scans (mean uptake in [^{18}F]SiFA*lin*-TATE PET: SUV_{mean} 0.2 ± 0.01, $p < 0.001$). Similar results were recorded for the myocardium (mean [^{18}F]FDG uptake: SUV_{mean} 2.9 ± 0.6; mean uptake in [^{18}F]SiFA*lin*-TATE PET: SUV_{mean} 0.9 ± 0.05, $p < 0.001$). The mean SUV_{mean} values measured in the myocardium from the SSTR-PET scan were not statistically significantly different from those of blood pool measurements (mean SUV_{mean} blood pool 1.1 ± 0.08, $p = 0.21$).

The mean ACTs of the tumor lesions in the [^{18}F]FDG PET scan was 1820 ± 152.7 Bq/mL. The estimated residual [^{18}F]FDG activity was 273.3 ± 22.9 Bq/mL for R15% and 364.4 ± 30.5 Bq/mL for R20%. In contrast, the measured mean ACTs of all tumor lesions in the [^{18}F]SiFA*lin*-TATE PET scan were significantly higher (13882 ± 1073 Bq/; $p < 0.0001$). This data indicates that residual [^{18}F]FDG ACTs resulted in only a minor proportion of activity concentrations of tumor lesions in the [^{18}F]SiFA*lin*-TATE PET at 5.2 ± 0.9% and 6.8 ± 1.2% for R15% and R20%, respectively. R15% and R20% exert only a minimal influence on the semi-quantification of [^{18}F]SiFA*lin*-TATE. Consequently, there would be no relevant clinical implications, such as incorrect classification of tumor lesions. Furthermore, the mean CoV in the healthy liver tissue in the low activity [^{18}F]FDG PET images in HS and UHS was 18.2 ± 0.7% and 13.3 ± 0.6%, respectively. CoV values

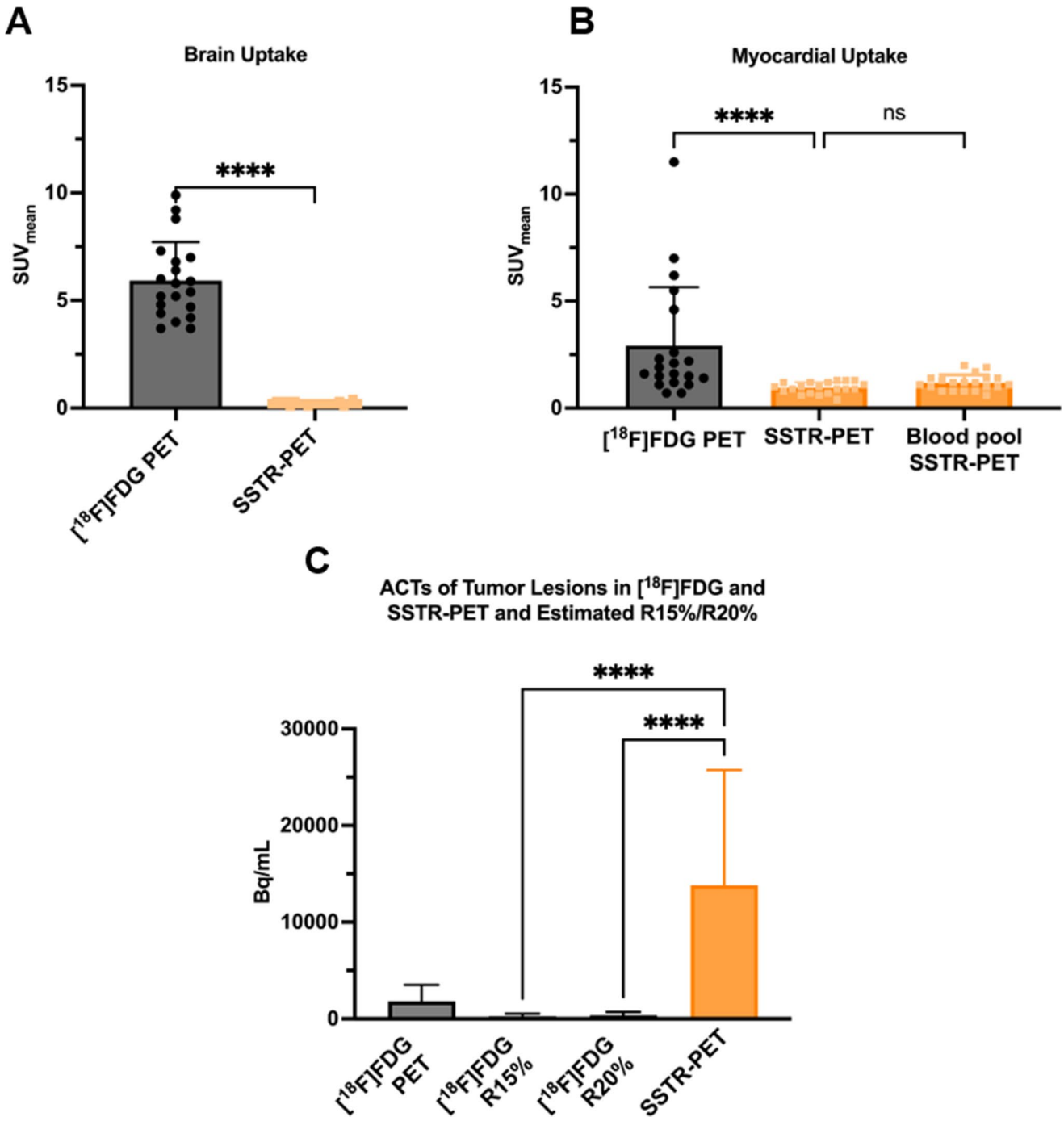

Fig. 1 Column bars displaying SUV_{mean} values of brain parenchyma (**A**) and myocardium (**B**) and activity concentrations (ACTs) of tumor lesions (**C**) in the [^{18}F]FDG and SSTR-PET. No relevant residual [^{18}F]FDG activity was measured in brain parenchyma in subsequent SSTR-PET images. For the myocardium, a similar decrease in uptake values was noted, with assessed uptake values in the myocardium of SSTR-PET images showing no statistically significant difference from blood pool measurements. The estimated residual ACTs of [^{18}F]FDG activity (R15%/R20%) are significantly lower in comparison to tumor ACTs observed in the SSTR-PET ($p < 0.0001$). Each bar represents the mean, while the error bars represent the standard deviation. Scatter plots represent individual values. Wilcoxon matched-pairs signed ranked test, and the Kruskal-Wallis test were performed to compare uptake values. *ns = non-significant.* **** *refers to* $p < 0.001$

in UHS were statistically significantly lower compared to HS values, denoting the improved noise performance of UHS mode ($p < 0.001$), which clearly supports low activity imaging and complies with the recommended values by the EANM/EFOMP (Fig. 2).

Tumor lesion classification and semi-quantification

Four patients showed no tumor lesions on either PET scan after surgical resection of known tumor/metastases, chemotherapy, selective internal radiation therapy (SIRT), or PRRT. Thirteen patients (65%) had evidence of [^{18}F]FDG-avid tumor lesions, highlighting the high proportion of [^{18}F]FDG-avid disease burden in our cohort of NEN patients. Furthermore, nine patients (45%) had evidence of tumor lesions with increased [^{18}F]FDG uptake and no relevant SSTR expression (FDG+/SSTR-), nine patients (45%) showed lesions with increased SSTR expression, but no [^{18}F]FDG avidity (FDG-/SSTR+), and seven patients (35%) showed tumor lesions with concordant tracer uptake (FDG+/SSTR+). Overall, one hundred and twenty-five tumor lesions were analyzed in both PET scans. 25/125 (20%) of the NEN-lesions showed concordant increased [^{18}F]FDG uptake and SSTR expression with a mean TLR_{mean} of 3.1 ± 0.3 and 2.8 ± 0.3 (FDG+/SSTR+), 55/125 (44%) showed discordant uptake with increased [^{18}F]FDG uptake and no relevant SSTR expression with a TLR_{mean} of 3.4 ± 0.3 and 0.7 ± 0.03 (FDG+/SSTR-), and 45/125 lesions (36%) showed only increased SSTR expression (FDG-/SSTR+) with a TLR_{mean} of 0.9 ± 0.03 and 2.8 ± 0.2, respectively (Fig. 3). Lesion classification according to dual-tracer uptake and organ distribution can be found in Table 2.

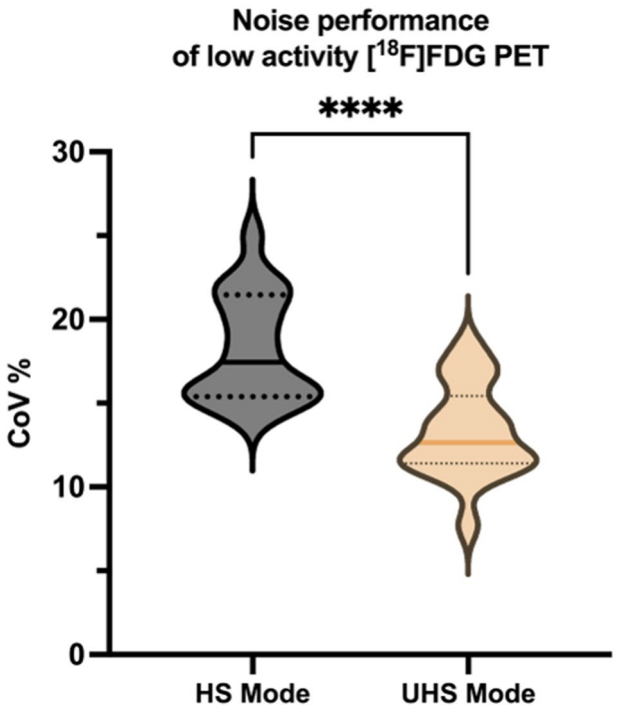

Fig. 2 Violin plots displaying the coefficient of variation (CoV) percentage values of the liver background of low activity [^{18}F]FDG PET images. Images reconstructed in the high-sensitivity mode (HS) showed a mean CoV of 18.2 ± 3.2%. In comparison, CoV values of images in ultra-high sensitivity mode (UHS) were statistically significantly lower (mean 13.2 ± 2.8%, $p < 0.001$), denoting the improved noise performance of UHS mode. Wilcoxon matched-pairs signed rank test was used to compare variables. The bold line represents the median, the upper dotted line represents the 75th percentile, and the lower dotted line represents the 25th percentile. **** *refers to* $p < 0.001$

Impact on clinical management

One of the primary factors affecting the treatment stratification was the tumor burden, as assessed by SSTR-MTV and FDG-MTV. These volumes per patient are presented in Table 3. Prior to the dual-tracer PET, the treatment plans included PRRT ($n = 5$), PRRT + RS ($n = 1$), chemotherapy ($n = 9$), active surveillance (AS) ($n = 2$), SIRT ($n = 2$) and SSA ($n = 1$) (Table 3). A Sankey-flow diagram illustrating the treatment stratification is presented in Fig. 4.

In the PRRT group ($n = 6$; PRRT and PRRT + RS), dual-tracer PET supported the previously considered treatment in three patients primarily by excluding discordant FDG+/SSTR- lesions (patients 2, 10, 12). In the remaining three patients, dual-tracer PET findings changed their treatment plans. In patient 1, only a low SSTR-MTV and no FDG-MTV were detected, so PRRT was not performed, and AS was initiated. In patient 11, discordant tracer uptake (FDG+/SSTR-) led to a change in treatment strategy to chemotherapy. Finally, in patient 14, a high SSTR + tumor burden with concordant [^{18}F]FDG uptake was detected (Fig. 5), prompting the ITB to recommend intensified PRRT combined with RS.

In the chemotherapy group ($n = 9$), dual-tracer PET led to treatment plan changes to locoregional approaches in two patients ($n = 1$ SIRT, $n = 1$ surgery). In patient 15, due to a large discordant tumor volume (FDG+/SSTR-) identified in the liver, SIRT was chosen, while SSAs were introduced to address the low extrahepatic SSTR-MTV. In patient 16, surgical resection of tumor lesions was conducted as an individualized treatment.

From the remaining patients ($n = 7$), four patients also benefited from dual-tracer PET due to the delineation of extensive discordant tumor disease (FDG+/SSTR-), receiving regimen adaptations primarily based on disease progression or new histological findings. For example, patient 17, with an initial diagnosis of a colon NET G3 (Ki-67 30%), had been treated with first-line chemotherapy (FOLFOX) according to German NET guidelines [27]. Dual-tracer PET/CT revealed progressive disease with multiple FDG+/

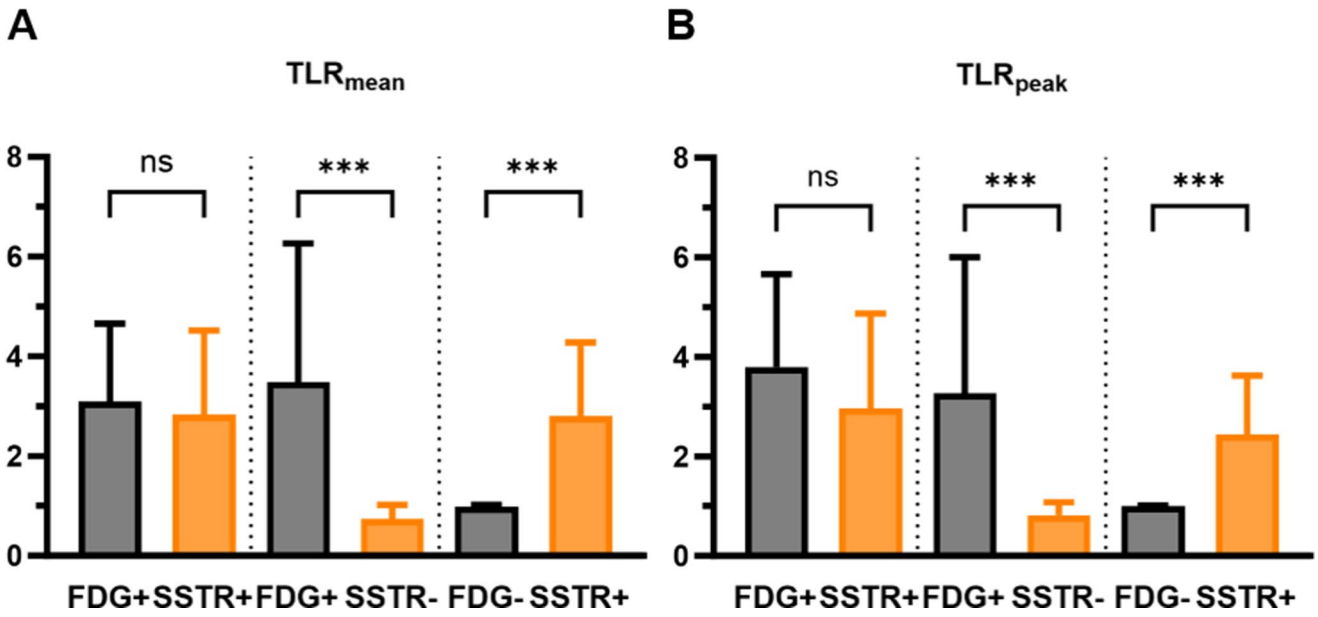

Fig. 3 TLR$_{mean}$ (**A**) and TLR$_{peak}$ (**B**) results of all 125 analyzed lesions. Regarding their [^{18}F]FDG and [^{18}F]SiFA*lin*-TATE uptake, lesions were classified as FDG+/SSTR-, FDG+/SSTR+, and FDG-/SSTR+. Each bar represents the mean, while the error bars represent the standard deviation. The Kruskal-Wallis test was used to compare the difference in median uptake values between lesions in each classification. *TLR = tumor-to-liver ratio. ns = non-significant. *** refers to p < 0.001*

Table 2 Distribution of metastatic tumor lesions according to dual-tracer uptake and involved region

Region	FDG + / SSTR +	FDG + / SSTR -	FDG - / SSTR +
Liver	15	16	25
Lymph nodes	1	23	7
Bone	6	1	12
Lung	3	6	0
Other			
Peritoneum	0	5	0
Myocardium	0	2	0
Ovary	0	1	0
Colon/Small intestine	0	1	1
Total	**25**	**55**	**45**

SSTR- metastases. Subsequently, a PET-guided biopsy of one FDG+/SSTR- liver metastasis was performed (**red arrow**, Fig. 6E), leading to the histologic diagnosis of NEC (Ki67 49.7%) and initiation of carboplatin-etoposide chemotherapy (Fig. 6G-L). In the SIRT group ($n=2$), AS was introduced because there was either no evidence of disease or only minimal extrahepatic FDG-MTV. Additionally, patients scheduled for AS and SSAs did not experience any modifications to their treatment plans. In summary, the findings from dual-tracer PET/CT scans directly impacted the therapy stratification of eleven patients (55%).

Discussion

In cases of high-proliferating NENs, adequate patient management often requires additional [^{18}F]FDG PET in conjunction with an SSTR-PET, as outlined in the ESMO clinical practice guidelines [7]. However, this has proven challenging to implement in routine clinical practice. Following the promising results of the recent NETTER2 trial in untreated G2 and G3 NEN patients (Ki67≥10%), PRRT may now be the treatment of choice for this population, which aligns with the patient cohort presented in this study. An accurate patient stratification will be necessary to better take advantage of this expensive treatment, where combined PET imaging with [^{18}F]FDG and radiolabeled SSAs can be of great importance.

Accordingly, the need for timely dual-tracer PET/CT scans for initial staging will increase. Due to the disadvantages of ^{68}Ge/^{68}Ga-generators involving high costs and low production yields, ^{18}F-labeled tracers, such as [^{18}F]SiFA*lin*-TATE, are on the rise [6]. Until now, due to the 109.8 min half-life of fluorine-18, the acquisition of two PET scans with ^{18}F-labeled radiotracers necessitates a second visit to a nuclear medicine center on a separate day. This would result in an additional burden for cancer patients, who are already under psychological and physical stress. Particularly in this subset of untreated, rapidly progressing NENs, an inappropriate delay in treatment initiation and characterization of tumor biology is a considerable issue. However,

Table 3 FDG-MTV and SSTR-MTV for each PET examination and implications of dual-tracer PET in therapy stratification

P.	FDG MTV (mL)	SSTR-MTV (mL)	G	Therapy concept before DT-PET	Therapy concept after DT-PET	Considered PET information by ITB
1	0	1,2	G2	PRRT	AS	Low SSTR + MTV
2	0	1090	G2	PRRT	PRRT	No discordant MTV (FDG+/STTR-)
3	0	0	G3	AS	AS	No MTV
4	16	0	G2	SIRT	AS	Low extrahepatic [^{18}F]FDG MTV
5	0	0	G3	SIRT	AS	No MTV
6	94,6	148	G3	Chx	Chx	FDG + disease; No discordant MTV (FDG+/STTR-)
7	130	0	G3	Chx	Chx Change	Discordant MTV (FDG+/STTR-)
8	568	31,4	G3	Chx	Chx Change	Predominant Discordant MTV (FDG+/STTR-)
9	0	0	G3	SSA	SSA	No MTV
10	3,8	72,8	G3	PRRT	PRRT	No discordant MTV (FDG+/STTR-); FDG + disease
11	1,3	0	G3	PRRT	Chx	Discordant MTV (FDG+/STTR-)
12	0,5	65,2	G2	PRRT + RS	PRRT + RS	No discordant MTV (FDG+/STTR-); FDG + disease
13	0	0	G3	AS	AS	No MTV
14	556	836	G3	PRRT	PRRT + RS	No discordant MTV (FDG+/STTR-); Extensive FDG + disease
15	212	12,8	G2	Chx	SIRT	Discordant MTV (FDG+/STTR-) liver predominant
16	23,2	0	G3	Chx	Surgery	Discordant MTV (FDG+/STTR-)
17	917	61,8	G3	Chx	Chx Change	Predominant Discordant MTV (FDG+/STTR-)
18	122	0	G3	Chx	Chx	Discordant MTV (FDG+/STTR-)
19	236	0	G3	Chx	Chx Change	Discordant MTV (FDG+/STTR-)
20	0	616	G3	Chx	Chx	No discordant MTV (FDG+/STTR-)

P. = Patient; G = Grading; DT-PET = dual-tracer PET; ITB = interdisciplinary tumor board; PRRT = peptide receptor radionuclide therapy; AS = active surveillance; SIRT = selective internal radiotherapy; Chx = Chemotherapy; SSA = somatostatin analogue

by exploiting the increased sensitivity of LAFOV PET/CT scanners, a significant injected activity reduction of the first administered radiotracer may shorten the interval between two separate PET examinations, providing a viable solution [18].

This work proposes a one-day dual-tracer protocol with a low activity [^{18}F]FDG and a standard activity [^{18}F]SiFA*lin*-TATE PET for patients with high-proliferating NENs. The protocol foresees a 10 min scan with reduced activity of 0.5 MBq/kg [^{18}F]FDG PET and a subsequent 5 min scan with 3.0 MBq/kg [^{18}F]SiFA*lin*-TATE PET.

Our findings demonstrated that tissue with high physiological glucose metabolism (myocardium and brain) without physiological SSTR expression showed no relevant residual activity in the second PET scan. In the case of the myocardium, the amount of assessable tracer uptake did not differ significantly from that in the blood pool, indicating that measured values correspond to blood pool activity. Furthermore, we analyzed the impact of the residual tumor ACTs of [^{18}F]FDG in the second scan. The estimated residual ACT of R20%, which considers the physical decay of fluorine-18 and a potential increase of [^{18}F]FDG uptake over time, resulted in an only minor percentual proportion of 6.8 ± 1.2% of the measured ACTs in the [^{18}F]SiFA*lin*-TATE PET. Both physiological uptake and tumor ACTs assessments illustrate that the potential residual activity has no significant influence on [^{18}F]SiFA*lin*-TATE semi-quantification, even considering this conservative approach. This is an essential aspect of the proposed protocol, as the accurate non-invasive assessment of SSTR expression is paramount for treatment stratification in NENs.

Regarding noise performance and image quality, we recommend using the UHS mode of the Biograph Vision Quadra for the low activity [^{18}F]FDG scan. The increased event statistics lead to a reduction in image noise (CoV of 13.3 ± 0.6% (UHS), 18.2% ± 0.7% (HS)), which outweighs the slight degradation of the spatial resolution due to the parallax error [28]. Furthermore, optimizing time intervals between examinations may be feasible, including approaches employing correction methods that account for the physical decay and tracer kinetics to mitigate the impact of tracer "spill-over".

In our patient cohort, 55% of patients had their management plans altered due to dual-tracer PET findings. This was mainly due to the identification of tumor lesions with discordant tracer uptake, which would not have been assessed

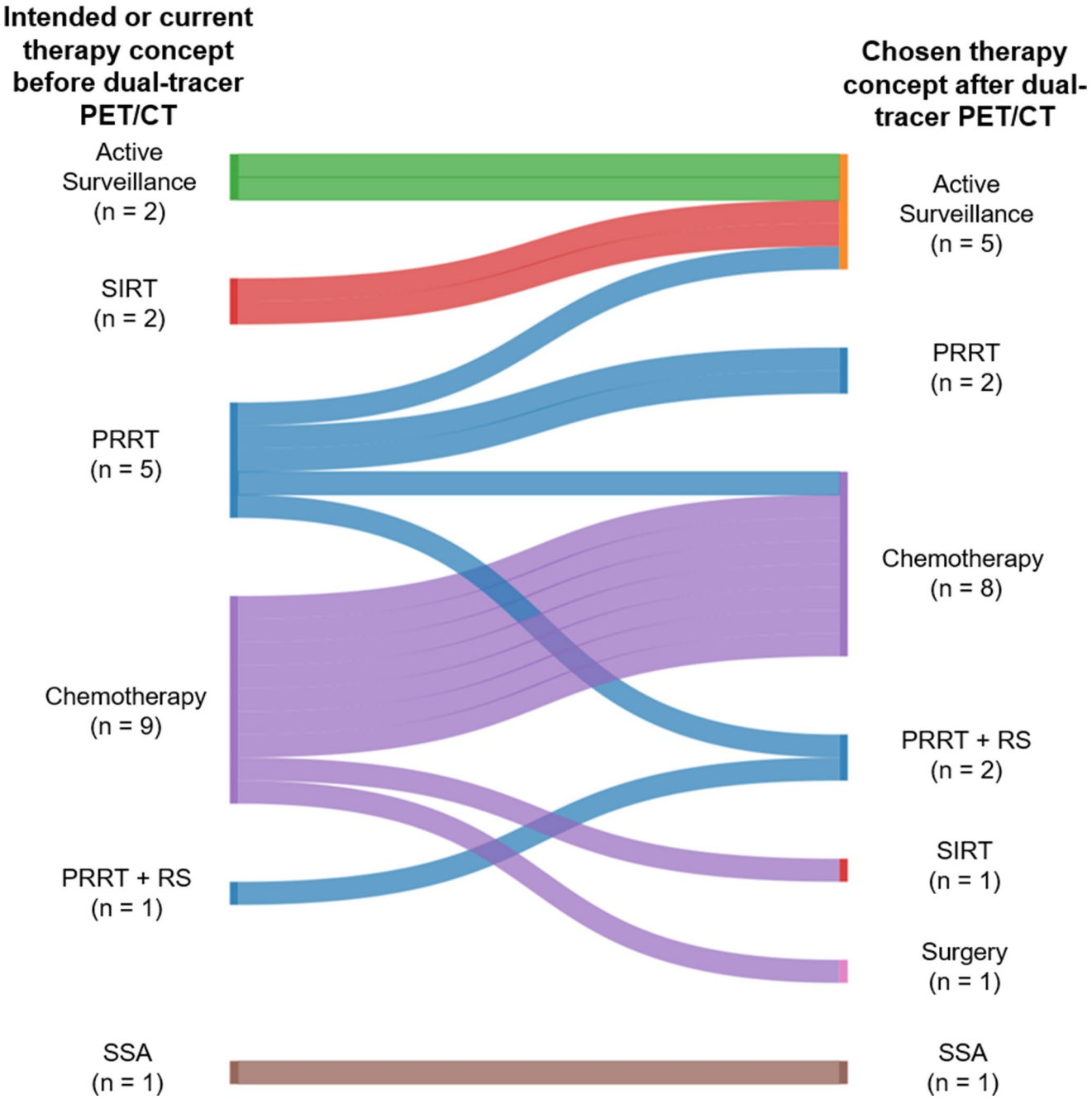

Fig. 4 A Sankey diagram illustrating the therapy stratification for patients undergoing dual-tracer PET/CT. 6/20 patients were initially assigned to PRRT ± RS. The initial treatment stratification was maintained in 3/6 patients while a change to therapy intensification was decided in 2/7 patients ($n = 1$ chemotherapy, 1 PRRT ± RS) and therapy de-escalation to AS in one patient. 2/9 patients in the chemotherapy group received locoregional treatments ($n = 1$ SIRT, $n = 1$ surgery), with the majority remaining in the chemotherapy approach. For both patients in the SIRT group, AS approaches were chosen due to the lack of evidence of active disease, whereas dual-tracer PET/CT scans were performed due to suspicious CT findings. SIRT = selective internal radiation therapy; PRRT = peptide receptor radionuclide therapy; RS = Radiosensitizing; SSA = somatostatin analogue; AS = active surveillance; CT = computed tomography

by SSTR-PET alone. This demonstrates the meaningful application of dual-tracer approaches in G2/G3 NENs and aligns with the findings of other studies demonstrating the importance of combining [^{18}F]FDG and SSTR-PET [13, 29].

Moreover, the assessment of metabolic and molecular tumor volume has shown to be a relevant prognostic factor [30–32], also when specifically evaluating discordant tumor volumes, i.e., consideration of only [^{18}F]FDG-avid disease without relevant SSTR expression, which is also related to

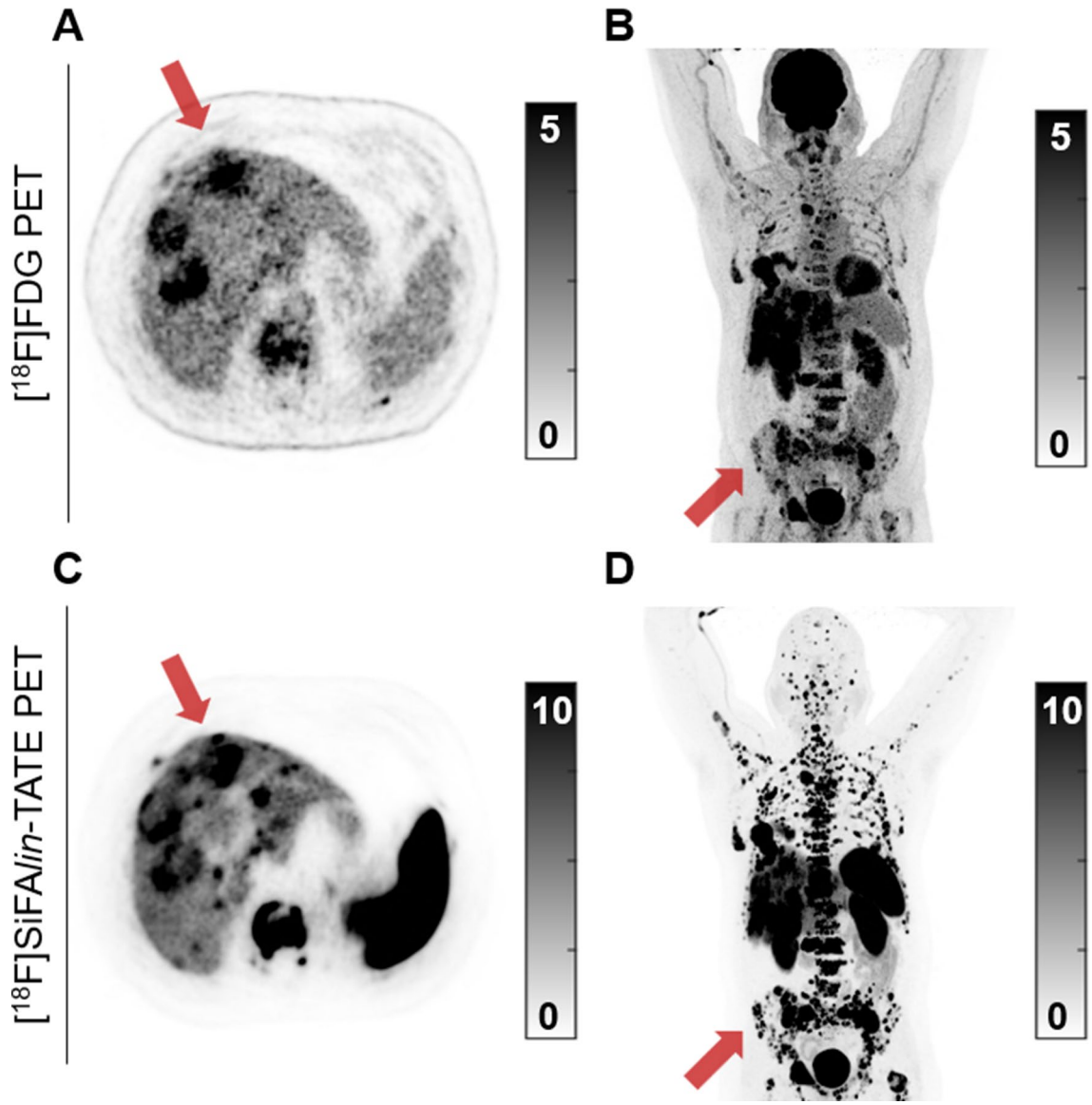

Fig. 5 Axial PET images and maximum intensity projections of the low activity [^{18}F]FDG PET (69 MBq) (**A**, **B**) and subsequent standard activity [^{18}F]SiFA*lin*-TATE PET (367 MBq) (**C**, **D**) of a patient with newly diagnosed CUP NET G2 (Ki67 13.4%). A significant tumor burden is noted in this patient (SSTR-MTV: 836 mL; FDG-MTV: 556 mL), predominantly affecting the liver and bones. Additionally, numerous lesions exhibit concordant uptake of both tracers (FDG+/SSTR+), highlighted by the **red arrows**, which suggests increased tumor aggressiveness and a poorer prognosis. Therefore, a more aggressive treatment plan combining PRRT with RS was recommended and subsequently administered

poorer overall survival in GEP-NENs [24]. Furthermore, as shown in the patient in Fig. 6, dual-tracer PET approaches may guide histologic sampling, allowing the identification of more aggressive tumor sites with increased glucose metabolism that will require more aggressive or multimodal therapeutic regimes. Our streamlined approach can benefit research and clinical studies and improve patient comfort while reducing the logistical challenges of dual-tracer PET examinations. On the patient's experience side, although a directed evaluation of patient comfort was not performed, on-site patient feedback was generally positive. This is especially relevant since, as an ENETS Center of Excellence, many patients have long travel times to our facility and often have to arrange solutions for related issues, such as companions in the case of sedation requirements due to claustrophobia or arranging childcare. Because of these issues, on-site patient feedback was generally positive since both examinations could be completed in one visit.

The proposed imaging procedure might also be applied to different radiotracers, including using radionuclides

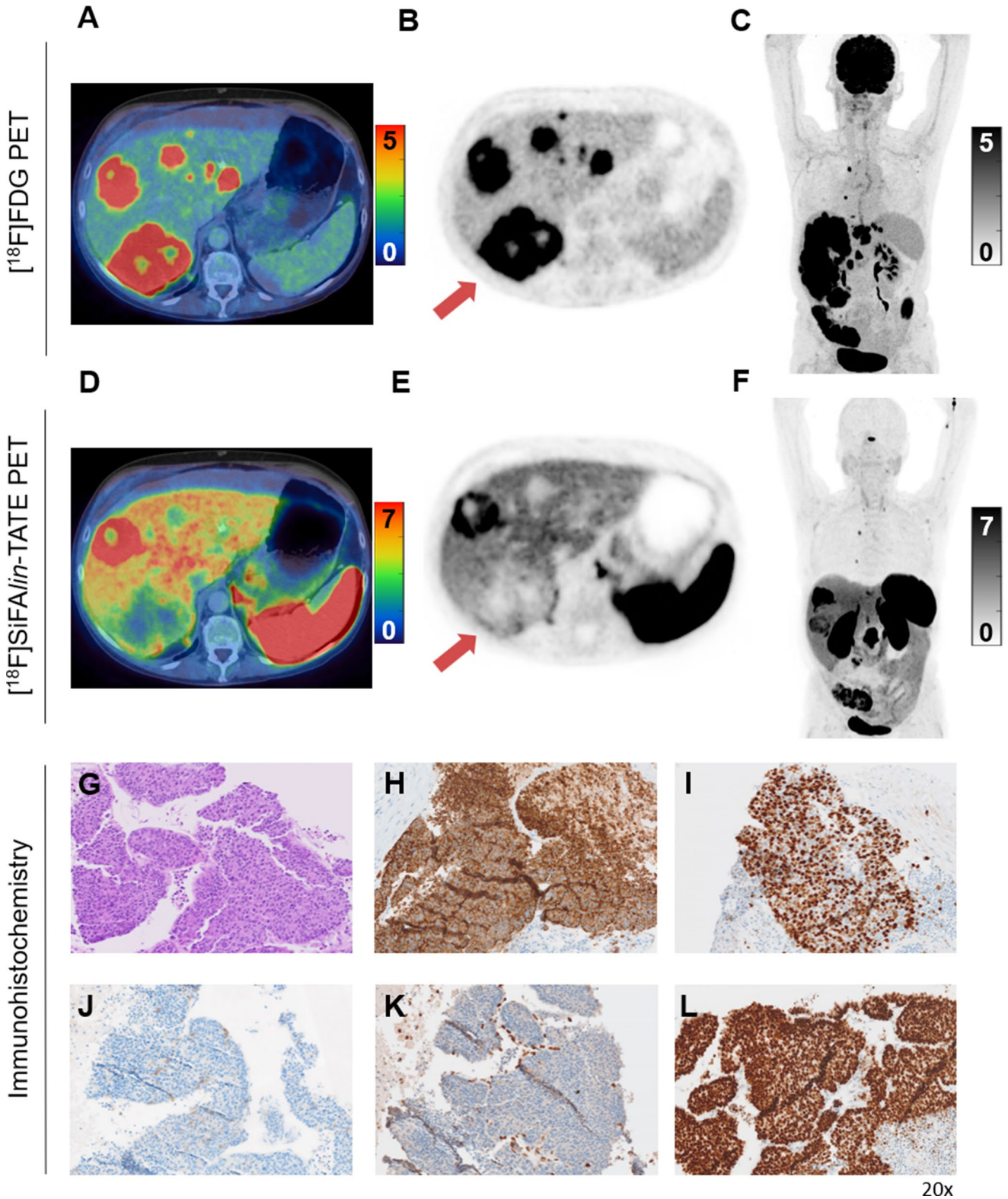

Fig. 6 Axial PET images and maximum intensity projections of low activity [^{18}F]FDG PET (27 MBq) (**A**-**C**) followed six hours later by a standard activity [^{18}F]SiFA*lin*-TATE PET (167 MBq) (**D**-**F**). In this 65-year-old female patient initially diagnosed with a G3 colon NET, a dual-tracer PET/CT was conducted following indications of progressive disease. To further evaluate tumor aggressiveness, a PET-targeted biopsy of a liver lesion exhibiting discordant tracer uptake was carried out (**red arrow**). Histopathological analysis with H&E staining (**G**), positivity for Synaptophysin (**H**), a Ki67 of 49.7% (**I**), negativity for SSTR2 (**J**), and a pathognomonic combination of RB loss (**K**) together with an abnormal p53 expression (**L**), confirmed tumor dedifferentiation into NEC

other than fluorine-18 or involving other tumor entities, such as prostate cancer, i.e., by combining [^{18}F]FDG and [^{18}F]PSMA-1007. The recent TheraP study highlighted the potential benefit of combining [^{18}F]FDG and PSMA-PET for treatment stratification and prognosis assessment since patients displaying [^{18}F]FDG-avid discordant disease generally showed a shorter median overall survival [33]. Regarding prostate cancer patients, a dual-tracer protocol in a single imaging session combining [^{68}Ga]Ga-PSMA-11 and [^{18}F]FDG has already been developed for the Biograph Vision Quadra by Alberts et al. [34], allowing the detection of mismatch lesions. However, this protocol differs significantly from the current study, as quantification of the second radiotracer is not achievable due to the short time interval between scans and the resulting radiotracer superimposition (low activity [^{18}F]FDG PET being performed 1 h after the conclusion of the PSMA-PET).

LAFOV PET/CT scanners are increasingly being installed in different hospitals worldwide because of their significantly increased sensitivity, leading to many clinical advantages. Several studies have shown that reductions of the injected activity are feasible using LAFOV PET scanners, which are undoubtedly worthwhile for pediatric examinations [35, 36]. Still, some critics question whether the reduction in radiation exposure may be negligible in adult oncological patients. However, performing two ^{18}F-labeled PET scans in one day could be considered a clinical "killer application" for LAFOV PET/CT scanners, facilitating quantifiable, one-day multi-tracer PET examinations. Furthermore, we deem scalability feasible due to the reduced acquisition times of low activity [^{18}F]FDG PET scans and the generally higher patient throughput that can be attained with LAFOV PET/CT scanners. Our study showed that the proposed protocol was feasible, even if the limited number of patients reported in this study must be considered a potential limitation.

Conclusion

Our study demonstrates that LAFOV PET scanners enable a one-day dual-tracer protocol with good image quality and preserved semi-quantification of two ^{18}F-labeled radiotracers. Our approach facilitates the assessment of tumor biology and tumor heterogeneity while reducing the logistical burden. In addition, we claim that one real advantage of low activity PET imaging is enabling one-day dual-tracer PET examinations.

Supplementary Information The online version contains supplementary material available at https://doi.org/10.1007/s00259-025-07073-w.

Acknowledgements The LAFOV PET/CT scanner was funded by the Deutsche Forschungsgemeinschaft (DFG, German Research Foundation) — INST 37/1145-1 FUGG, and the Deutsche Forschungsgemeinschaft (DFG, German Research Foundation) under Germany's Excellence Strategy — EXC 2180—390900677. Nils F. Trautwein was supported by the Clinician Scientist Program Tuebingen (525-0-0).

Author contributions E.C, H.D., C.lF., N.T., conceived and designed the study. E.C., N.T., L.K., A.B, C.R., M.H., H.D, C.lF., acquired the patient data and performed the medical evaluation. E.C, N.T., L.K., A.S., performed the image analysis and statistics. S.S. performed the histology staining. G.R. was in charge of tracer production. F.S., W.L., performed necessary additional image reconstructions. E.C, N.T., C.lF., F.S., L.K., wrote the first draft of the manuscript. All of the authors critically reviewed, read, and approved the final manuscript.

Funding Open Access funding enabled and organized by Projekt DEAL. The LAFOV PET/CT scanner was funded by the Deutsche Forschungsgemeinschaft (DFG, German Research Foundation) — INST 37/1145-1 FUGG, and the Deutsche Forschungsgemeinschaft (DFG, German Research Foundation) under Germany's Excellence Strategy — EXC 2180—390900677. Nils F. Trautwein was supported by the Clinician Scientist Program Tuebingen (525-0-0).

Data availability The datasets generated during and/or analyzed during the current study are available from the corresponding author on reasonable request.

Declarations

Ethics approval and informed consent The study was conducted according to the guidelines of the Declaration of Helsinki and approved by the Institutional Review Board of the University Hospital of Tuebingen (#082/2024BO2). Informed consent for study participation and publication was obtained from all individual participants included in the study.

Conflicts of interest Fabian P. Schmidt and Christian la Fougère have received research support from Siemens. Nils F. Trautwein reports personal fees from Novartis. All other authors have no conflicts of interest regarding this study to report.

References

1. Rindi G, Klimstra DS, Abedi-Ardekani B, et al. A common classification framework for neuroendocrine neoplasms: an International Agency for Research on Cancer (IARC) and World Health

Organization (WHO) expert consensus proposal. Mod Pathol Dec. 2018;31(12):1770–86. https://doi.org/10.1038/s41379-018-0110-y.
2. Rindi G, Mete O, Uccella S, et al. Overview of the 2022 WHO classification of neuroendocrine neoplasms. Endocr Pathol Mar. 2022;33(1):115–54. https://doi.org/10.1007/s12022-022-09708-2.
3. Zamora V, Cabanne A, Salanova R, et al. Immunohistochemical expression of somatostatin receptors in digestive endocrine tumours. Dig Liver Dis Mar. 2010;42(3):220–5. https://doi.org/10.1016/j.dld.2009.07.018.
4. Park S, Parihar AS, Bodei L, et al. Somatostatin Receptor Imaging and theranostics: current practice and future prospects. J Nucl Med Oct. 2021;62(10):1323–9. https://doi.org/10.2967/jnumed.120.251512.
5. Geijer H, Breimer LH. Somatostatin receptor PET/CT in neuroendocrine tumours: update on systematic review and meta-analysis. Eur J Nucl Med Mol Imaging Oct. 2013;40(11):1770–80. https://doi.org/10.1007/s00259-013-2482-z.
6. Leupe H, Ahenkorah S, Dekervel J, et al. (18)F-Labeled somatostatin analogs as PET Tracers for the somatostatin receptor: ready for clinical use. J Nucl Med Jun. 2023;64(6):835–41. https://doi.org/10.2967/jnumed.123.265622.
7. Pavel M, Oberg K, Falconi M, et al. Gastroenteropancreatic neuroendocrine neoplasms: ESMO Clinical Practice guidelines for diagnosis, treatment and follow-up. Ann Oncol Jul. 2020;31(7):844–60. https://doi.org/10.1016/j.annonc.2020.03.304.
8. Kuwabara H, Toriihara A, Yuasa-Nakagawa K, Toda K, Tateishi U, Yoshimura R. Prognostic value of metabolic tumor burden calculated using dual-time-point 18F-fluorodeoxyglucose positron emission tomography/CT in patients with oropharyngeal or hypopharyngeal cancer. Head Neck Jan. 2019;41(1):103–9. https://doi.org/10.1002/hed.25490.
9. Carlsen EA, Johnbeck CB, Loft M, et al. Semiautomatic tumor delineation for evaluation of (64)Cu-DOTATATE PET/CT in patients with neuroendocrine neoplasms: Prognostication based on lowest lesion uptake and total tumor volume. J Nucl Med Nov. 2021;62(11):1564–70. https://doi.org/10.2967/jnumed.120.258392.
10. Singh S, Halperin D, Myrehaug S, et al. [(177)Lu]Lu-DOTA-TATE plus long-acting octreotide versus high–dose long-acting octreotide for the treatment of newly diagnosed, advanced grade 2–3, well-differentiated, gastroenteropancreatic neuroendocrine tumours (NETTER-2): an open-label, randomised, phase 3 study. Lancet Jun. 2024;29(10446):2807–17. https://doi.org/10.1016/S0140-6736(24)00701-3.
11. Binderup T, Knigge U, Loft A, Federspiel B, Kjaer A. 18F-fluorodeoxyglucose positron emission tomography predicts survival of patients with neuroendocrine tumors. Clin Cancer Res Feb. 2010;1(3):978–85. https://doi.org/10.1158/1078-0432.CCR-09-1759.
12. Binderup T, Knigge U, Johnbeck CB, et al. (18)F-FDG PET is Superior to WHO Grading as a Prognostic Tool in neuroendocrine neoplasms and useful in guiding PRRT: a prospective 10-Year follow-up study. J Nucl Med Jun. 2021;1(6):808–15. https://doi.org/10.2967/jnumed.120.244798.
13. Chan DL, Pavlakis N, Schembri GP, et al. Dual Somatostatin Receptor/FDG PET/CT Imaging in metastatic neuroendocrine tumours: proposal for a Novel Grading Scheme with Prognostic significance. Theranostics. 2017;7(5):1149–58. https://doi.org/10.7150/thno.18068.
14. Ambrosini V, Caplin M, Castano JP, et al. Use and perceived utility of [(18) F]FDG PET/CT in neuroendocrine neoplasms: a consensus report from the European Neuroendocrine Tumor Society (ENETS) Advisory Board Meeting 2022. J Neuroendocrinol Jan. 2024;36(1):e13359. https://doi.org/10.1111/jne.13359.
15. Alberts I, Hunermund JN, Prenosil G, et al. Clinical performance of long axial field of view PET/CT: a head-to-head intra-individual comparison of the Biograph Vision quadra with the Biograph Vision PET/CT. Eur J Nucl Med Mol Imaging Jul. 2021;48(8):2395–404. https://doi.org/10.1007/s00259-021-05282-7.
16. Prenosil GA, Hentschel M, Weitzel T, et al. EARL compliance measurements on the biograph vision quadra PET/CT system with a long axial field of view. EJNMMI Phys Apr. 2022;8(1):26. https://doi.org/10.1186/s40658-022-00455-1.
17. Sachpekidis C, Pan L, Kopp-Schneider A, Weru V, Hassel JC, Dimitrakopoulou-Strauss A. Application of the long axial field-of-view PET/CT with low-dose [(18)F]FDG in melanoma. Eur J Nucl Med Mol Imaging Mar. 2023;50(4):1158–67. https://doi.org/10.1007/s00259-022-06070-7.
18. Calderon E, Schmidt FP, Lan W, et al. Image quality and quantitative PET parameters of low-dose [(18)F]FDG PET in a long Axial Field-of-view PET/CT scanner. Diagnostics (Basel) Oct. 2023;18(20). https://doi.org/10.3390/diagnostics13203240.
19. Boellaard R, Delgado-Bolton R, Oyen WJ, et al. FDG PET/CT: EANM procedure guidelines for tumour imaging: version 2.0. Eur J Nucl Med Mol Imaging Feb. 2015;42(2):328–54. https://doi.org/10.1007/s00259-014-2961-x.
20. Beyer L, Gosewisch A, Lindner S, et al. Dosimetry and optimal scan time of [(18)F]SiTATE-PET/CT in patients with neuroendocrine tumours. Eur J Nucl Med Mol Imaging Oct. 2021;48(11):3571–81. https://doi.org/10.1007/s00259-021-05351-x.
21. Lindner S, Wangler C, Bailey JJ, et al. Radiosynthesis of [(18)F]SiFAlin-TATE for clinical neuroendocrine tumor positron emission tomography. Nat Protoc Dec. 2020;15(12):3827–43. https://doi.org/10.1038/s41596-020-00407-y.
22. De Luca GMR, Habraken JBA. Method to determine the statistical technical variability of SUV metrics. EJNMMI Phys Jun. 2022;6(1):40. https://doi.org/10.1186/s40658-022-00470-2.
23. EFOMP Protocol for Quality Control in PET/CT and PET/MRI. Accessed May 22. 2023, https://www.efomp.org/index.php?r=news/view&id=277
24. Chan DL, Hayes AR, Karfis I, et al. [(18)F]FDG PET/CT-Avid discordant volume as a biomarker in patients with gastroenteropancreatic neuroendocrine neoplasms: a Multicenter Study. J Nucl Med Feb. 2024;1(2):185–91. https://doi.org/10.2967/jnumed.123.266346.
25. Trautwein NF, Schwenck J, Jacoby J, et al. Long-term prognostic factors for PRRT in neuroendocrine tumors. Front Med (Lausanne). 2023;10:1169970. https://doi.org/10.3389/fmed.2023.1169970.
26. Trautwein NF, Hinterleitner C, Kiefer LS, et al. Radiosensitizing Favors Response to peptide receptor Radionuclide Therapy in patients with highly proliferative neuroendocrine malignancies: preliminary evidence from a clinical pilot study. Clin Nucl Med. Mar 2024;1(3):207–14. https://doi.org/10.1097/RLU.0000000000005006.
27. Netzwerk Neuroendokrine Tumoren e V, Authors. Deutsche Gesellschaft für Gastroenterologie V-uS, S2k-Leitlinie Neuroendokrine Tumore. Practice guideline neuroendocrine tumors. *AWMF-Reg 021–27*. 2018/06/11 2018;56(06):583–681. https://doi.org/10.1055/a-0604-2924
28. Schmidt FP, Mannheim JG, Linder PM, et al. Impact of the maximum ring difference on image quality and noise characteristics of a total-body PET/CT scanner. Z Med Phys Oct. 2023;20. https://doi.org/10.1016/j.zemedi.2023.09.001.
29. Kaewput C, Vinjamuri S. Role of combined (68)Ga DOTA-Peptides and (18)F FDG PET/CT in the evaluation of

gastroenteropancreatic neuroendocrine neoplasms. Diagnostics (Basel) Jan. 2022;22(2). https://doi.org/10.3390/diagnostics12020280.
30. Langen Stokmo H, Aly M, Bowitz Lothe IM, et al. Volumetric parameters from [(18) F]FDG PET/CT predicts survival in patients with high-grade gastroenteropancreatic neuroendocrine neoplasms. J Neuroendocrinol Jul. 2022;34(7):e13170. https://doi.org/10.1111/jne.13170.
31. Chan DL, Bernard EJ, Schembri G, et al. High metabolic tumour volume on 18-Fluorodeoxyglucose Positron Emission Tomography predicts poor survival from neuroendocrine neoplasms. Neuroendocrinology. 2020;110(11–12):950–8. https://doi.org/10.1159/000504673.
32. Alevroudis E, Spei ME, Chatziioannou SN, et al. Clinical utility of (18)F-FDG PET in neuroendocrine tumors prior to peptide receptor Radionuclide Therapy: a systematic review and Meta-analysis. Cancers (Basel) Apr. 2021;10(8). https://doi.org/10.3390/cancers13081813.
33. Hofman MS, Emmett L, Sandhu S, et al. Overall survival with [(177)Lu]Lu-PSMA-617 versus cabazitaxel in metastatic castration-resistant prostate cancer (TheraP): secondary outcomes of a randomised, open-label, phase 2 trial. Lancet Oncol Jan. 2024;25(1):99–107. https://doi.org/10.1016/S1470-2045(23)00529-6.
34. Alberts I, Schepers R, Zeimpekis K, Sari H, Rominger A, Afshar-Oromieh A. Combined [68 Ga]Ga-PSMA-11 and low-dose 2-[18F]FDG PET/CT using a long-axial field of view scanner for patients referred for [177Lu]-PSMA-radioligand therapy. Eur J Nucl Med Mol Imaging Feb. 2023;50(3):951–6. https://doi.org/10.1007/s00259-022-05961-z.
35. Mingels C, Spencer BA, Nalbant H, et al. Dose reduction in Pediatric Oncology patients with delayed total-body [(18)F]FDG PET/CT. J Nucl Med Jul. 2024;1(7):1101–6. https://doi.org/10.2967/jnumed.124.267521.
36. van Rijsewijk ND, van Leer B, Ivashchenko OV, et al. Ultra-low dose infection imaging of a newborn without sedation using long axial field-of-view PET/CT. Eur J Nucl Med Mol Imaging Jan. 2023;50(2):622–3. https://doi.org/10.1007/s00259-022-05979-3.

Authors and Affiliations

Eduardo Calderón[1] · Lena S. Kiefer[1] · Fabian P. Schmidt[1,2] · Wenhong Lan[1] · Andreas S. Brendlin[3] · Christian P. Reinert[3] · Stephan Singer[4] · Gerald Reischl[2,7] · Martina Hinterleitner[5,6,7] · Helmut Dittmann[1,6] · Christian la Fougère[1,6,7,8] · Nils F. Trautwein[1,6]

Christian la Fougère
christian.lafougere@med.uni-tuebingen.de

Eduardo Calderón
eduardo.calderon-ochoa@med.uni-tuebingen.de

1 Nuclear Medicine and Clinical Molecular Imaging, University Hospital Tuebingen, Otfried-Mueller-Str. 14, 72076 Tuebingen, Germany

2 Werner Siemens Imaging Center, Preclinical Imaging and Radiopharmacy, Eberhard-Karls University, Roentgenweg 13, 72076 Tuebingen, Germany

3 Diagnostic and Interventional Radiology, University Hospital Tuebingen, Hoppe-Seyler-Str. 3, 72076 Tuebingen, Germany

4 Department of Pathology, University Hospital Tuebingen, Liebermeisterstr. 8, 72076 Tuebingen, Germany

5 Medical Oncology and Pneumology (Internal Medicine VIII), University Hospital Tuebingen, Otfried- Mueller-Str. 14, 72076 Tuebingen, Germany

6 University Hospital Tuebingen, ENETS Center of Excellence, Otfried-Mueller-Str. 14, 72076 Tuebingen, Germany

7 DFG Cluster of Excellence 2180 'Image-Guided and Functional Instructed Tumor Therapy' (iFIT), University of Tuebingen, Roentgenweg 11, 72076 Tuebingen, Germany

8 German Cancer Consortium (DKTK), German Cancer Research Center (DKFZ) Partner Site Tuebingen, Auf der Morgenstelle 15, 72076 Tuebingen, Germany

3. Discussion

With the introduction of LAFOV PET/CT scanners, multiple novel PET applications appear to be within reach of clinical translation, marking an exciting era for diagnostic nuclear medicine. This work had two complementary aims: first, to develop and establish a practical low-dose [^{18}F]FDG PET/CT protocol that preserves diagnostic performance and semi-quantitative robustness comparable to a standard full-dose [^{18}F]FDG PET examination; and second, to leverage the significant reduction in applied [^{18}F]FDG activity to establish a clinically feasible one-day dual-tracer PET examination by pairing an initial low-activity [^{18}F]FDG scan with a standard-dose SSTR-PET/CT for NEN patients, thereby evaluating the clinical impact of dual-tracer PET findings on patient management. However, the generated data and evidence could also be useful for establishing other clinical applications, such as low-dose [^{18}F]FDG PET in pediatric examinations and pregnant patients, oncology screening(Slart, Tsoumpas et al. 2021), and multi-tracer examinations beyond NEN.

3.1 Why do we need low-dose PET examinations?

As previously mentioned, these scanners provide a significant increase in sensitivity, enabling high-quality PET images even in low-count scenarios, such as PET with reduced tracer activity or ultra-fast examinations. A feasible low-dose [^{18}F]FDG PET protocol opens up several additional applications that have not yet been considered due to radiation safety concerns, such as PET imaging of pregnant women. The group of Korshol et al.(Korsholm, Aleksyniene et al. 2023) examined a 30-week pregnant female patient with breast cancer using a dose of 24 MBq of [^{18}F]FDG (or 1/10 of the standard applied dose of 3.0 MBq/kg) with a scan time of 30 minutes. This chosen protocol resulted in excellent-quality PET images, enabling adequate staging of the malignant disease. Thereby, including the radiation exposure coming from the low-dose CT component, the female patient received 1.4 mSv. In comparison, the fetus received only about 1 mSv, suggesting that low-dose PET imaging can be used in complex scenarios for

staging cancer patients during pregnancy without significant radiation exposure. Although promising, the results in this study were achieved with a considerably long scan time of 30 minutes. A similar case series was published by Smith et al., in which two pregnant women in the second and third trimester underwent low-dose [^{18}F]FDG PET for oncological staging. As in the protocol of Korsholm et al., 1/10 of the standard dose (0.3 MBq/kg of [^{18}F]FDG) was administered, with a slightly shorter scan time of 20 minutes. Here, excellent image quality sufficient for staging was also reported, with an estimated maximum fetal radiation exposure of 0.44 mGy, notably lower than in similar studies performed on SAFOV PET/CT scanners, which reported a mean fetal radiation exposure of 1.82±0.55 mGy (Smith, Yaqub et al. 2024).

These case series demonstrate the potential of LAFOV PET to evaluate and reduce fetal radiation exposure during clinically necessary staging of pregnant oncology patients. Nonetheless, with the limited number of patients examined, there isn't sufficient evidence to establish a standard for clinical practice, and these studies mainly serve as proof of principle. In particular, the clinical scenario of required oncological staging during pregnancy, although complex, is rare, with an incidence of 1 per 1,000-2,000 pregnancies(Schwab, Anic et al. 2021). However, due to increasing maternal age in developed countries, the prevalence of cancer during pregnancy is rising(Van Calsteren, Heyns et al. 2010), implying that the need for such examinations may increase in the future.

In pediatric cases, depending on the clinical context or patient age, one could perform a low-dose PET examination with a relatively short scan time or administer a standard tracer activity and perform a fast examination, thereby avoiding the need for sedation. In a case report, Reichkendler et al. performed a sedation-free PET examination with a standard dose of [^{18}F]FDG (3.0 MBq/kg) in a 17-month-old girl with incomplete Kawasaki disease(Reichkendler, Andersen et al. 2022). In this case, the scan duration was 5 minutes. Thereafter, additional reconstructions were performed using the first 120 seconds of the scan, as the patient showed little to no movement during this time frame. The resulting images

were of good quality, and the protocol demonstrated that these scanners may also allow avoidance of sedation for PET examinations, thereby reducing the logistical difficulties associated with it. Furthermore, van Rijsewijk et al. examined a 10-week-old newborn with sepsis of unknown origin using a protocol with an applied [^{18}F]FDG activity of 12 MBq and a scan time of 3 min without sedation. Thereafter, the source of the infection could be localized, including a septic thrombus in the right atrium. These LAFOV PET-enabled approaches promise to revolutionize pediatric PET imaging by reducing radiation exposure and eliminating the need for sedation(van Rijsewijk, van Leer et al. 2023).

Even though these approaches exemplify the possibilities, they do not provide sufficient data to establish a clinically feasible protocol. In the previously published analysis(Calderon, Schmidt et al. 2023), we systematically evaluated subjective image quality, lesion detection rates, noise performance, and changes in SUV across simulated PET images in both HS and UHS modes with reduced [^{18}F]FDG doses of 1.0, 0.5, 0.25, and 0.125 MBq/kg, compared with standard PET images at 3.0 MBq/kg. This assessment was performed on the Biograph Vision Quadra PET/CT scanner and evaluated 26 oncology patients. Evaluated PET images had a scan duration of 5 minutes. The analysis demonstrated that 1.0 MBq/kg PET images preserved diagnostic performance, with 100% lesion detection rates, and displayed acceptable noise levels when reconstructed in the UHS mode with a CoV of 13.0 $\pm$ 1.3% (compared to the recommended CoV% of the EFOMP $<$15.0%)(Calderon, Schmidt et al. 2023). At 0.5 MBq/kg, a few small lesions were missed, with lesion detection rates of 95% and 98% in HS and UHS modes, respectively. Furthermore, of the three evaluated SUV metrics (SUVmax, SUVmean, and SUVpeak), only SUVmax showed significant differences, and only between PET images with 3.0 MBq/kg and 0.125 MBq/kg in HS mode(Calderon, Schmidt et al. 2023). This was, to some extent, expected, since SUVmax can be strongly affected by increased noise and by worsened count statistics, as is the case in PET images with only 1/24 of the standard applied activity. Therefore, both SUVmean and SUVpeak are more robust metrics for semi-quantification in low-count imaging scenarios.

Considering all evaluated parameters, a [^{18}F]FDG activity dose of 0.5 MBq/kg with a scan time of 10 minutes was found to be a potentially practicable low-dose [^{18}F]FDG PET protocol for our proposed dual-tracer protocol. The prolonged scan time, compared to the 5-minute examination performed in the study, was introduced to ensure that the resulting count statistics reflect those from a 5-minute scan at 1.0 MBq/kg, as in our study. Moreover, to our knowledge, this work represents the first systematic evaluation of the effects of reduced [^{18}F]FDG activity on diagnostic performance and radiotracer semi-quantification in both sensitivity modes for the Biograph Vision Quadra system (Calderon, Schmidt et al. 2023).

Regarding radiation safety, using this aforementioned protocol and the ICRP coefficient for [^{18}F]FDG (~0.019 mSv/MBq), a low-dose [^{18}F]FDG PET coupled with a low-dose CT scan would yield approximately a 0.8 mSv radiation exposure for a whole-body PET/CT examination from the skull apex to the mid-thighs in a 70-kg patient (35 MBq [^{18}F]FDG activity). Thereby, approximately 0.6 mSv would come from the PET examination. Given this substantial decrease in radiation exposure, these protocols might also be suitable for widespread screening of patients in high-risk groups, providing a comprehensive assessment through a whole-body PET/CT scan at a “cost” well below half the average annual background dose of 2.1 mSv in Germany(BfS 2024). In this context, some groups have already proposed blood sampling to assess molecular markers, combined with [^{18}F]FDG PET/CT, as a screening approach to facilitate the detection and localization of malignancies in high-risk populations without a prior cancer diagnosis(Lennon, Buchanan et al. 2020).

Although LAFOV PET systems may facilitate such screening concepts concerning radiation exposure and image quality for low-dose whole-body [^{18}F]FDG PET examinations, translating technical feasibility into routine use depends on other factors, including health-economic value. Such a screening strategy must first demonstrate that earlier detection changes management and outcomes. Furthermore, reimbursement remains a practical barrier: coverage

policies differ markedly across health systems, hospital clinics, and countries, and may depend on the indication, referral pathway, and whether the scan is performed in a hospital or at an outpatient PET/CT center. Therefore, implementation should be restricted to well-defined high-risk cohorts and malignancy types. Prospective studies would then also be required to evaluate budget impact and cost-benefit endpoints.

In summary, our findings provided the groundwork for the evaluation and clinical implementation of various low-dose [^{18}F]FDG PET applications. Nonetheless, we considered that the main novel use of a low-dose [^{18}F]FDG PET would be to enable one-day dual-tracer protocols using two ^{18}F-labeled radiotracers, in this case combining [^{18}F]FDG and [^{18}F]SiTATE, also known as [^{18}F]SiFA*lin*-TATE, for comprehensive molecular imaging in NEN patients.

3.3. Assessing tumor heterogeneity with one-day dual-tracer PET examinations in NEN

As previously mentioned, NENs are a heterogeneous group of rare tumors that can arise from almost any anatomical site but are most often found in the gastroenteropancreatic tract and the lung, with both sites together accounting for around 80-85% of NEN origins(Nordstrand, Lea et al. 2025). According to the 2022 WHO classification, NENs are primarily classified by histopathological grade as well-differentiated NET or poorly differentiated NEC. NETs are further classified by proliferation activity, with tumors designated as G1, G2, or G3 based on Ki67 proliferation indices of <3%, 3-20%, and more than 20%, respectively. NEC can be further categorized into small cell and large cell NEC(Rindi, Mete et al. 2022).

The therapeutic landscape and prognosis of these tumor entities can vary widely depending on tumor grade, primary tumor site, and clinical stage, with a typically worse prognosis in higher-grade tumors and in the presence of metastatic disease(Polee, Hermans et al. 2022). NEC has the worst prognosis among all

NENs, including NET G3(Sorbye, Hjortland et al. 2025). For example, a population-based analysis of survival probabilities for patients with pancreatic NEN through the German Cancer Registry data from 2017-2021 showed that NET G1 patients have a 5-year relative survival of 88%, which is excellent compared with the relative survival of 37% and 9% for NET G3 and NEC, respectively(Stang, Wellmann et al. 2024). Furthermore, in the same study, the overall 5-year relative survival for all NET tumors with localized disease was excellent at 92.8%, whereas the presence of distant metastatic disease considerably reduced survival to 45%. In comparison, a similar evaluation in patients with colorectal NETs showed that rectal NETs had a better overall 5-year relative survival rate of 95.9%, and of 54% if evidence of distant metastasis was present (Moller, Szentkiralyi et al. 2025). This places the histologic subtype, Ki67, initial clinical stage, and primary tumor location as useful prognostic factors for risk stratification of NEN patients(Man, Wu et al. 2018, Tao, Xue et al. 2023, Lagana, Gallo et al. 2025). Therefore, the clinical management of this heterogeneous patient group requires accurate staging and ongoing assessment of tumor biology and heterogeneity to enable optimal therapy stratification.

In this regard, molecular imaging with SSTR-PET/CT is a diagnostic tool with high sensitivity and specificity for staging patients with well-differentiated NETs(Park, Parihar et al. 2021). It can also provide prognostic information. Studies have demonstrated that patients with NEN tumor lesions exhibiting higher SSTR expression, as evidenced by higher SUVmax values on SSTR-PET, have a better prognosis than those with evidence of tumor disease with lower or missing SSTR expression(Campana, Ambrosini et al. 2010, Refardt, Zandee et al. 2020). The proposed hypothesis to explain the worse clinical outcome is that the amount of SSTR expression correlates with tumor grade, meaning that SSTR-negative tumor lesions indicate a higher grade and, consequently, a more aggressive tumor biology(Chan, Moseley et al. 2019). This places SSTR-PET imaging at the forefront for the in vivo whole-body assessment of SSTR expression in NEN patients and is the current gold standard for staging and therapy stratification, especially before SSA-targeted therapies, such as PRRT.

However, the presence of SSTR-negative disease cannot be reliably assessed by SSTR-PET alone, which is why many authors have evaluated the complementary use of [^{18}F]FDG PET/CT to assess the SSTR-negative tumor burden and its potential role in risk stratification and patient prognosis. [^{18}F]FDG PET is not routinely used for staging well-differentiated NET, since the majority of these tumors are considered slow-growing or indolent, and therefore have a low glycolytic activity. Nonetheless, due to the increased likelihood of [^{18}F]FDG avid disease that correlates with higher tumor grade and increased tumor dedifferentiation(Rinzivillo, Partelli et al. 2018, Liu, Li et al. 2020), the ENETS and ESMO clinical NEN guidelines include an optional recommendation for the use of [^{18}]FDG PET in patients with Ki67 >10% NET G2, NET G3, and NEC(Sundin, Arnold et al. 2017, Pavel, Oberg et al. 2020). Through these dual-tracer approaches, combining [^{18}]FDG with SSTR-PET, it is possible to non-invasively assess the tumor biology at any given time point during the clinical course of NEN patients.

Chan et al. developed a scoring system, the so-called NETPET score, using a small retrospective cohort of NET G1-G3 patients (*n* = 62). The score categorizes dual-tracer PET/CT findings into labels ranging from P1 to P5. Specifically, P1 indicates only SSTR-positive tumor burden without [^{18}F]FDG-avid disease; P2-4 categorize different ranges of SSTR positivity and [^{18}F]FDG-positive tumor lesions; and P5 indicates only [^{18}F]FDG-avid disease without any SSTR-positive lesions(Chan, Pavlakis et al. 2017). The score was then validated in a larger multi-center NET cohort of 319 patients, in which patients with a scoring label of P1 had a significantly longer overall survival (OS) of 101.8 months compared to patients with a scoring label of P5 (OS = 11.5 months)(Chan, Hayes et al. 2023). Furthermore, recent studies evaluating SUV-based analysis using the total [^{18}F]FDG-positive MTV in advanced GEP-NET patients have shown that this metric is highly effective for identifying high-risk patients with potentially worse clinical outcomes. In a study evaluating 231 NET G1-G3 patients with a median follow-up of 27 months, the group with high [^{18}F]FDG MTV had an OS of 23.8

months, whereas the group with low [^{18}F]FDG MTV did not reach endpoint(Chan, Hayes et al. 2025).

Although the evidence supporting the use of [^{18}F]FDG PET/CT in NEN patients is growing, its regular implementation in clinical practice faces challenges. As previously mentioned, such dual-tracer PET/CT examinations combining [^{18}F]FDG with either ^{18}F- or ^{68}Ga-labelled SSAs require separate imaging days to preserve tracer semi-quantification. This requires two visits to PET/CT centers by usually frail oncology patients, increasing the burden related to diagnostic examinations, which can be even greater for patients who may require sedation due to claustrophobia or premedication due to allergies to contrast material. All of these logistical factors have hampered widespread implementation. As previously mentioned, some dual-tracer protocols have been proposed for other tumor entities, where sequential [^{68}Ga]Ga-PSMA-11 and [^{18}F]FDG PET examinations are performed in a single imaging session for prostate cancer patients before radioligand therapy(Alberts, Schepers et al. 2023), enabling the detection of tracer “mismatches”, that is, PSMA-negative and [^{18}F]FDG-positive tumor lesions. However, SUV-based estimates of the entire [^{18}F]FDG-positive tumor burden are not possible due to tracer superimposition, thereby losing valuable information.

Our proposed approach aimed to preserve semi-quantitative analysis of the two independent tracers, to perform two high-quality PET/CT examinations in a single visit, and to assess the influence of dual-tracer PET findings on patient management, as previously reported(Calderon, Kiefer et al. 2025). To perform this, we first acquired a low-dose [^{18}F]FDG PET scan with an applied activity of 0.5 MBq/kg (10-minute scan time), followed by an SSTR-PET/CT with [^{18}F]SiTATE with 3.0 MBq/kg in 20 NEN G2 and G3 patients. To estimate the influence of residual [^{18}F]FDG in the second scan, we assessed the activity concentrations in organs with physiological [^{18}F]FDG uptake, namely the brain and myocardium, as well as in all assessed tumor lesions. Following this, we estimated the residual activity concentrations by accounting for the decay of

fluorine-18 and the shortest time interval between the two independent PET examinations, approximately 5 hours. This assessment showed that the [^{18}F]FDG minimal residual activity concentrations present at the time point of the second examination had no relevant influence on the semi-quantification of [^{18}F]SiTATE(Calderon, Kiefer et al. 2025). Visual assessments of the brain and myocardium also supported these results. With preserved semi-quantification of both radiotracers, lesions could then be easily categorized as [^{18}F]FDG-positive or SSTR-negative (or vice versa), followed by complete estimations of [^{18}F]FDG-MTV and SSTR-MTV. Moreover, in 80% of patients, at least one tumor lesion exhibited increased [^{18}F]FDG uptake, and 45% showed tumor lesions with discordant tracer uptake ([^{18}F]FDG-positive, SSTR-negative)(Calderon, Kiefer et al. 2025). Based on the detection of total tumor burden by this dual-tracer assessment, 55% of patients had changes in their chosen therapy concepts prior to dual-tracer PET. Furthermore, the resulting mean CoV of PET images with 0.5 MBq/kg (10-minute scan time) in UHS mode was 13.2±2.8%, similar to the value reported in our first assessment of simulated low-dose [^{18}F]FDG PET images with 1.0 MBq (5-minute scan time) of 13.1±1.3%, which confirmed our results regarding low-dose performance(Calderon, Kiefer et al. 2025).

These results demonstrated, for the first time, the feasibility of a dual-tracer PET/CT protocol that preserves the diagnostic quality of PET examinations performed on two separate days, thereby also establishing the groundwork for other low-dose [^{18}F]FDG PET applications. Although the effects of dual-tracer PET on long-term survival in NEN patients were not evaluated in this work, this streamlined approach represents a step toward implementing dual-tracer PET in daily medical practice, improving personalized treatment in the era of precision oncology, while also facilitating the evaluation of these long-term effects in future prospective studies.

3.7 Outlook

This work developed a clinically feasible low-dose [^{18}F]FDG PET/CT examination and a one-day dual-tracer PET/CT protocol, both achieved using a highly conservative approach. In the following studies, the time interval between PET examinations could be further optimized. Modifications to the low-dose [^{18}F]FDG PET protocol that shorten the total examination time of both PET scans could support this optimization. Further reductions in administered activity could be feasible by either prolonging scan time or improving the diagnostic performance of these ultra-low-dose PET examinations with novel AI-denoising algorithms. Furthermore, several other oncological diseases, such as prostate cancer, may benefit from the proposed dual-tracer PET assessment, and our streamlined approach opens the way for a straightforward evaluation of the potential clinical impact in these other tumor entities.

3.8 Conclusions

LAFOV PET/CT scanners enable substantial reductions in administered radiotracer activity without compromising semi-quantification of the tracer or diagnostic performance, thereby establishing feasible low-dose [^{18}F]FDG PET examinations. Within this framework, a one-day dual-tracer PET examination with preserved semi-quantification of two ^{18}F-labelled radiotracers is technically feasible and facilitates optimal therapy stratification of NEN patients. These strategies reduce radiation dose, simplify patient care, and enable comprehensive in vivo assessment of tumor biology and heterogeneity.

4. Summary

This cumulative dissertation investigated how the markedly increased sensitivity of long axial field-of-view (LAFOV) PET/CT can be translated into clinically feasible low-dose [^{18}F]FDG PET protocols and how such protocols can be exploited to enable one-day dual-tracer PET examinations combining two ^{18}F-labelled radiotracers, while preserving diagnostic performance and semi-quantitative reliability.

The first part of this work established a low-dose [^{18}F]FDG PET/CT protocol on a LAFOV PET/CT scanner, the Biograph Vision Quadra. In 26 oncology patients, simulated [^{18}F]FDG PET images reflecting various reduced activity doses (1.0, 0.5, 0.25, and 0.125 MBq/kg) were systematically compared with a standard activity dose of 3.0 MBq/kg. Image quality, lesion detectability, noise performance, and changes of SUVmax, SUVmean, and SUVpeak were assessed. [^{18}F]FDG PET images at 1.0 MBq/kg preserved diagnostic performance, with acceptable noise levels in images reconstructed in the UHS mode. At 0.5 MBq/kg, lesion detectability remained high with only minor losses of small lesions. SUVmax showed a tendency to increase in PET images with significantly reduced applied activity, whereas SUVmean and SUVpeak remained stable. Based on these findings, a practical low-dose protocol of 0.5 MBq/kg with a prolonged 10-minute acquisition in UHS mode was defined, corresponding to a PET-related radiation exposure of approximately 0.6 mSv and a total PET/CT exposure of about 0.8 mSv when combined with low-dose CT.

The second part adapted this low-dose [^{18}F]FDG PET protocol into a one-day dual-tracer PET/CT workflow for NEN patients, in which the combined assessment of SSTR expression and glycolytic activity is clinically relevant but is usually performed on separate imaging days. Twenty patients with NEN G2/G3 underwent low-dose [^{18}F]FDG PET/CT (0.5 MBq/kg, 10-minute acquisition), followed by standard-dose [^{18}F]SiTATE PET/CT (3.0 MBq/kg) after a minimal time interval of three and a half hours. Estimated residual [^{18}F]FDG activity at the time of the second scan was evaluated in physiological reference organs and tumour

lesions, accounting for radioactive decay of fluorine-18 and time elapsed between examinations. Maximal estimated residual activity concentrations had no relevant influence on visual interpretation or SUV-based semi-quantification of [^{18}F]SiTATE, allowing both examinations to be interpreted as independent datasets. Most patients exhibited FDG-avid disease, and nearly half showed discordant lesions with FDG positivity and absent SSTR expression, reflecting clinically relevant tumour heterogeneity. Dual-tracer findings were associated with changes in therapeutic management in more than half of the patients.

In conclusion, LAFOV PET/CT enables substantial reductions in injected [^{18}F]FDG activity while maintaining diagnostic and semi-quantitative performance. This capability can be translated into a robust one-day dual-tracer PET/CT protocol using two ^{18}F-labelled radiotracers without compromising semi-quantification. The approach reduces radiation exposure and patient burden and enables a more comprehensive in vivo assessment of tumour biology with direct clinical impact. Future work should focus on further optimizing acquisition times and inter-scan intervals, evaluating additional dose reductions, validating clinical impact in larger prospective cohorts, and extending this concept to other oncologic entities where multiparametric PET imaging may be relevant.

5. German Summary

Diese kumulative Dissertation untersuchte, wie die deutlich erhöhte Sensitivität von PET/CT-Geräten mit langem axialem Sichtfeld (LAFOV) in klinisch praktikable Low-Dose-[^{18}F]FDG-PET-Protokolle umgesetzt werden kann und wie solche Protokolle eingesetzt werden können, um Ein-Tages-Dual-Tracer-PET-Untersuchungen zu ermöglichen, bei denen zwei ^{18}F-markierte Radiotracer kombiniert werden, während die diagnostische Leistung und die semiquantitative Zuverlässigkeit erhalten bleiben.

Im ersten Teil dieser Arbeit wurde ein Low-Dose-[^{18}F]FDG-PET/CT-Protokoll für den LAFOV-PET/CT-Scanner Biograph Vision Quadra etabliert. Bei 26 onkologischen Patienten wurden [^{18}F]FDG-PET-Bilder, die verschiedene reduzierte Aktivitätsdosen (1,0, 0,5, 0,25 und 0,125 MBq/Kg/KG) widerspiegeln, systematisch mit einer Standardaktivitätsdosis von 3,0 MBq/Kg/KG verglichen. Die Bildqualität, die Detektion von Tumorläsionen, das Bildrauschverhalten sowie die Veränderungen von SUVmax, SUVmean und SUVpeak wurden bewertet. [^{18}F]FDG-PET-Bilder bei 1,0 MBq/Kg/KG behielten ihre diagnostische Leistungsfähigkeit bei, wobei die Rauschwerte in den im UHS-Modus rekonstruierten Bildern akzeptabel waren. Bei 0,5 MBq/Kg/KG blieb die Detektionsrate von Läsionen erhalten, mit nur geringfügigen Verlusten bei kleinen Läsionen. SUVmax zeigte eine Tendenz zur Zunahme in den PET-Bildern mit deutlich reduzierter [^{18}F]FDG-Aktivität, während SUVmean und SUVpeak stabil blieben. Auf der Grundlage dieser Ergebnisse wurde ein Low-Dose-PET-Protokoll mit 0,5 MBq/Kg/KG und einer verlängerten 10-minütigen Aufnahme im UHS-Modus definiert, was einer PET-bezogenen Strahlenexposition von etwa 0,6 mSv und einer Gesamt-PET/CT-Exposition von etwa 0,8 mSv in Kombination mit einer Low-Dose-CT entspricht.

Im zweiten Teil wurde dieses Low-Dose-[^{18}F]FDG-PET-Protokoll in einen eintägigen Dual-Tracer-PET/CT-Workflow für NEN-Patienten adaptiert, bei dem die kombinierte Beurteilung der SSTR-Expression und des Glukosestoffwechsels

klinisch relevant ist, jedoch in der Regel an getrennten Bildgebungstagen erfolgt. 20 Patienten mit NEN G2/G3 wurden einer Low-Dose-[^{18}F]FDG-PET/CT (0,5 MBq/kg, 10-minütige Aufnahme) unterzogen, gefolgt von einer Standarddosis [^{18}F]SiTATE-PET/CT (3,0 MBq/kg) nach einem Mindestzeitintervall von 3,5 Stunden. Die geschätzte Restaktivität von [^{18}F]FDG zum Zeitpunkt der zweiten Untersuchung wurde in physiologischen Referenzorganen und Tumorläsionen unter Berücksichtigung des radioaktiven Zerfalls von Fluor-18 sowie der zwischen den Untersuchungen verstrichenen Zeit bewertet. Die maximal geschätzten Restaktivitätskonzentrationen hatten keinen relevanten Einfluss auf die visuelle Interpretation oder die SUV-basierte Semiquantifizierung von [^{18}F]SiTATE, sodass beide Untersuchungen als unabhängige Datensätze interpretiert werden konnten. Die meisten Patienten wiesen [^{18}F]FDG-avide Tumorläsionen auf, und fast die Hälfte zeigte diskordante Läsionen mit [^{18}F]FDG-Positivität und fehlender SSTR-Expression, was die klinisch relevante Tumorheterogenität widerspiegelte. Die Ergebnisse der Dual-Tracer-Untersuchung führten bei mehr als der Hälfte der Patienten zu Änderungen in der therapeutischen Behandlung.

Zusammenfassend lässt sich sagen, dass LAFOV-PET/CT-Geräte eine signifikante Reduktion der injizierten [^{18}F]FDG-Aktivität ermöglichen, während die diagnostische und semiquantitative Leistungsfähigkeit erhalten bleibt. Diese Fähigkeit lässt sich in ein robustes, Ein-Tages-Dual-Tracer-PET/CT-Protokoll mit zwei ^{18}F-markierten Radiotracern umsetzen, ohne die semiquantitative Auswertung der Tracer-Aufnahme zu beeinträchtigen. Der Ansatz reduziert die Strahlenbelastung sowie die Belastung für den Patienten und ermöglicht eine umfassendere in-vivo-Evaluation der Tumorbiologie mit direkter klinischer Auswirkung. Zukünftige Arbeiten sollten sich auf die weitere Optimierung der Akquisitionszeiten und der Intervalle zwischen den Scans, die Bewertung zusätzlicher Dosisreduktionen, die Validierung der klinischen Auswirkungen in größeren prospektiven Kohorten sowie die Ausweitung dieses Konzepts auf andere onkologische Entitäten konzentrieren, bei denen die multiparametrische PET-Bildgebung relevant sein könnte.

6. Bibliography/List of References:

Adams, M. C., T. G. Turkington, J. M. Wilson and T. Z. Wong (2010). "A systematic review of the factors affecting accuracy of SUV measurements." AJR Am J Roentgenol **195**(2): 310-320.

Afshar-Oromieh, A., E. Avtzi, F. L. Giesel, T. Holland-Letz, H. G. Linhart, M. Eder, M. Eisenhut, S. Boxler, B. A. Hadaschik, C. Kratochwil, W. Weichert, K. Kopka, J. Debus and U. Haberkorn (2015). "The diagnostic value of PET/CT imaging with the (68)Ga-labelled PSMA ligand HBED-CC in the diagnosis of recurrent prostate cancer." Eur J Nucl Med Mol Imaging **42**(2): 197-209.

Alberts, I., J. N. Hunermund, G. Prenosil, C. Mingels, K. P. Bohn, M. Viscione, H. Sari, B. Vollnberg, K. Shi, A. Afshar-Oromieh and A. Rominger (2021). "Clinical performance of long axial field of view PET/CT: a head-to-head intra-individual comparison of the Biograph Vision Quadra with the Biograph Vision PET/CT." Eur J Nucl Med Mol Imaging **48**(8): 2395-2404.

Alberts, I., R. Schepers, K. Zeimpekis, H. Sari, A. Rominger and A. Afshar-Oromieh (2023). "Combined [68 Ga]Ga-PSMA-11 and low-dose 2-[18F]FDG PET/CT using a long-axial field of view scanner for patients referred for [177Lu]-PSMA-radioligand therapy." Eur J Nucl Med Mol Imaging **50**(3): 951-956.

Alevroudis, E., M. E. Spei, S. N. Chatziioannou, M. Tsoli, G. Wallin, G. Kaltsas and K. Daskalakis (2021). "Clinical Utility of (18)F-FDG PET in Neuroendocrine Tumors Prior to Peptide Receptor Radionuclide Therapy: A Systematic Review and Meta-Analysis." Cancers (Basel) **13**(8).

Amaral, T., M. Ottaviano, A. Arance, C. Blank, V. Chiarion-Sileni, M. Donia, R. Dummer, C. Garbe, J. E. Gershenwald, H. Gogas, M. Guckenberger, J. Haanen, O. Hamid, A. Hauschild, C. Holler, C. Lebbe, R. J. Lee, G. V. Long, P. Lorigan, E. Munoz Couselo, P. Nathan, C. Robert, E. Romano, D. Schadendorf, V. Sondak, K. P. M. Suijkerbuijk, A. C. J. van Akkooi, O. Michielin, P. A. Ascierto and E. G. C. E. a. clinicalguidelines@esmo.org (2025). "Cutaneous melanoma: ESMO Clinical Practice Guideline for diagnosis, treatment and follow-up." Ann Oncol **36**(1): 10-30.

Ambrosini, V., M. Caplin, J. P. Castano, E. Christ, T. Denecke, C. M. Deroose, C. Dromain, M. Falconi, S. Grozinsky-Glasberg, R. J. Hicks, J. Hofland, A. Kjaer, U. P. Knigge, B. Kos-Kudla, A. Koumarianou, B. Krishna, A. Lamarca, M. Pavel, N. S. Reed, A. Scarpa, R. Srirajaskanthan, A. Sundin, C. Toumpanakis and V. Prasad (2024). "Use and perceived utility of [(18) F]FDG PET/CT in neuroendocrine neoplasms: A consensus report from the European Neuroendocrine Tumor Society (ENETS) Advisory Board Meeting 2022." J Neuroendocrinol **36**(1): e13359.

Ayati, N., R. Sadeghi, Z. Kiamanesh, S. T. Lee, S. R. Zakavi and A. M. Scott (2021). "The value of (18)F-FDG PET/CT for predicting or monitoring

immunotherapy response in patients with metastatic melanoma: a systematic review and meta-analysis." Eur J Nucl Med Mol Imaging **48**(2): 428-448.

Barrington, S. F. and R. Kluge (2017). "FDG PET for therapy monitoring in Hodgkin and non-Hodgkin lymphomas." Eur J Nucl Med Mol Imaging **44**(Suppl 1): 97-110.

Basu, S., T. C. Kwee, S. Surti, E. A. Akin, D. Yoo and A. Alavi (2011). "Fundamentals of PET and PET/CT imaging." Ann N Y Acad Sci **1228**: 1-18.

Beyer, L., A. Gosewisch, S. Lindner, F. Volter, L. M. Mittlmeier, R. Tiling, M. Brendel, C. C. Cyran, M. Unterrainer, J. Rubenthaler, C. J. Auernhammer, C. Spitzweg, G. Boning, F. J. Gildehaus, K. Jurkschat, C. Wangler, B. Wangler, R. Schirrmacher, V. Wenter, A. Todica, P. Bartenstein and H. Ilhan (2021). "Dosimetry and optimal scan time of [(18)F]SiTATE-PET/CT in patients with neuroendocrine tumours." Eur J Nucl Med Mol Imaging **48**(11): 3571-3581.

BfS. (2024, Accessed on: 12.12.2025). "Natural radiation in Germany." from https://www.bfs.de/EN/topics/ion/environment/natural-radiation/natural-radiation.html.

Binderup, T., U. Knigge, A. Loft, B. Federspiel and A. Kjaer (2010). "18F-fluorodeoxyglucose positron emission tomography predicts survival of patients with neuroendocrine tumors." Clin Cancer Res **16**(3): 978-985.

Boellaard, R., I. Buvat, C. Nioche, L. Ceriani, A. S. Cottereau, L. Guerra, R. J. Hicks, S. Kanoun, C. Kobe, A. Loft, H. Schoder, A. Versari, C. A. Voltin, G. J. C. Zwezerijnen, J. M. Zijlstra, N. G. Mikhaeel, A. Gallamini, T. C. El-Galaly, C. Hanoun, S. Chauvie, R. Ricci, E. Zucca, M. Meignan and S. F. Barrington (2024). "International Benchmark for Total Metabolic Tumor Volume Measurement in Baseline (18)F-FDG PET/CT of Lymphoma Patients: A Milestone Toward Clinical Implementation." J Nucl Med **65**(9): 1343-1348.

Boellaard, R., R. Delgado-Bolton, W. J. Oyen, F. Giammarile, K. Tatsch, W. Eschner, F. J. Verzijlbergen, S. F. Barrington, L. C. Pike, W. A. Weber, S. Stroobants, D. Delbeke, K. J. Donohoe, S. Holbrook, M. M. Graham, G. Testanera, O. S. Hoekstra, J. Zijlstra, E. Visser, C. J. Hoekstra, J. Pruim, A. Willemsen, B. Arends, J. Kotzerke, A. Bockisch, T. Beyer, A. Chiti, B. J. Krause and M. European Association of Nuclear (2015). "FDG PET/CT: EANM procedure guidelines for tumour imaging: version 2.0." Eur J Nucl Med Mol Imaging **42**(2): 328-354.

Calderon, E., L. S. Kiefer, F. P. Schmidt, W. Lan, A. S. Brendlin, C. P. Reinert, S. Singer, G. Reischl, M. Hinterleitner, H. Dittmann, C. la Fougere and N. F. Trautwein (2025). "One-day dual-tracer examination in neuroendocrine neoplasms: a real advantage of low activity LAFOV PET imaging." Eur J Nucl Med Mol Imaging.

Calderon, E., F. P. Schmidt, W. Lan, S. Castaneda-Vega, A. S. Brendlin, N. F. Trautwein, H. Dittmann, C. la Fougere and L. S. Kiefer (2023). "Image Quality and Quantitative PET Parameters of Low-Dose [(18)F]FDG PET in a Long Axial Field-of-View PET/CT Scanner." Diagnostics (Basel) **13**(20).

Campana, D., V. Ambrosini, R. Pezzilli, S. Fanti, A. M. Labate, D. Santini, C. Ceccarelli, F. Nori, R. Franchi, R. Corinaldesi and P. Tomassetti (2010). "Standardized uptake values of (68)Ga-DOTANOC PET: a promising prognostic tool in neuroendocrine tumors." J Nucl Med **51**(3): 353-359.

Chan, D. L., E. J. Bernard, G. Schembri, P. J. Roach, M. Johnson, N. Pavlakis, S. Clarke and D. L. Bailey (2020). "High Metabolic Tumour Volume on 18-Fluorodeoxyglucose Positron Emission Tomography Predicts Poor Survival from Neuroendocrine Neoplasms." Neuroendocrinology **110**(11-12): 950-958.

Chan, D. L., A. Hayes, I. Karfis, A. Conner, M. Mileva, E. Bernard, S. Navalkissoor, G. Gnanasekaran, S. J. Clarke, P. J. Roach, P. Flamen, M. E. Caplin, N. Pavlakis, C. Toumpanakis and D. L. Bailey (2025). "[(18)F]FDG Metabolic Tumor Volume as a Prognostic Marker in Neuroendocrine Neoplasm: A Multicenter Study." J Nucl Med **66**(7): 1012-1017.

Chan, D. L., A. R. Hayes, I. Karfis, A. Conner, L. Furtado O'Mahony, M. Mileva, E. Bernard, P. Roach, G. Marin, N. Pavlakis, G. Schembri, G. Gnanasegaran, C. Marin, B. Vanderlinden, S. Navalkissoor, M. E. Caplin, P. Flamen, C. Toumpanakis and D. L. Bailey (2023). "Dual [(68)Ga]DOTATATE and [(18)F]FDG PET/CT in patients with metastatic gastroenteropancreatic neuroendocrine neoplasms: a multicentre validation of the NETPET score." Br J Cancer **128**(4): 549-555.

Chan, D. L., N. Pavlakis, G. P. Schembri, E. J. Bernard, E. Hsiao, A. Hayes, T. Barnes, C. Diakos, M. Khasraw, J. Samra, E. Eslick, P. J. Roach, A. Engel, S. J. Clarke and D. L. Bailey (2017). "Dual Somatostatin Receptor/FDG PET/CT Imaging in Metastatic Neuroendocrine Tumours: Proposal for a Novel Grading Scheme with Prognostic Significance." Theranostics **7**(5): 1149-1158.

Chan, H., C. Moseley, L. Zhang, E. K. Bergsland, M. H. Pampaloni, K. Van Loon and T. A. Hope (2019). "Correlation of DOTATOC Uptake and Pathologic Grade in Neuroendocrine Tumors." Pancreas **48**(7): 948-952.

Cheson, B. D., R. I. Fisher, S. F. Barrington, F. Cavalli, L. H. Schwartz, E. Zucca, T. A. Lister, A. L. Alliance, G. Lymphoma, G. Eastern Cooperative Oncology, C. European Mantle Cell Lymphoma, F. Italian Lymphoma, R. European Organisation for, G. Treatment of Cancer/Dutch Hemato-Oncology, O. Grupo Espanol de Medula, G. German High-Grade Lymphoma Study, G. German Hodgkin's Study, G. Japanese Lymphorra Study, A. Lymphoma Study, N. C. T. Group, G. Nordic Lymphoma Study, G. Southwest Oncology and I. United Kingdom National Cancer Research (2014). "Recommendations for initial evaluation, staging, and response assessment of Hodgkin and non-Hodgkin lymphoma: the Lugano classification." J Clin Oncol **32**(27): 3059-3068.

Delpassand, E. S., D. Ranganathan, N. Wagh, A. Shafie, A. Gaber, A. Abbasi, A. Kjaer, I. Tworowska and R. Nunez (2020). "(64)Cu-DOTATATE PET/CT for Imaging Patients with Known or Suspected Somatostatin Receptor-Positive Neuroendocrine Tumors: Results of the First U.S. Prospective, Reader-Masked Clinical Trial." J Nucl Med **61**(6): 890-896.

Dimitrakopoulou-Strauss, A., L. Pan and C. Sachpekidis (2023). "Long axial field of view (LAFOV) PET-CT: implementation in static and dynamic oncological studies." Eur J Nucl Med Mol Imaging **50**(11): 3354-3362.

Forschner, A., S. C. Olthof, B. Guckel, P. Martus, W. Vach, C. la Fougere, K. Nikolaou, U. Keim, T. K. Eigentler, C. Garbe and C. Pfannenberg (2017). "Impact of (18)F-FDG-PET/CT on surgical management in patients with advanced melanoma: an outcome based analysis." Eur J Nucl Med Mol Imaging **44**(8): 1312-1318.

Fueger, B. J., K. Yeom, J. Czernin, J. W. Sayre, M. E. Phelps and M. S. Allen-Auerbach (2009). "Comparison of CT, PET, and PET/CT for staging of patients with indolent non-Hodgkin's lymphoma." Mol Imaging Biol **11**(4): 269-274.

Gambhir, S. S. (2002). "Molecular imaging of cancer with positron emission tomography." Nat Rev Cancer **2**(9): 683-693.

Geijer, H. and L. H. Breimer (2013). "Somatostatin receptor PET/CT in neuroendocrine tumours: update on systematic review and meta-analysis." Eur J Nucl Med Mol Imaging **40**(11): 1770-1780.

Giesel, F. L., B. Hadaschik, J. Cardinale, J. Radtke, M. Vinsensia, W. Lehnert, C. Kesch, Y. Tolstov, S. Singer, N. Grabe, S. Duensing, M. Schafer, O. C. Neels, W. Mier, U. Haberkorn, K. Kopka and C. Kratochwil (2017). "F-18 labelled PSMA-1007: biodistribution, radiation dosimetry and histopathological validation of tumor lesions in prostate cancer patients." Eur J Nucl Med Mol Imaging **44**(4): 678-688.

Guttikonda, R., B. R. Herts, F. Dong, M. E. Baker, K. B. Fenner and B. Pohlman (2014). "Estimated radiation exposure and cancer risk from CT and PET/CT scans in patients with lymphoma." Eur J Radiol **83**(6): 1011-1015.

He, Y., Y. Gu, H. Yu, B. Wu, S. Wang, H. Tan, Y. Cao, S. Chen, X. Sui, Y. Zhang and H. Shi (2022). "Optimizing acquisition times for total-body positron emission tomography/computed tomography with half-dose (18)F-fluorodeoxyglucose in oncology patients." EJNMMI Phys **9**(1): 45.

Hofman, M. S., L. Emmett, S. Sandhu, A. Iravani, J. P. Buteau, A. M. Joshua, J. C. Goh, D. A. Pattison, T. H. Tan, I. D. Kirkwood, S. Ng, R. J. Francis, C. Gedye, N. K. Rutherford, A. Weickhardt, A. M. Scott, S. T. Lee, E. M. Kwan, A. A. Azad, S. Ramdave, A. D. Redfern, W. Macdonald, A. Guminski, E. Hsiao, W. Chua, P. Lin, A. Y. Zhang, M. R. Stockler, S. G. Williams, A. J. Martin, I. D. Davis, P. T. I. Thera, A. the, U. New Zealand and G. Prostate Cancer Trials (2024). "Overall

survival with [(177)Lu]Lu-PSMA-617 versus cabazitaxel in metastatic castration-resistant prostate cancer (TheraP): secondary outcomes of a randomised, open-label, phase 2 trial." Lancet Oncol **25**(1): 99-107.

Hofman, M. S., N. Lawrentschuk, R. J. Francis, C. Tang, I. Vela, P. Thomas, N. Rutherford, J. M. Martin, M. Frydenberg, R. Shakher, L. M. Wong, K. Taubman, S. Ting Lee, E. Hsiao, P. Roach, M. Nottage, I. Kirkwood, D. Hayne, E. Link, P. Marusic, A. Matera, A. Herschtal, A. Iravani, R. J. Hicks, S. Williams, D. G. Murphy and P. S. G. C. pro (2020). "Prostate-specific membrane antigen PET-CT in patients with high-risk prostate cancer before curative-intent surgery or radiotherapy (proPSMA): a prospective, randomised, multicentre study." Lancet **395**(10231): 1208-1216.

Korsholm, K., R. Aleksyniene, E. Albrecht-Beste, E. S. Vadstrup, F. L. Andersen and B. M. Fischer (2023). "Staging of breast cancer in pregnancy with ultralow dose [18F]-FDG-PET/CT." Eur J Nucl Med Mol Imaging **50**(5): 1534-1535.

Lagana, M., F. Gallo, M. Salvetti, D. Smussi, A. Esposito, G. Carola, M. Carpani, F. Morocutti, D. Cosentini, R. Pedersini, S. Grisanti, A. Berruti and V. Amoroso (2025). "Predictors of survival outcomes in patients with neuroendocrine neoplasms: a real-world retrospective study." Endocr Relat Cancer **32**(12).

Lennon, A. M., A. H. Buchanan, I. Kinde, A. Warren, A. Honushefsky, A. T. Cohain, D. H. Ledbetter, F. Sanfilippo, K. Sheridan, D. Rosica, C. S. Adonizio, H. J. Hwang, K. Lahouel, J. D. Cohen, C. Douville, A. A. Patel, L. N. Hagmann, D. D. Rolston, N. Malani, S. Zhou, C. Bettegowda, D. L. Diehl, B. Urban, C. D. Still, L. Kann, J. I. Woods, Z. M. Salvati, J. Vadakara, R. Leeming, P. Bhattacharya, C. Walter, A. Parker, C. Lengauer, A. Klein, C. Tomasetti, E. K. Fishman, R. H. Hruban, K. W. Kinzler, B. Vogelstein and N. Papadopoulos (2020). "Feasibility of blood testing combined with PET-CT to screen for cancer and guide intervention." Science **369**(6499).

Leupe, H., S. Ahenkorah, J. Dekervel, M. Unterrainer, E. Van Cutsem, C. Verslype, F. Cleeren and C. M. Deroose (2023). "(18)F-Labeled Somatostatin Analogs as PET Tracers for the Somatostatin Receptor: Ready for Clinical Use." J Nucl Med **64**(6): 835-841.

Lewis, K. L. and J. Trotman (2023). "Integration of PET in DLBCL." Semin Hematol **60**(5): 291-304.

Lindner, S., C. Wangler, J. J. Bailey, K. Jurkschat, P. Bartenstein, B. Wangler and R. Schirrmacher (2020). "Radiosynthesis of [(18)F]SiFAlin-TATE for clinical neuroendocrine tumor positron emission tomography." Nat Protoc **15**(12): 3827-3843.

Liu, X., N. Li, T. Jiang, H. Xu, Q. Ran, Z. Shu, J. Wu, Y. Li, S. Zhou and B. Zhang (2020). "Comparison of gallium-68 somatostatin receptor and (18)F-fluorodeoxyglucose positron emission tomography in the diagnosis of

neuroendocrine tumours: A systematic review and meta-analysis." Hell J Nucl Med **23**(2): 188-200.

Lodge, M. A., M. A. Chaudhry and R. L. Wahl (2012). "Noise considerations for PET quantification using maximum and peak standardized uptake value." J Nucl Med **53**(7): 1041-1047.

Lucignani, G. (2009). "SUV and segmentation: pressing challenges in tumour assessment and treatment." Eur J Nucl Med Mol Imaging **36**(4): 715-720.

Man, D., J. Wu, Z. Shen and X. Zhu (2018). "Prognosis of patients with neuroendocrine tumor: a SEER database analysis." Cancer Manag Res **10**: 5629-5638.

Mattsson, S., L. Johansson, S. Leide Svegborn, J. Liniecki, D. Nosske, K. A. Riklund, M. Stabin, D. Taylor, W. Bolch, S. Carlsson, K. Eckerman, A. Giussani, L. Soderberg, S. Valind and Icrp (2015). "Radiation Dose to Patients from Radiopharmaceuticals: a Compendium of Current Information Related to Frequently Used Substances." Ann ICRP **44**(2 Suppl): 7-321.

Mochizuki, T., E. Tsukamoto, Y. Kuge, K. Kanegae, S. Zhao, K. Hikosaka, M. Hosokawa, M. Kohanawa and N. Tamaki (2001). "FDG uptake and glucose transporter subtype expressions in experimental tumor and inflammation models." J Nucl Med **42**(10): 1551-1555.

Moller, L., A. Szentkiralyi, C. Eisfeld, I. Wellmann, F. Rees, K. Claassen, F. Oesterling, H. Kajuter and A. Stang (2025). "Incidence trends and relative survival of colorectal neuroendocrine neoplasms: A population-based study using German cancer registry data." Int J Cancer **157**(1): 116-125.

Nordstrand, M. A., D. Lea and J. A. Soreide (2025). "Incidence of gastroenteropancreatic neuroendocrine neoplasms (GEP-NENs): An updated systematic review of population-based reports from 2010 to 2023." J Neuroendocrinol **37**(4): e70001.

Olivier, T., K. Powell and V. Prasad (2023). "Lutetium-177-PSMA-617 in Metastatic Castration-resistant Prostate Cancer: Limitations of the VISION Trial." Eur Urol **84**(1): 4-6.

Park, S., A. S. Parihar, L. Bodei, T. A. Hope, N. Mallak, C. Millo, K. Prasad, D. Wilson, K. Zukotynski and E. Mittra (2021). "Somatostatin Receptor Imaging and Theranostics: Current Practice and Future Prospects." J Nucl Med **62**(10): 1323-1329.

Pauwels, E. K., M. J. Ribeiro, J. H. Stoot, V. R. McCready, M. Bourguignon and B. Maziere (1998). "FDG accumulation and tumor biology." Nucl Med Biol **25**(4): 317-322.

Pavel, M., K. Oberg, M. Falconi, E. P. Krenning, A. Sundin, A. Perren, A. Berruti and E. G. C. E. a. clinicalguidelines@esmo.org (2020). "Gastroenteropancreatic

neuroendocrine neoplasms: ESMO Clinical Practice Guidelines for diagnosis, treatment and follow-up." Ann Oncol **31**(7): 844-860.

Petersen, R. K., S. Hess, A. Alavi and P. F. Hoilund-Carlsen (2014). "Clinical impact of FDG-PET/CT on colorectal cancer staging and treatment strategy." Am J Nucl Med Mol Imaging **4**(5): 471-482.

Phelps, M. E., E. J. Hoffman, N. A. Mullani and M. M. Ter-Pogossian (1975). "Application of annihilation coincidence detection to transaxial reconstruction tomography." J Nucl Med **16**(3): 210-224.

Polee, I. N., B. C. M. Hermans, J. M. van der Zwan, S. A. W. Bouwense, M. W. Dercksen, F. Eskens, B. Havekes, J. Hofland, T. M. A. Kerkhofs, H. J. Klumpen, L. M. Latten-Jansen, E. M. Speel, F. A. Verburg, A. M. E. Walenkamp, S. M. E. Geurts and J. de Vos-Geelen (2022). "Long-term survival in patients with gastroenteropancreatic neuroendocrine neoplasms: A population-based study." Eur J Cancer **172**: 252-263.

Pozdnyakov, A., R. Kulanthaivelu, G. Bauman, C. Ortega, P. Veit-Haibach and U. Metser (2023). "The impact of PSMA PET on the treatment and outcomes of men with biochemical recurrence of prostate cancer: a systematic review and meta-analysis." Prostate Cancer Prostatic Dis **26**(2): 240-248.

Prenosil, G. A., M. Hentschel, T. Weitzel, H. Sari, K. Shi, A. Afshar-Oromieh and A. Rominger (2022). "EARL compliance measurements on the biograph vision Quadra PET/CT system with a long axial field of view." EJNMMI Phys **9**(1): 26.

Prenosil, G. A., H. Sari, M. Furstner, A. Afshar-Oromieh, K. Shi, A. Rominger and M. Hentschel (2022). "Performance Characteristics of the Biograph Vision Quadra PET/CT System with a Long Axial Field of View Using the NEMA NU 2-2018 Standard." J Nucl Med **63**(3): 476-484.

Queisser, A., S. A. Hagedorn, M. Braun, W. Vogel, S. Duensing and S. Perner (2015). "Comparison of different prostatic markers in lymph node and distant metastases of prostate cancer." Mod Pathol **28**(1): 138-145.

Rausch, I., J. G. Mannheim, J. Kupferschlager, C. la Fougere and F. P. Schmidt (2022). "Image quality assessment along the one metre axial field-of-view of the total-body Biograph Vision Quadra PET/CT system for (18)F-FDG." EJNMMI Phys **9**(1): 87.

Refardt, J., W. T. Zandee, T. Brabander, R. A. Feelders, G. J. H. Franssen, L. J. Hofland, E. Christ, W. W. de Herder and J. Hofland (2020). "Inferior outcome of neuroendocrine tumor patients negative on somatostatin receptor imaging." Endocr Relat Cancer **27**(11): 615-624.

Reichkendler, M., F. L. Andersen, L. Borgwardt, U. Nygaard, E. Albrecht-Beste, K. F. Andersen, A. Ljunggren, N. Abrahamsen, A. Loft, L. Hojgaard and B. M.

Fischer (2022). "A Long Axial Field of View Enables PET/CT in Toddler Without Sedation." J Nucl Med **63**(12): 1962.

Rindi, G., O. Mete, S. Uccella, O. Basturk, S. La Rosa, L. A. A. Brosens, S. Ezzat, W. W. de Herder, D. S. Klimstra, M. Papotti and S. L. Asa (2022). "Overview of the 2022 WHO Classification of Neuroendocrine Neoplasms." Endocr Pathol **33**(1): 115-154.

Rinzivillo, M., S. Partelli, D. Prosperi, G. Capurso, P. Pizzichini, E. Iannicelli, E. Merola, F. Muffatti, F. Scopinaro, O. Schillaci, M. Salgarello, M. Falconi, G. Delle Fave and F. Panzuto (2018). "Clinical Usefulness of (18)F-Fluorodeoxyglucose Positron Emission Tomography in the Diagnostic Algorithm of Advanced Entero-Pancreatic Neuroendocrine Neoplasms." Oncologist **23**(2): 186-192.

Sachpekidis, C., L. Pan, A. Kopp-Schneider, V. Weru, J. C. Hassel and A. Dimitrakopoulou-Strauss (2023). "Application of the long axial field-of-view PET/CT with low-dose [(18)F]FDG in melanoma." Eur J Nucl Med Mol Imaging **50**(4): 1158-1167.

Sadowski, S. M., V. Neychev, C. Millo, J. Shih, N. Nilubol, P. Herscovitch, K. Pacak, S. J. Marx and E. Kebebew (2016). "Prospective Study of 68Ga-DOTATATE Positron Emission Tomography/Computed Tomography for Detecting Gastro-Entero-Pancreatic Neuroendocrine Tumors and Unknown Primary Sites." J Clin Oncol **34**(6): 588-596.

Sathekge, C., J. Maes, A. Maes and C. Van de Wiele (2025). "FDG PET/CT for Staging Lung Carcinoma: An Update." Semin Nucl Med **55**(2): 167-174.

Schmidt, F. P., J. G. Mannheim, P. M. Linder, P. Will, L. S. Kiefer, M. Conti, C. la Fougere and I. Rausch (2023). "Impact of the maximum ring difference on image quality and noise characteristics of a total-body PET/CT scanner." Z Med Phys.

Schwab, R., K. Anic and A. Hasenburg (2021). "Cancer and Pregnancy: A Comprehensive Review." Cancers (Basel) **13**(12).

Slart, R., C. Tsoumpas, A. Glaudemans, W. Noordzij, A. T. M. Willemsen, R. J. H. Borra, R. Dierckx and A. A. Lammertsma (2021). "Long axial field of view PET scanners: a road map to implementation and new possibilities." Eur J Nucl Med Mol Imaging **48**(13): 4236-4245.

Smith, C. L. C., M. Yaqub, R. H. H. Wellenberg, J. J. Knip, R. Boellaard and G. J. C. Zwezerijnen (2024). "Ultra-low foetal radiation exposure in (18)F-FDG PET/CT imaging with a long axial field-of-view PET/CT system." EJNMMI Phys **11**(1): 45.

Sorbye, H., G. O. Hjortland, L. W. Vestermark, M. Ladekarl, J. Svensson, A. Sundlov, E. T. Janson, H. Garresori, E. Hofsli, C. Kersten, H. Elvebakken, P. Pfeiffer, S. Morken, J. Assmus, I. M. B. Lothe, E. Tabaksblat, U. Knigge, A. Couvelard, A. Perren and S. W. Langer (2025). "Characteristics and treatment outcome in a prospective cohort of 639 advanced high-grade digestive

neuroendocrine neoplasms (NET G3 and NEC). The NORDIC NEC 2 study." Br J Cancer **133**(3): 316-324.

Spencer, B. A., E. Berg, J. P. Schmall, N. Omidvari, E. K. Leung, Y. G. Abdelhafez, S. Tang, Z. Deng, Y. Dong, Y. Lv, J. Bao, W. Liu, H. Li, T. Jones, R. D. Badawi and S. R. Cherry (2021). "Performance Evaluation of the uEXPLORER Total-Body PET/CT Scanner Based on NEMA NU 2-2018 with Additional Tests to Characterize PET Scanners with a Long Axial Field of View." J Nucl Med **62**(6): 861-870.

Squires, M. H., 3rd, N. Volkan Adsay, D. M. Schuster, M. C. Russell, K. Cardona, K. A. Delman, J. H. Winer, D. Altinel, J. M. Sarmiento, B. El-Rayes, N. Hawk, C. A. Staley, 3rd, S. K. Maithel and D. A. Kooby (2015). "Octreoscan Versus FDG-PET for Neuroendocrine Tumor Staging: A Biological Approach." Ann Surg Oncol **22**(7): 2295-2301.

Stang, A., I. Wellmann, B. Holleczek, S. Z. Kim-Wanner, J. Muller-Nordhorn, E. Sirri, I. Wittenberg, J. T. Siveke, H. Kajuter and R. German Network of Cancer (2024). "Incidence and survival of patients with malignant pancreatic neuroendocrine neoplasms in Germany, 2009-2021." Cancer Epidemiol **93**: 102659.

Strosberg, J. R., M. E. Caplin, P. L. Kunz, P. B. Ruszniewski, L. Bodei, A. Hendifar, E. Mittra, E. M. Wolin, J. C. Yao, M. E. Pavel, E. Grande, E. Van Cutsem, E. Seregni, H. Duarte, G. Gericke, A. Bartalotta, M. F. Mariani, A. Demange, S. Mutevelic, E. P. Krenning and N.-. investigators (2021). "(177)Lu-Dotatate plus long-acting octreotide versus high-dose long-acting octreotide in patients with midgut neuroendocrine tumours (NETTER-1): final overall survival and long-term safety results from an open-label, randomised, controlled, phase 3 trial." Lancet Oncol **22**(12): 1752-1763.

Sundin, A., R. Arnold, E. Baudin, J. B. Cwikla, B. Eriksson, S. Fanti, N. Fazio, F. Giammarile, R. J. Hicks, A. Kjaer, E. Krenning, D. Kwekkeboom, C. Lombard-Bohas, J. M. O'Connor, D. O'Toole, A. Rockall, B. Wiedenmann, J. W. Valle, M. P. Vullierme and p. Antibes Consensus Conference (2017). "ENETS Consensus Guidelines for the Standards of Care in Neuroendocrine Tumors: Radiological, Nuclear Medicine & Hybrid Imaging." Neuroendocrinology **105**(3): 212-244.

Surti, S., A. R. Pantel and J. S. Karp (2020). "Total Body PET: Why, How, What for?" IEEE Trans Radiat Plasma Med Sci **4**(3): 283-292.

Tan, H., X. Sui, H. Yin, H. Yu, Y. Gu, S. Chen, P. Hu, W. Mao and H. Shi (2021). "Total-body PET/CT using half-dose FDG and compared with conventional PET/CT using full-dose FDG in lung cancer." Eur J Nucl Med Mol Imaging **48**(6): 1966-1975.

Tao, Z., R. Xue, Z. Wei, L. Qin, R. Bai, N. Liu, J. Wang and C. Wang (2023). "The assessment of Ki-67 for prognosis of gastroenteropancreatic neuroendocrine

neoplasm patients: a systematic review and meta-analysis." Transl Cancer Res **12**(8): 1980-1991.

Van Calsteren, K., L. Heyns, F. De Smet, L. Van Eycken, M. M. Gziri, W. Van Gemert, M. Halaska, I. Vergote, N. Ottevanger and F. Amant (2010). "Cancer during pregnancy: an analysis of 215 patients emphasizing the obstetrical and the neonatal outcomes." J Clin Oncol **28**(4): 683-689.

van Rijsewijk, N. D., B. van Leer, O. V. Ivashchenko, E. H. Scholvinck, F. van den Heuvel, J. H. van Snick, R. Slart, W. Noordzij and A. Glaudemans (2023). "Ultra-low dose infection imaging of a newborn without sedation using long axial field-of-view PET/CT." Eur J Nucl Med Mol Imaging **50**(2): 622-623.

van Sluis, J., R. Borra, C. Tsoumpas, J. H. van Snick, M. Roya, D. Ten Hove, A. H. Brouwers, A. A. Lammertsma, W. Noordzij, R. Dierckx, R. Slart and A. Glaudemans (2022). "Extending the clinical capabilities of short- and long-lived positron-emitting radionuclides through high sensitivity PET/CT." Cancer Imaging **22**(1): 69.

Vandenberghe, S., P. Moskal and J. S. Karp (2020). "State of the art in total body PET." EJNMMI Phys **7**(1): 35.

Warburg, O., F. Wind and E. Negelein (1927). "The Metabolism of Tumors in the Body." J Gen Physiol **8**(6): 519-530.

Weber, W. A. (2005). "Use of PET for monitoring cancer therapy and for predicting outcome." J Nucl Med **46**(6): 983-995.

Yoo, K. H. (2022). "Staging and response assessment of lymphoma: a brief review of the Lugano classification and the role of FDG-PET/CT." Blood Res **57**(S1): 75-78.

7. Declaration regarding the author´s contribution and the contribution of others

Publication 1: "Image Quality and Quantitative PET Parameters of Low-Dose [^{18}F]FDG PET in a Long Axial Field-of-View PET/CT Scanner."

Authors: Eduardo Calderón, Fabian P. Schmidt, Wenhong Lan, Salvador Castaneda-Vega, Andreas S. Brendlin, Nils F. Trautwein, Helmut Dittmann, Christian la Fougère, Lena S. Kiefer.

Published in: Diagnostics (Basel), **Volume:** 13**, Article Number:** 20**, Year:** 2023

Publication 2: "One-day dual-tracer examination in neuroendocrine neoplasms: a real advantage of low activity LAFOV PET imaging."

Authors: Eduardo Calderón, Lena S. Kiefer, Fabian P. Schmidt, Wenhong Lan, Andreas S. Brendlin, Christian P. Reinert, Stephan Singer, Gerald Reischl, Martina Hinterleitner, Helmut Dittmann, Christian la Fougère, Nils F. Trautwein.

Published in: European Journal of Nuclear Medicine and Molecular Imaging, **Volume:** 52**, Issue:** 7**, Pages:** 2463-2476**, Year:** 2025

Both publications were produced as collaborative efforts involving the above-mentioned co-authors, who mainly contributed to study execution, including patient recruitment and data acquisition, and, to a lesser extent, to data analysis, interpretation of results, and manuscript preparation. Moreover, across both studies, the doctoral candidate was a key contributor to the development of the research concepts, the selection and implementation of study methods, and the interpretation of the results, and performed most of the data analysis. He also wrote the initial manuscripts of both research articles and led the review process before publication.

Furthermore, I confirm that I have written this manuscript independently and have not used any sources other than those I have cited. The program Grammarly was used to check spelling and grammar.

Tübingen, den

Acknowledgements

I wish to express my gratitude to my family and friends, who have provided unwavering support from afar over the years. Especially, I would like to express my sincere gratitude to my wife, whose daily support is one of my primary sources of motivation.

Furthermore, I wish to express my gratitude to the entire Department of Nuclear Medicine Team in Tübingen, particularly acknowledging the consistent support of Prof. Dr. Christian La Fougère, Dr. sc. hum. Fabian P. Schmidt, and PD Dr. med. Lena S. Kiefer.